UNIVERSITAT DE BARCELONA

Role of kinase DYRK1A in the neurogenesis of the embryonic telencephalon

Alejandro Trujillano Fernández

Role of the kinase DYRK1A in the neurogenesis of the embryonic telencephalon

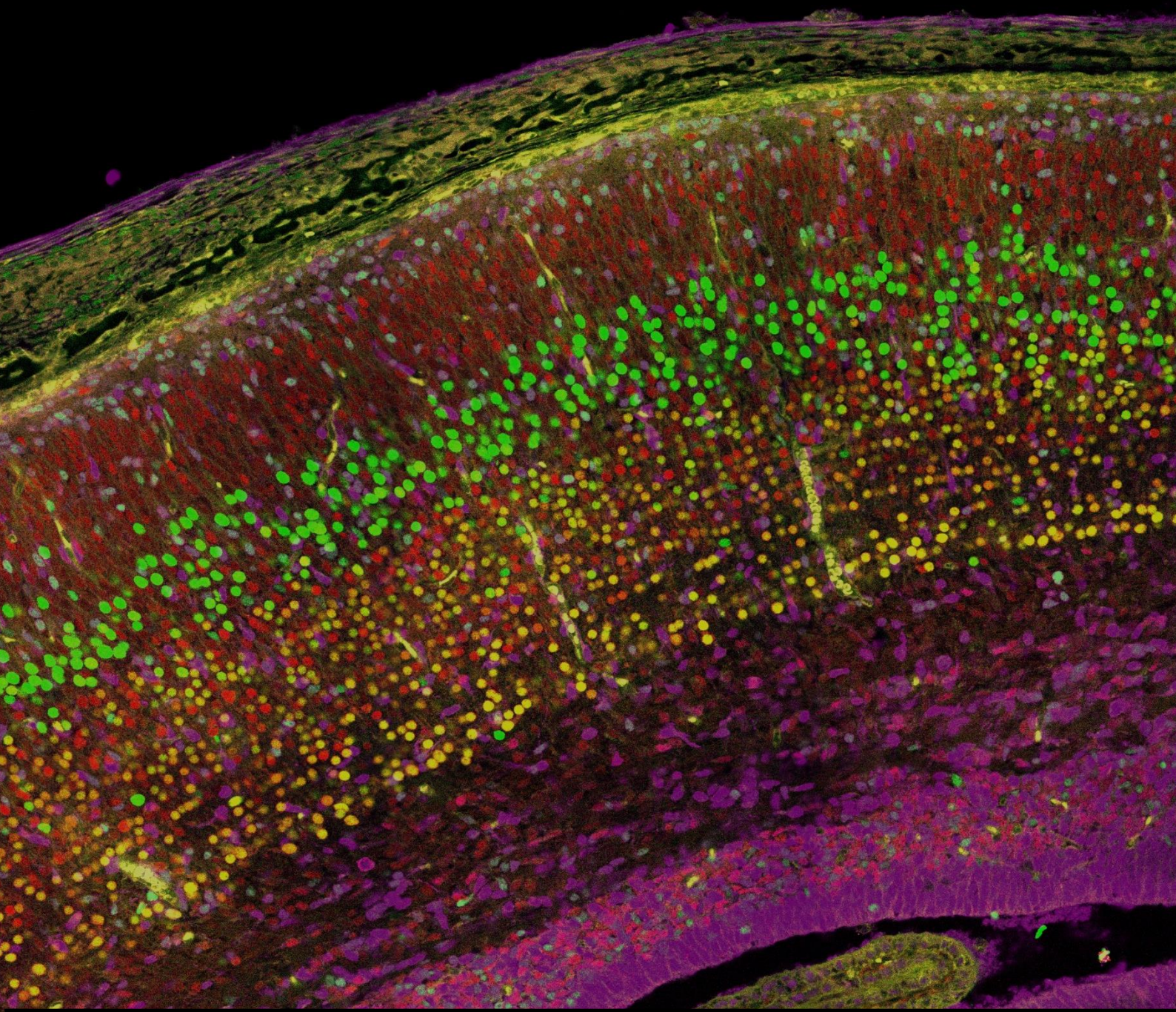

Alejandro Trujillano Fernández

Barcelona, 2023

PROGRAMA DE DOCTORADO EN BIOMEDICINA

FACULTAD DE BIOLOGÍA

2023

Role of the kinase DYRK1A in the neurogenesis of the embryonic telencephalon

Memoria presentada por Alejandro Trujillano Fernández para optar al Grado de Doctor por la Universidad de Barcelona.

Trabajo realizado bajo la dirección de la Dra. Mª Lourdes Arbonés de Rafael en el Instituto de Biología Molecular de Barcelona (IBMB-CSIC).

DIRECTOR	TUTOR
Mª Lourdes Arbonés de Rafael	Ferrán Burgaya Márquez

DOCTORANDO

Alejandro Trujillano Fernández

Alejandro Trujillano was supported by a predoctoral fellowship of the Spanish Ministry of Education and Science (*Ayudas para contratos predoctorales para la formación de doctores* 2017; BES-2017-080478). This work was supported by grants of the Spanish Ministry of Education and Science (SAF2016-77971-R and PID2019-105902RB-100).

ACKNOWLEDGEMENTS

I would like to give special thanks to my thesis director, Mariona, for her devoted dedication along the thesis and for the valuable knowledges and competences that I have obtained due to its constant and thorough guidance. Thank you as well to have teach me to be patience, think twice and not be impulsive, and be more self-critical with my work. I also want to thank all my laboratory mates María José, Isabel, Laia and David for been always willing to help me with my experiments and doubts and encourage me to be more positive and self-aware of my capacities. Many thanks as well to the members of the Elisa Marti's lab for its kindness, support, and assistance. Special thanks too to Elena Rebollo, of the molecular imaging platform, for its patience, constant assistance, and will help me with any of my problems regarding microscopes usage. You have been very helpful and great part of the merit for the quality of the images presented here is because her guidance. Also, thanks to Ferrán, my thesis tutor, for being always willing to help me and give me feedback of my work. Special thanks to the Spanish Ministry of Education and Science and the AEI (*Agencia estatal de investigación)* for the economic support of this project and to Dr. Weimin Zhong (Yale University), Dr. Jhon Crispino (Northwestern University of Chicago) and Dra. Silvia Nicolis (*Universitá degli Studi di Milano-Bicocca*, UNIMIB) for kindly providing us the transgenic mice used in this project.

ABSTRACT

DYRK1A is a kinase that is expressed in virtually all tissues and cell types and is implicated in human diseases. Several studies indicate that *DYRK1A* is a dose-dependent gene with a prevalent function in brain development by regulating neurogenesis, neuronal differentiation and physiological apoptosis. *DYRK1A* is on chromosome 21 and its trisomy contributes to some of the neurodevelopmental defects in Down syndrome. Furthermore, *de novo* mutations in *DYRK1A* in heterozygosity cause DYRK1A syndrome, a syndromic form of intellectual disability and autism that presents, among other neurological features, developmental delay, microcephaly, motor and speech problems, and early-onset epilepsy.

With the aim of providing evidence on the functions regulated by DYRK1A in early brain development, we have generated a conditional mouse mutant with a mutation in the *Dyrk1a* gene in neural progenitors. The conditional null mutant (*NesCre:Dyrk1a*-KO) dies in perinatal stages, presenting at the end of embryonic development a severe reduction in brain size, complete loss of ventral structures such as the *striatum* and morphological alterations in the neocortex. The loss of brain parenchyma in this mutant is caused by an increase in apoptosis that affects progenitors and postmitotic cells. In the progenitors, the cell death is due to defects in DNA replication and/or repair and is dependent on p53. At the beginning of neurogenesis, the cortical radial glia of *NesCre:Dyrk1a*-KO mutants present an elongation of the S phase of the cell cycle and alterations in the morphology of the nucleus that correlate with less differentiation. At the end of neurogenesis, *NesCre:Dyrk1a*-KO mutants show an early depletion of cortical progenitors caused by an increase in differentiating symmetric divisions. The conditional mutant with the *Dyrk1a* mutation in heterozygosity (*NesCre*:*Dyrk1a*-HET) reaches adulthood, presenting at the end of embryonic development a reduction in the size of the telencephalic vesicles, the *striatum,* and other ventral structures. These results show that DYRK1A is an essential kinase for the proliferation and differentiation of embryonic brain stem cells and suggests that alterations in cortical circuits involving the *striatum* may contribute to the neurological deficits in patients with DYRK1A syndrome.

In order to eliminate DYRK1A specifically in dorsal brain progenitors we generated the tamoxifen-induced mouse mutant *Sox2CreERT2:Dyrk1a*. The experiments carried out in this conditional mutant have not revealed alterations in the morphology or cellularity of the dorsal telencephalon of tamoxifen-treated *Sox2CreERT2:Dyrk1a*$^{Fl/Fl}$ embryos, probably because the mutation is in mosaicism, or because the depletion of DYRK1A in the progenitors that express Cre-recombinase is not complete and/or occurs after the critical period for DYRK1A in cortical neurogenesis.

RESUMEN

DYRK1A es una quinasa que se expresa prácticamente en todos los tejidos y tipos celulares y está implicada en enfermedades humanas. Diversos estudios indican que *DYRK1A* es un gen dosis-dependiente con una función prevalente en el desarrollo del cerebro regulando neurogénesis, diferenciación neuronal y apoptosis fisiológica. *DYRK1A* está en el cromosoma 21 y su trisomía contribuye a algunos de los defectos del neurodesarrollo en el síndrome de Down. Además, mutaciones *de novo* en *DYRK1A* en heterocigosis causan el síndrome de DYRK1A, una forma sindrómica de discapacidad intelectual y autismo que presenta, entre otras características neurológicas, retraso del desarrollo, microcefalia, problemas motores y del habla y epilepsia de inicio temprano.

Con el objetivo de aportar evidencias sobre las funciones reguladas por DYRK1A en el desarrollo cerebral temprano, hemos generado un mutante de ratón con una mutación nula en el gen *Dyrk1a* en progenitores neurales. El mutante nulo condicional (*NesCre*:*Dyrk1a*-KO) muere en estadios perinatales, presentando al final del desarrollo embrionario una severa reducción del tamaño del cerebro, pérdida completa de estructuras ventrales como el estriado y alteraciones morfológicas en el neocórtex. La pérdida de parénquima cerebral en este mutante está causada por un aumento de la apoptosis que afecta a progenitores y a células postmitóticas. En los progenitores, la muerte es debida a defectos en la replicación y/o reparación del DNA y es dependiente de p53. Al inicio de la neurogénesis, la glía radial cortical de los mutantes *NesCre*:*Dyrk1a*-KO presenta un alargamiento de la fase S del ciclo celular y alteraciones en la morfología del núcleo que correlacionan con una menor diferenciación. Al final de la neurogénesis, los mutantes *NesCre*:*Dyrk1a*-KO muestran una depleción adelantada de progenitores corticales causada por un aumento de divisiones simétricas diferenciadoras. El mutante condicional con la mutación *Dyrk1a* en heterocigosis (*NesCre*:*Dyrk1a*-HET) alcanza la edad adulta, presentando al final del desarrollo embrionario una reducción en el tamaño de las vesículas telencefálicas, del estriado y otras estructuras ventrales. Estos resultados muestran que DYRK1A es una quinasa esencial para la proliferación y diferenciación de las células madre cerebrales embrionarias y sugieren que alteraciones en circuitos corticales que impliquen el estriado pueden contribuir a los déficits neurológicos en pacientes con síndrome DYRK1A.

Para eliminar DYRK1A específicamente en los progenitores del telencéfalo dorsal, generamos el mutante de ratón inducido por tamoxifeno *Sox2CreERT2*:*Dyrk1a.* Los experimentos realizados en este mutante condicional no han revelado alteraciones en la morfología o celularidad del telencéfalo dorsal de embriones *Sox2CreERT2*:*Dyrk1a*$^{Fl/Fl}$ tratados con tamoxifeno, probablemente porque la mutación está en mosaicismo, o debido

a que la depleción de DYRK1A en los progenitores que expresan Cre-recombinasa no es completa y/o ocurre después del periodo crítico para DYRK1A en la neurogénesis cortical.

TABLE OF CONTENTS

ABBREVIATIONS

aIP: apical intermediate progenitor
ASD: autism spectrum disorder
ATM: ataxia telangiectasia mutated
ATR: ataxia telangiectasia and RAD3-related
bIP: basal intermediate progenitor
bRG: basal radial glia
BrdU: 5-bromo-2'-deoxyuridine
CDK: cyclin-dependent kinase
CGE: caudal ganglionic eminence
CNS: central nervous system
CP: cortical plate
DAPI: 4′,6-diamidino-2-phenylindole, dihydrochloride
DDR: DNA-damage response
DNA-PK: DNA-dependent protein kinase
DSB: DNA double strand break
DYRK: Dual-specificity tyrosine-regulated Kinase
E: embryonic day
EdU: 5-ethynyl-2′-deoxyuridine
HR: homologous recombination
ID: intellectual disability
IP: intermediate progenitor
IZ: intermediate zone
LGE: lateral ganglionic eminence
MGE: medial ganglionic eminence
MRN: MRE11-RAD50-NBS1
MSN: medium spiny neuron
MZ: mantle zone
NesCre:*Dyrk1a*-HET: *NestinCre*+: *Dyrk1a* Fl/+
NesCre:*Dyrk1a*-KO: *NestinCre*+: *Dyrk1a* Fl/Fl
NHEJ: non-homologous end joining
NSC: neural stem cell
N-WAP: neuronal Wiskott-Aldrich syndrome protein
P: postnatal day
PBS: phosphate buffer saline

pH3: phosphorylated histone H3 (Ser28)

pVim: phosphorylated Vimentin (Ser55)

RG: radial glia

ROS: reactive oxygen species

Sox2CreERT2:*Dyrk1a*-KO: *Sox2CreERT2*+:*Dyrk1a*Fl/Fl

SSB: DNA single strand break

ssDNA: single stranded DNA

SVZ: subventricular zone

tdTomato reporter: mB6.Cg-Gt (ROSA) 26Sortm14 (CAG-tdTomato) Hze/J reporter

VZ: ventricular zone

ɣ-H2AX: phosphorylated histone H2A (Ser139)

INTRODUCTION

1. The Neocortex and *Striatum*

The brain is the part of the central nervous system (CNS) located inside the skull. This structure is originated from the most anterior part of the embryonic neural tube and can be subdivided in three parts: the rhombencephalon or hindbrain, the mesencephalon or midbrain, and the prosencephalon or forebrain. The rhombencephalon encompasses the cerebellum, the medulla oblongata and the pons, which together with the caudal part of the mesencephalon form the brain stem. The mesencephalon also includes the *tectum* and the *substantia nigra* in the ventral tegmentum. The prosencephalon is further divided into the diencephalon, that comprises the thalamus and the hypothalamus, and the telencephalon, which is formed by the neocortex, the *striatum*, the *globus pallidus*, the amygdala, the hippocampus, and the olfactory bulb (Nieuwenhuys et al., 2007).

The gross anatomy, function and development of the neocortex and *striatum* are described in the sections bellow.

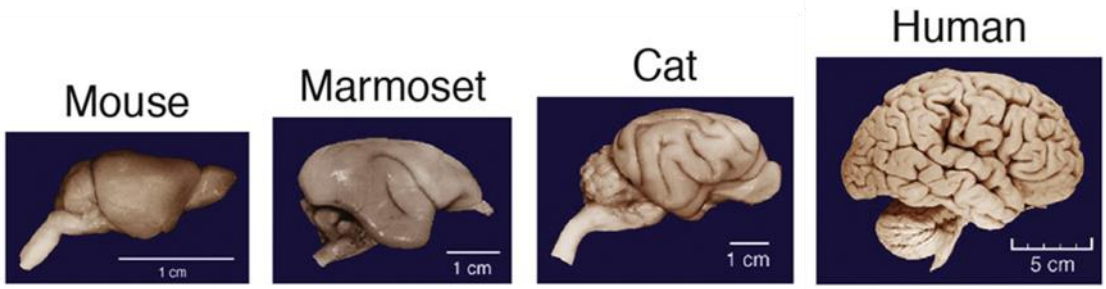

Figure I.1. Brain size and folding across mammalian evolution. *From Hawkes and Finlay, 2018.*

1.1. The Neocortex: anatomical organization and functions

The neocortex is the covert of the two cerebral hemispheres and constitutes the largest part of the human brain. This structure oversees complex functions such as cognition, emotion, motor control and consciousness and is a hallmark of mammals (Villalba et al., 2021). The size of the neocortex varies drastically across mammalian evolution. For example, the human neocortex is around 1000 times larger and contains around 3.2 x 10^3 more neurons than the mouse neocortex. Moreover, the human neocortex has a convoluted surface with fissures (sulci) and ridges (giry), while the surface of the mouse brain is smooth (see examples of gyrencephalic (with gyrus) and lissencephalic (smooth) brains in **Figure I.1**). The notorious folding of the human and other gyrencephalic species evolved as an efficient way to pack large cortical surface areas (large number of neurons) into a limited skull volume (Azevedo et al., 2009; Zilles et al., 2013).

The neocortex is formed by six horizontal anatomical layers (layer I to VI) each of them with different cell densities and neuron types. These neurons form functional units, called cortical columns, that extend across the layers and are heavily interconnected with each other along the vertical axis. Tangentially, neocortical neurons organize into areas that

are dedicated to the processing of sensory, motor, and associative functions and present different cytoarchitectonic features and specialized patterns of afferent-efferent connectivity (**Figure I.2**).

In the mouse, there are four primary areas: the somatosensory cortex, which processes sensory inputs, the auditory cortex, which processes sound, the visual cortex, which processes the sense of sight, and the motor cortex, which controls fine motor behaviour (Lodato and Arlotta, 2015; Jabaudon, 2017) (**Figure I.2A**).

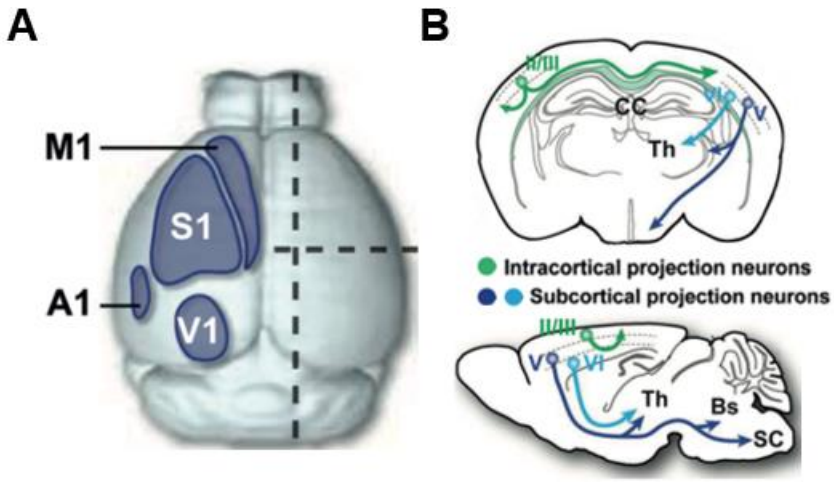

Figure I.2. Primary functional areas, laminar organization, and connectivity of the adult mouse neocortex. (A) Representation of the four primary areas (primary auditory cortex (A1), primary motor cortex (M1), primary somatosensory cortex (S1) and primary visual cortex (V1)) of the mouse neocortex. (B) Scheme of coronal and sagittal views of the brain indicating the layer-specific connectivity of neocortical projections neurons. Bs, brain stem; CC, corpus callosum; SC, spinal cord; Th, thalamus. *From Jabaudon, 2017.*

Neocortical neurons can be projection neurons or interneurons. Projection neurons are excitatory neurons that use glutamate as neurotransmitter and represent the vast majority of neurons in the neocortex (70-80%). These neurons comprise different neuron subtypes that differ in the expression of transcription factors, have different morphologies and electrophysiological properties, and project within the cortex (intracortical neurons) or to subcortical or subcerebral regions (corticofugal neurons). Intracortical neurons are predominantly located in the upper layers II and III and can be further classified into associative neurons, which target the same hemisphere (ipsilateral), and commissural neurons, which extend their axons to the opposite hemisphere (contralateral) through the *corpus callosum* or the anterior commissure. Corticofugal projection neurons are mainly located in the deeper layers (layers V and VI) and target neurons in different thalamic nuclei, the brainstem, and the spinal cord (Molyneaux et al., 2007; Lodato and Arlotta, 2015; Jabaudon, 2017) (**Figure I.2B**). Some types of projection neurons do not fit in this classification. An example of these neurons is the corticostriatal neurons, which are

intratelencephalic neurons that extend their axons to the ipsilateral and contralateral *striatum* and to the contralateral cortex (Shepherd, 2013).

The interneurons of the neocortex are inhibitory GABAergic neurons that establish local connections. These neurons may expand several layers and like the excitatory neurons display a notorious morphological and functional diversity. Cortical interneurons can be classified by their morphology or by the expression of the calcium-binding protein Parvalbumin, the neuropeptides Somatostatin and VIP (Vasoactive Intestinal Peptide) or the secreted signalling protein Reelin. Functionally, these neurons ensure that excitation remains in check, and modulate the timing, shape, and coordination of the circuits (Wamsley and Fishell, 2017; Lim et al., 2018).

1.2. The *striatum*: anatomical organization and functions

The *striatum* is the gateway of the basal ganglia and receives massive inputs from the cerebral cortex and the thalamus. The *striatum* has a compartmental organization in which specialized zones called striosomes are embedded in the much larger matrix compartment (Graybiel, 1978). The dorsal part of the *striatum* includes the caudate nucleus and the putamen and is involved in motor control and cognitive functions (Floresco, 2015). The ventral *striatum* is formed by the subcommissural region of the main body of the *striatum*, the nucleus *accumbens* and part of the olfactory tubercle. This brain region is in the crossroad of neuronal networks involved in the processing of several aspects of motivation and reward (Kravitz and Matikainen-Ankney, 2020).

Around 95% of the neurons in the *striatum* are output spiny projection neurons, commonly known as medium spiny neurons (MSNs). These neurons are GABAergic and display a characteristic branched and spiny dendrite morphology (Wilson and Groves, 1980). The remaining neurons of the *striatum* are GABAergic and cholinergic interneurons that act in different but complementary ways to modulate local activity (Kawaguchi et al., 1995; Tepper et al., 2004). MSNs located in the striosomes receive inputs from limbic regions and project primarily to the *substantia nigra* engaging dopamine and serotonin-mediated neuromodulation of aspects such as decision-making and reward (Crittenden and Graybiel, 2011; Friedman et al., 2015; Brimblecombe and Cragg, 2017). In contrast, matrix MSNs receive inputs from sensorimotor and associative cortical regions and project to output nucleus in the basal ganglia that target premotor regions and thalamocortical circuits, thus translating cortical action plans to action execution (Amemori et al., 2011; Hikosaka et al., 2014).

Motor activity is modulated by the direct and the indirect corticostriatal pathways. These pathways have been proposed to effect movement in opposite ways (see **Figure I.3**). However, recent evidence indicate that MSNs might facilitate or inhibit movement

depending on the form of synaptic plasticity at a certain moment and not of the inputs and outputs of the neurons (Calabresi et al., 2014).

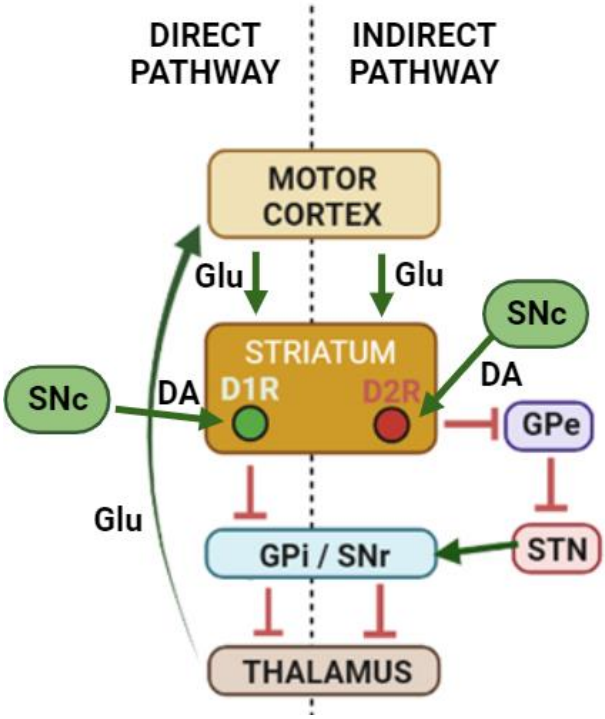

Figure I.3. Corticostriatal pathway involved in motor control. Direct medium spiny neurons are activated by dopaminergic neurons of the substantia nigra pars compacta (SNc) and neurons from different regions of the motor cortex. Striatal afferents innervate the internal segment of the globus pallidus (GPi) and the substantia nigra pars reticulata (SNr), leading to a disinhibition of subthalamocortical neurons (STN) and excitation of the motor cortex (direct pathway), or the external segment of the GP (GPe), leading to an inhibition of thalamocortical neurons (indirect pathway). D1R, dopamine receptor type 1; D2R, dopamine receptor type 2. *From Ferrini et al., 2021.*

1.3. Neurogenic niches in the developing telencephalon

Neurons in the cerebral cortex and basal ganglia are originated in the most anterior part of the neural tube, the telencephalon. In the mouse, at embryonic day (E) 8.5 the telencephalic primordium is subdivided into different territories that express specific transcription factors through the action of morphogens. After this early patterning event, subsequent patterning within the telencephalon give rise to the dorsal telencephalon or *pallium* and a series of ventral eminences (lateral ganglionic eminence (LGE), medial ganglionic eminence (MGE) and caudal ganglionic eminence (CGE)) located at different rostro-caudal positions of the *subpallium* (**Figure I.4A**). The dorsal-ventral pattering of the telencephalon lasts until E11 and overlaps with the initiation of neurogenesis in this region (Hebert and Fishell, 2008; Borello and Pierani, 2010; Azzarelli et al., 2016).

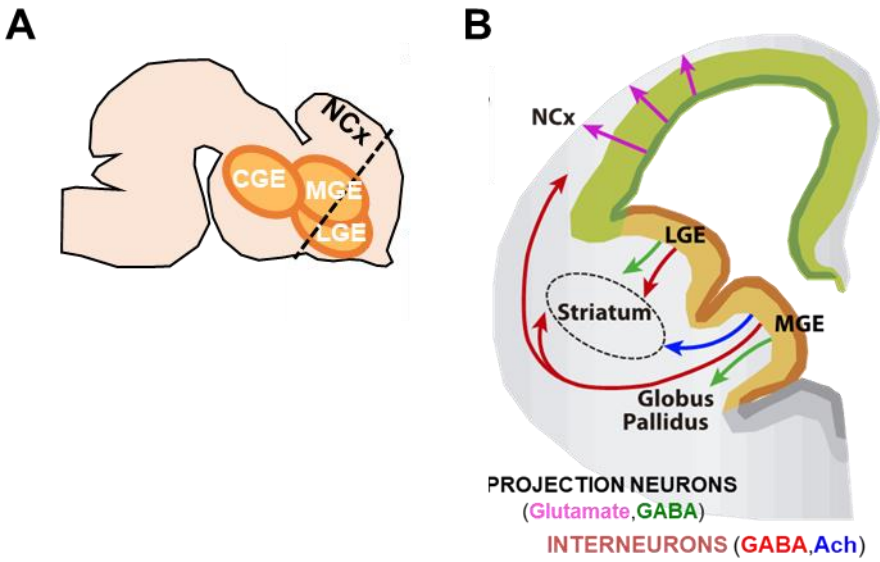

Figure I.4. Neuron types and migratory routes in the embryonic telencephalon. (A) Scheme of a sagittal view of the telencephalon indicating the position of the ganglionic eminences (LGE, lateral ganglionic eminence; MGE, medial ganglionic eminence; CGE, caudal ganglionic eminence). (B) Scheme of a coronal section of the telencephalon at the anterior-posterior level indicated by the dashed line in A showing the different neurogenic areas and migration routes of the neurons. Glutamatergic neurons are generated in the dorsal telencephalon (prospective neocortex (Ncx) in green) and migrate short distances towards their destination in the cortical plate (radial migration indicated by pink arrows). Cortical and striatal interneurons are generated in the LGE and the MGE and undergo tangential migration (red and blue arrows). GABAergic projection neurons of the striatum and the *globus pallidus* are generated in the LGE and the MGE, respectively. The migratory route of these neurons is indicated by green arrows.

Telencephalic neurons originate from pluripotent neural stem cells (NSCs) either directly (direct neurogenesis) or through other transit amplifying progenitors (indirect neurogenesis). Before the onset of neurogenesis, NSCs elongate the apical and basal processes, lose the tight junctions in the apical surface and start to express glial markers. These NSCs originate all the neurons in the CNS and are usually named radial glial (RG) cells. Like other neuroepithelial cells, the RG presents interkinetic nuclei migration, a characteristic that consists in the movement of the nuclei between the apical surface of the ventricular zone (VZ) where the cells divide and the basal surface in synchronization with the cell cycle (Anthony et al., 2004; Gotz and Huttner, 2005) (**Figure I.5A**). Transit amplifying progenitors present different shapes and modes of division and divide in distinct apical-basal positions of the VZ and the above subventricular zone (SVZ) (Florio and Huttner, 2014). These progenitors are particularly abundant and diverse in the ventral ganglionic eminences, which are the regions of the mouse embryonic brain with the largest SVZ (Turrero Garcia and Harwell, 2017) (**Figure I.5B**).

The distinct neurons of the telencephalon are generated in specific temporal windows and in different territories (domains and subdomains) of the *pallium* and *subpallium* (**Figure**

I.4B). For example, cortical excitatory neurons are produced in the *pallium* whereas cortical inhibitory neurons are produced in the MGE, CGE and the preoptic area (Wonders and Anderson, 2006; Molyneaux et al., 2007; Lodato and Arlotta, 2015; Lim et al., 2018). The cholinergic interneurons of the *striatum* and the projecting GABAergic neurons of the *globus pallidus* are generated in the MGE, and striatal MSNs and GABAergic interneurons in the LGE (Marin et al., 2000; Flandin et al., 2010; Fjodorova et al., 2015; Kelly et al., 2018). Newborn neurons then migrate radially or tangentially to reach their final positions in the *pallium* or the *subpallium* (Lodato and Arlotta, 2015; Turrero Garcia and Harwell, 2017; Lim et al., 2018) (**Figure I.4B**).

In the next two sections I will summarize the histogenesis of the projection neurons of the neocortex and the *striatum*.

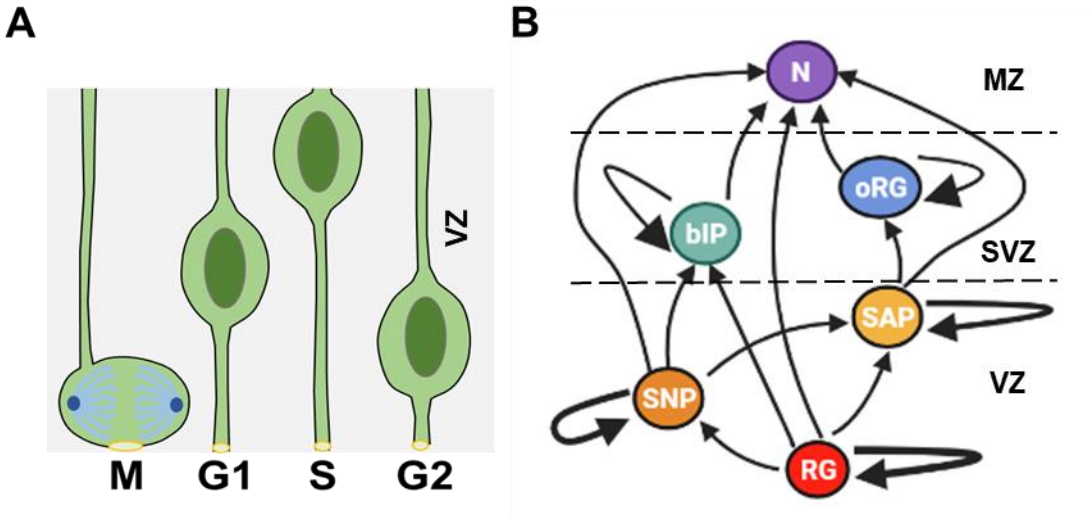

Figure I.5. Interkinetic nuclear migration of radial glia and lineage progression of ventral brain progenitors. (A) Scheme showing the interkinetic nuclear migration of the radial glia (RG) within the ventricular zone (VZ) along the cell cycle. (B) Scheme showing the different progenitors generated from the RG and the type and location of the divisions in the VZ and subventricular zone (SVZ). bIP, basal intermediate progenitor; N, neuron; MZ, mantel zone; oRG, outer radial glia; SAP, subapical progenitor; SNP, short neural progenitor. *From Turrero Garcia and Harwell, 2017.*

1.3.1. Generation of neocortical projection neurons

Neurogenesis in the mouse dorsal telencephalon stars at E11-E11.5 and ends around E17.5. During this period, dorsal RG cells express the transcription factor PAX6 (Gotz et al., 1998) and can divide symmetrically, producing two RG cells, or asymmetrically, producing one RG and either a neuron or an amplifying progenitor, known as intermediate progenitor (IP), that generates neurons directly or after one-three rounds of symmetric proliferative divisions. Symmetric RG divisions expand the progenitor pool and critically contribute to the lateral growth of the neocortex while asymmetric RG divisions

(differentiative divisions) are critical for the radial expansion (thickness of the neocortex) (Xing et al., 2021).

IPs and new-born neurons delaminate from the ventricular surface and move to more basal positions: the IPs to the SVZ where they divide and the neurons to the cortical plate (CP) located between the mantle zone and the intermediate zone (IZ) (**Figure I.6**). As soon as the cells delaminate from the ventricular surface, they downregulate PAX6 and start to express TBR2, a key transcription factor for dorsal IPs (Sessa et al., 2008). New-born neurons migrating towards the CP downregulate TBR2 and upregulate the transcription factor TBR1 (Englund et al., 2005). In addition to IPs, RG can generate another type of polarized progenitor that remains attached to the basal lamina and divide in a most basal position. This basal "radial glia" (bRG) is abundant in humans and non-human primates, where it contributes to the great expansion of the SVZ in these species but is very scarce in the mouse (Pinson et al., 2019). Another characteristic of dorsal neurogenesis is that the neurons are generated in an inside-out manner: first the neurons of the most internal layer and last the neurons of the superficial layers (Molyneaux *et al.*, 2007) (**Figure I.6**).

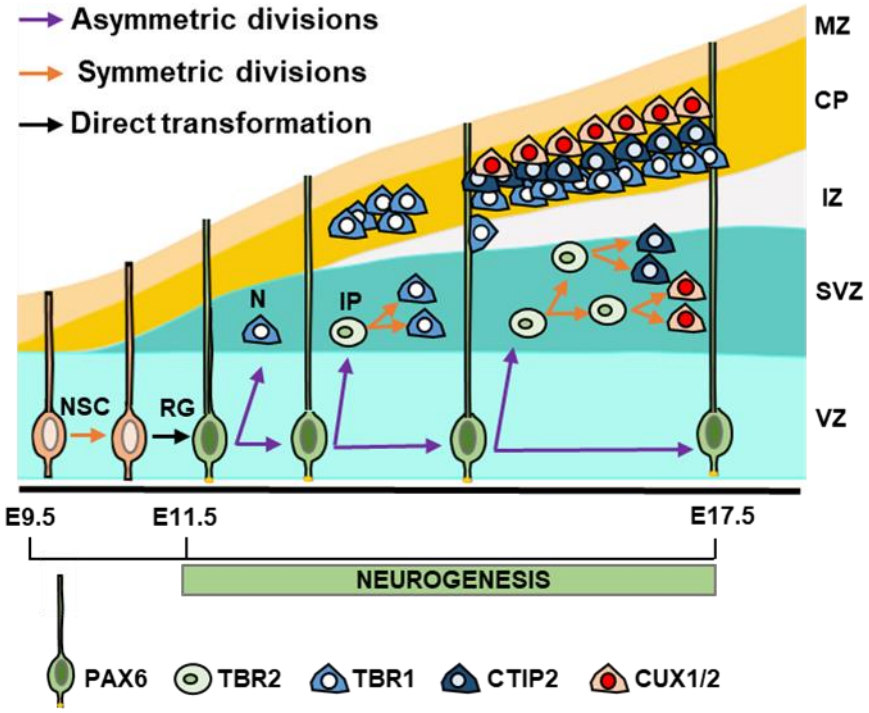

Figure I.6. Neurogenesis in the mice dorsal telencephalon. Scheme of the generation of cortical excitatory neurons. Neural stem cells (NSC in pink) divide symmetrically expanding the progenitor pool. At the onset of neurogenesis, NSCs transform to radial glial cells (RG, in green) that express PAX6 and divide asymmetrically giving rise to a neuron (N, TBR1 cell in blue) or an intermediate progenitor (IP, TBR2 cell in light green) and another RG. Neurons of the internal layers (TBR1 and CTIP2 cells in blue) and upper layer neurons (CUX1/2 cells in red) are generated sequentially from RGs or IPs. CP, cortical plate; IZ, intermediate zone; MZ, mantel zone; SVZ, subventricular zone; VZ, ventricular zone.

The neurogenic process just described relies on a complex interplay of internal factors and extracellular cues (Villalba et al., 2021). Pioneering studies performed in the mouse dorsal telencephalon indicated that cell cycle length in NSCs progressively increases as neurogenesis proceeds and that this increase is mainly due to a lengthening of the G1 (Takahashi et al., 1995; Caviness et al., 2003). Based on these experiments and others it was postulated that neural progenitors respond to external cues during G1, thereby determining the fate (remaining in the cell cycle or differentiate) of the daughter cells (Gotz and Huttner, 2005; Salomoni and Calegari, 2010). The link between G1 length and neurogenesis was further supported by different experiments in which the duration of G1-phase was artificially manipulated in RG progenitors (Lange et al., 2009). Moreover, the duration of the S-phase in apical and basal progenitors committed to produce neurons (differentiative divisions) is shorter than in those progenitors undergoing expanding proliferative divisions. The significance of this observation remains unknown, but gene expression studies suggest that expanding progenitors invest more time during S-phase into quality control of replicated DNA than those committed to neuron production (Arai et al., 2011).

1.3.2. Generation of striatal MSNs

Striatal MSNs are generated in the VZ and SVZ of the LGE and migrate radially to their final position in the *striatum* (**Figure I.4B**). Compared to the development of cortical neurons, the knowledge of the mechanisms underlying the generation and specification of MSNs is limited. Studies performed in the mouse, including live imaging studies, have provided valuable information regarding the abundance, diversity, and lineage progression of LGE progenitors during neurogenesis (Turrero Garcia and Harwell, 2017). The RG of the LGE produces IPs that divide in the SVZ (basal (b)IPs) and additional types of apical IPs (aIPs), such as the short neural progenitors (SNP) that divide close to the ventricle, and subapical progenitors (SAP) that divide in a more basal position of the VZ (Pilz et al., 2013). In the dorsal telencephalon the cell cycle in RG cells is shorter than in IPs (Arai et al., 2011), while in the LGE there is a progressive shortening of the cell cycle in each progenitor generation (the cell cycle of RG cells lasts about 25h, whereas in their daughters (SNPs and SAPs) last an average of 17h and in the subsequent generation of SAPs about 12h). The abundance of rapid amplifying progenitors and the progressive reduction of cell cycle duration in the LGE explain the vast expansion of the SVZ, and therefore its high neuronal output compared to the dorsal telencephalon (Pilz et al., 2013).

Studies performed in cats and rats suggested that striosome MSNs are generated before matrix MSNs (Fishell and van der Kooy, 1991; Newman et al., 2015). However, genetic fate mapping experiments performed in the mouse showed that striosome and matrix are

sequentially generated from a RG lineage program that involves the sequential production of IPs with different amplification capacities. At the early phase of this program (from E10 to E13.5), LGE RG cells are restricted to produce aIPs giving rise almost exclusively to striosomal MSNs. In contrast, matrix MSNs are generated later in development (from E12.5 to E17) from basal IPs (bIPs) produced by the same pool of RG cells (**Figure I.7**). Both aIPs and bIPs produce MSNs of the direct and the indirect pathways (Kelly et al., 2018). The developmental organization of MSNs in functional circuits remains unknown.

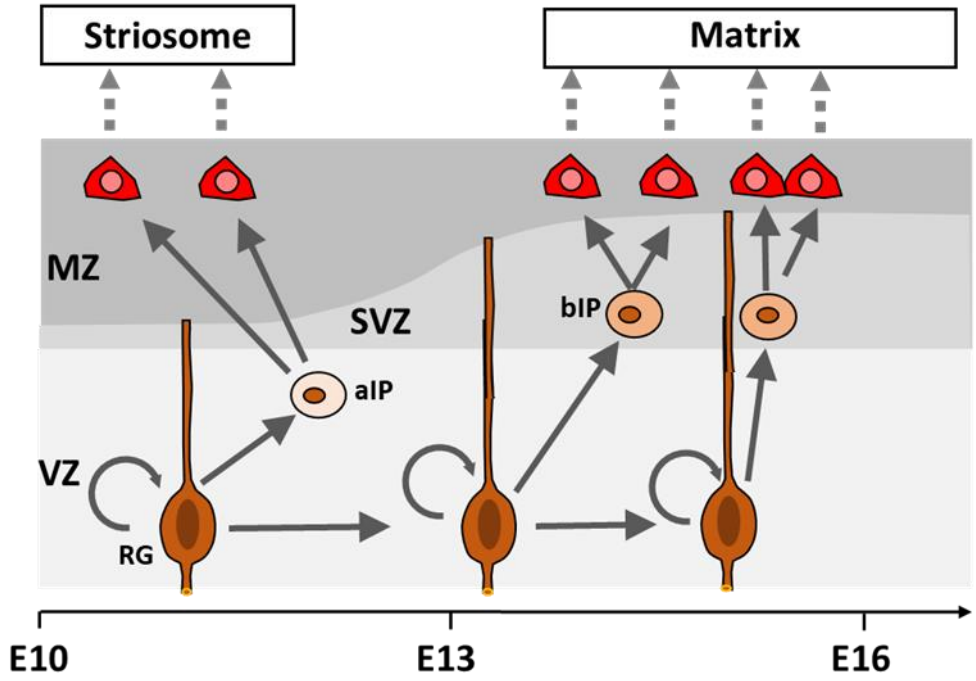

Figure I.7. Scheme illustrating the generation of medium spiny neurons in the embryonic lateral ganglionic eminence. Striosomal and Matrix medium spiny neurons are generated in two sequential waves along striatal development. aIP, apical intermediate progenitor; bIP, basal intermediate progenitor; MZ, mantle zone; RG, radial glia; SVZ, subventricular zone; VZ, ventricular zone. *From Kelly et al., 2018.*

2. DNA damage

2.1. Type of lesions and repair mechanisms

DNA damage is an alteration in the chemical structure of the DNA that can block genome replication and transcription. When DNA lesions are not repair or the reparation is not correct, they cause mutations or structural genome aberrations that compromise the viability of the cell or the whole organism. These lesions can be caused by endogenous factors, such as DNA mismatches that are occasionally introduced during DNA replication, DNA strand breaks caused by failed topoisomerase I and II activities, and reactive oxygen

species (ROS) generated as by-products of oxidative respiration, as well as by environmental agents such as ultraviolet light and ionising radiations. DNA single strand breaks (SSBs) and DNA double strand breaks (DSBs) are among the most prevalent DNA lesions (Jackson and Bartek, 2009).

To cope with DNA lesions, cells have evolved mechanisms that detect and sial the presence of these lesions and promote their repair. These mechanisms are collectively named DNA-damage response (DDR). Dysfunctions in DDR mechanisms sensitize the cells to DNA damage and might cause human diseases (O'Driscoll and Jeggo, 2008; Jackson and Bartek, 2009; see also section 2.3).

DSB is the most harmful DNA lesions and can cause cell lethality if unrepaired or cancer if improperly repaired. This lesion can arise directly by exposition to ionising radiation and other external agents and when telomeres become critically shortened. It can also arise from overlapping SSBs or following replication of ROS-induced SSBs. The origin of the DSB influences the processes factors that are required before break rejoining, while the cellular context determines the rejoining mechanism (Waterman et al., 2020). In mammalian cells, most DSBs are repair by non-homologous end joining (NHEJ), except when the damage occurs at DNA replication forks. In this case, homologous recombination (HR) is preferentially used (Karanam et al., 2012). NHEJ involves DSBs blunt ends ligation with limited or no DNA end processing and it is considered an error-prone mechanism. In contrast, HR rejoins DSBs using a sister homologue as a template, thus providing a high-fidelity DSB-rejoining mechanism (O'Driscoll and Jeggo, 2008; see **Figure I.8**).

The signal-transduction process activated by DNA strand breaks depends on the phosphatidylinositol 3-kinase related kinases (PIKKs), ataxia telangiectasia mutated (ATM), ataxia telangiectasia and RAD3-related (ATR) and DNA-dependent protein kinase (DNA-PK). DNA-PK is recruited and activated by Ku-bound DSB ends and repairs DSBs by NHEJ (**Figure I.8A**). ATM is activated and recruited to DSBs by the MRE11-RAD50-NBS1 (MRN) complex and repairs DNA by HR (**Figure I.8B**). In contrast to ATM and DNA-PK, which respond primarily to DSBs, ATR in complex with the ATR interacting protein (ATRIP) recognizes single stranded DNA (ssDNA) bound to Replication Protein A (RPA) (Blackford and Jackson, 2017).

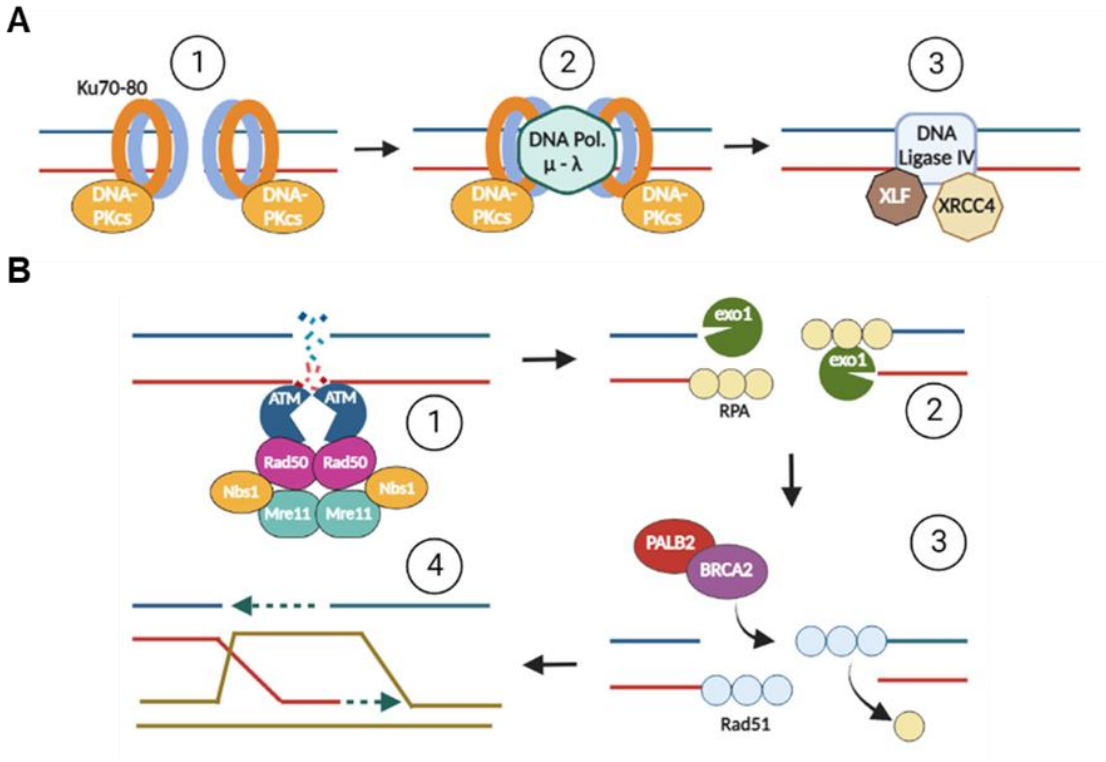

Figure I.8. Homologous recombination and non-homologous end joining repair of double strand breaks. (A) Scheme showing the main steps of non-homologous end joining: (1) DNA end recognition by the heterotrimeric complex composed by the catalytic subunit of DNA-PK (DNA-PKcs) and the Ku70-80 heterodimer; (2) DNA ends contact and nucleotide synthesis by the DNA polymerases Polμ and Polλ and DNA-PK complex activation; and (3) DNA end ligation by the DNA ligase IV in complex with XRCC4 and its associated factor XRCC4-like factor (XLF). (B) Scheme showing the main steps of DNA repair by homologous recombination. (1) Recognition of DNA unresected DNA ends by the MRN complex (MRE11-RAD50-NSB1) and ATM; (2) DNA end resection by the action of the BLM helicase and exonuclease exo1, generating a 3' ssDNA tail that is coated by the replication protein A (RPA); (3) Phosphorylation of the tumour suppressor protein partner and localizer of BRCA 2 (PALB2), which form a complex with BRCA2 that associates to damaged sites via BRCA1 promoting the association of Rad51 with several mediator proteins to form the Rad51 nucleoprotein filament, which displace RPA from DNA end; and (4) Rad51 mediated DNA sequence homology search and sister chromatid strands invasion and DNA ligation. *From Jiang and Chu, 2018.*

In response to DSBs, cells activate a DNA damage checkpoint response that arrest the cell cycle, reprograms gene expression, and mobilizes DNA repair factors to prevent the inheritance of unrepaired and broken chromosomes. ATM orchestrates these cellular responses phosphorylating numerous proteins (Shiloh and Ziv, 2013). In response to replicative stress, most ATM phosphorylated proteins are also phosphorylated by ATR (Blackford and Jackson, 2017).

ATM and ATR activate the downstream checkpoint kinases CHK2 and CHK1, which together mediate key checkpoint outcomes including cell-cycle arrest and apoptosis (**Figure I.9**). The early checkpoint signalling in response to DSBs is carried out preferentially through

the ATM-CHK2 signalling axis. Once ends are resected, ATR and ATRIP are recruited to ssDNA via RPA, leading to activation of CHK1 (Waterman et al., 2020). In addition to regulate cell-cycle checkpoint arrest, CHK2 and CDK1 phosphorylate proteins that influence other aspects of the DDR to promote genome integrity (Stracker et al., 2009).

An early step in the response to DSBs involves the phosphorylation of histone H2A on Ser129 (γ-H2AX) (Rogakou et al., 1998), an event primarily mediated by ATM. ATM also phosphorylates Mediator of DNA damage checkpoint 1 (MDC1), which together with γ-H2AX, activates a phosphorylation-ubiquitylation signalling cascade mediated by the E3 ubiquitin-protein ligases RNF8 and RNF168 resulting in the recruitment of the scaffolding protein 53BP1 to DSBs to direct repair towards NHEJ. ATM phosphorylation of 53BP1 promotes the recruitment of its effectors to incline the balance of DNA repair pathway choice in favour to NHEJ. DNA-end resection, a key process for HR, is initiated by MRN-CtIP generating short 3′-ssDNA. This ssDNA is further elongated by multiple nucleases and DNA helicases and provides a platform for recruiting HR repair-related proteins while prevents DNA repair by NHEJ. Some 53BP1 functions are antagonized by BRCA1, which major role seems to promote HR at the expense of 53BP1-mediated NHEJ (Blackford and Jackson, 2017). The choice of DSB repair pathway is fine-tuned regulated by RNF169, an E3 ubiquitin ligase paralogous to RNF168. This protein favours HR by two mechanisms: competing with 53BP1 and RAP80-BRCA1 for association with RNF168 modified chromatin (Poulsen et al., 2012) and promoting CtIP-dependent DSB resection (An et al., 2018).

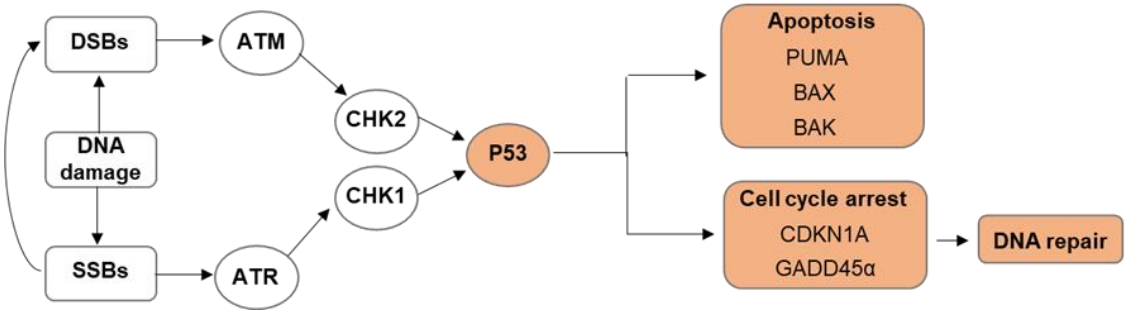

Figure I.9. DNA damage-mediated activation of p53. Upon DNA damage, checkpoint kinases are activated by the ATM (ataxia telangiectasia mutated) and ATR (ataxia telangiectasia and RAD3-related) pathways leading to p53 activation, which promotes cell cycle arrest enabling DNA repair or apoptosis. CDKN1A, cyclin-dependent kinase inhibitor 1A; CHK1, checkpoint kinase 1; CHK2, checkpoint kinase 2; DSBs, double strand breaks; GADD45α, growth arrest and DNA damage inducible alpha; SSBs, single strand breaks. *From Reinhardt and Schumacher, 2012.*

Activation of the DNA damage checkpoint signalling cascade activates the tumour suppressor protein p53 (**Figure I.9**). Upon activation, p53 induces the transcription of a multitude of target genes, such as the *Cyclin-dependent kinase inhibitor 1A* (*CDKN1A*) and *Growth arrest and DNA damage-inducible alpha* (*GADD45α)*, which promote cell cycle

arrest allowing for DNA repair. When DNA damage is severe, p53 undergoes several post-translational modifications, including phosphorylation at Ser46 and other serine residues inducing the death of the cell by promoting the transcription of BH3-only proteins such as PUMA, as well as the Blc2 associated X protein (BAX) and Bcl2 antagonist/killer1 (BAK), which are potent activators of apoptosis. Additionally, p53 phosphorylated at Ser46 can trigger apoptosis by transcription-independent mechanisms. For example, facilitating the interaction of p53 with PIN1 enhancing the translocation of p53 to the cytosol where interacts with BAX potentiating mitochondria outer membrane depolarization, cytochrome C release and the subsequent induction of apoptosis (Reinhardt and Schumacher, 2012; Liebl and Hofmann, 2019). Irreparable DNA damage and constitutive DNA damage checkpoint activation can also lead to an irreversible state of proliferative arrest called cellular senescence (Reinhardt and Schumacher, 2012).

2.2. DNA damage in the CNS

DNA damage in brain development primary affects proliferative cells. These cells are prompted to DNA damage, especially during early prenatal development, and have a low threshold for apoptosis. The primary source of DNA damage in prenatal brain development is replicative stress due to the high proliferative rates of the NSCs and rapid amplifying progenitors. As already mentioned, proliferative rates in brain progenitors change along neurogenesis (see section 1.3.1), and therefore there are important time differences in the susceptibility of these cells to DNA damage. Another source of DNA damage for both neural progenitors and the neuron progeny is the ROS generated in mitochondrial respiration, which represent a constant threat to both mitochondrial and nuclear genome stability. ROS in NSCs mainly arise from the massive energy supply required for the rapid proliferation rates of these progenitors, while in differentiating and mature neurons ROS are produced because of the high rates of metabolism required for active neuronal activity and for the transportation of molecules along neurites and axons from the cell body and *vice versa*. Fully mature neurons experience an additional source of DNA damage coming from defective transcription due to their high transcriptional activity needed to display a proper functionality (Abner and McKinnon, 2004; McKinnon, 2013; 2017; see **Figure I.10**).

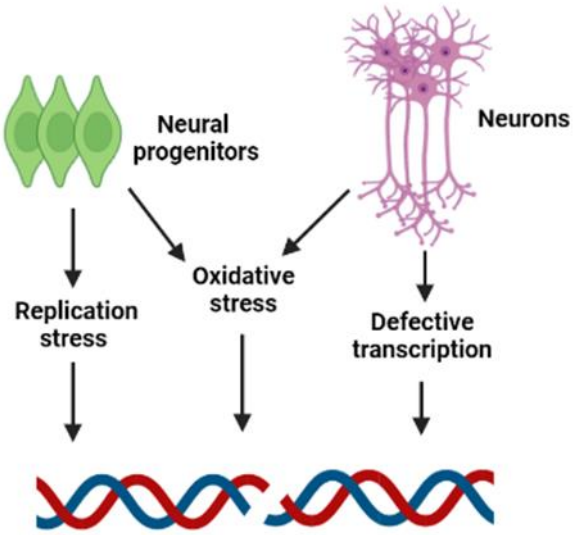

Figure I.10. Source of DNA damage in the distinct components of the neural tissue. *From McKinnon, 2017.*

2.3. DDR and human brain diseases

Dysfunctions in DNA repair pathways are on the bases of several human diseases including cancer and premature ageing (Jackson and Bartek, 2009). The CNS is particularly susceptible to DNA repair deficiency causing a variety of neurodevelopmental and neurodegenerative disorders. Indeed, DNA damage related human syndromes, such as ataxia telangiectasia (A-T), Seckel Syndrome and Nijmegen breakage syndrome particularly affect the CNS (Phillips and McKinnon, 2007).

The first evidence that DNA damage was an important pathogenic agent in neurological diseases came from the realization that the neurodegenerative syndrome A-T was associated to radiosensitivity. Later, it was discovered that A-T is caused by mutations in the *ATM* gene (McKinnon, 2017). The clinical symptoms in this disease commence when the child begins to walk, generally between 12 and 18 months of life. A-T patients display a progressive neurodegeneration that leads to progressive cerebellar ataxia, speech impairment and oculomotor apraxia with no affection in brain size (Chun and Gatti, 2004). In contrast, Seckel Syndrome, which is caused by mutations in the *ATR* gene, is characterized by the presence of microcephaly. Patients with this syndrome also present intrauterine and postnatal growth retardation, intellectual disability (ID), and unique facial features such as large eyes, beak-like nose, narrow face, and receding lower jaw (Faivre et al., 2002). The phenotype in children with Seckel Syndrome overlaps with some features of the Nijmegen breakage syndrome, which is caused by mutations in the gene encoding NBS1, which has already mentioned forms together with MRE11 and RAD50 the MRN complex that binds to DSBs to initiate repair by HR (Blackford and Jackson, 2017; see

Figure I.8B). People with this condition typically grow slowly during infancy and early childhood. Microcephaly is present at birth and progresses with age. Intellectual development is normal for the first year or two of life, but then development becomes delayed. Skills decline over time and most of the patients have mild to moderate ID (Chrzanowska et al., 2012).

The impact of DNA damage is also critical in the adult brain due to the low cell replacement of differentiated neurons, and it is linked to neuronal loss and memory defects. An excess of DNA damage in neurons has been implicated in the pathogenesis of neurodegenerative disorders including amyotrophic lateral sclerosis and Alzheimer's and Parkinson's diseases as well as in the neurodegeneration associated to Down syndrome and in cerebral ischemia and head trauma. Whether DNA lesions in these conditions are the cause of the cell death or the consequence of neurodegeneration is still not clear (Martin, 2008).

3. Cell death in CNS development

3.1. Types of cell death

Cell death can be broadly divided into non-programmed cell death and programmed cell death (Yan, 2020). Necrosis is the most prevalent form of non-programmed cell death. It is initiated by an unexpected cell injury caused by external factors such as toxins, a physical damage or an infection leading to a morphological cell alteration, plasma membrane rupture and further loss of intracellular organelles and DNA degradation with no chromatin condensation (Weerasinghe and Buja, 2012). Apoptosis is the most prevalent form of programmed cell death and the most common type of cell death in the prenatal and postnatal brain. Apoptosis implies a series of tightly regulated mechanisms that lead to chromatin condensation (pyknosis), loss of cell adhesion to neighbouring cells and to the extracellular matrix and ultimately nuclei fragmentation, DNA cleavage and cell membrane fragmentation (Kerr et al., 1972). These processes are exerted by the proteolytic cleavage of a family of cysteine proteases called caspases (LeBlanc, 2003). Caspases involved in cell death can be divided in initiator caspases and effector caspases. In humans, initiator caspases include caspases -2, -8, -9 and -10 and are activated after a death insult whereas effector caspases include caspases -3, -6 and -7 and are downstream caspases activated by initiator caspases. The activation of effector caspases leads to apoptotic cell death (Penaloza et al., 2008).

Depending on whether apoptosis is triggered by internal or external factors, apoptosis is classified in intrinsic and extrinsic apoptosis. Intrinsic apoptosis is initiated by a variety of cell intrinsic perturbations such as growth factor withdrawal, DNA damage induced by ROS or replication stress (DDR-dependent apoptosis initiated by p53 activation), alterations in the cytoskeleton or mitotic defects. The main event in intrinsic apoptosis is the depolarization of the outer membrane of the mitochondria by proapoptotic factors such as BAX and BAK, which causes the release of cytochrome C from the mitochondria to the cytosol where it binds to APAF-1. This protein together with the cofactor dATP/ATP form the apoptosome that activates the apoptotic pathway provoking caspase-9 cleavage and the subsequent activation of downstream caspases (caspase -3 and -7) (Ashe and Berry, 2003; Bao and Shi, 2007; Kale et al., 2012). Contrary, the extrinsic apoptotic pathway is initiated by the binding of a specific death ligand to a death receptor of the tumour necrosis factor (TNF) superfamily, which induces receptor oligomerization and the activation of the effector caspase -8 and -10 (Sprick et al., 2002; Bao and Shi, 2007; Mandal et al., 2020).

3.2. Programmed cell death

In physiological conditions apoptosis ensures the size and shape of the brain. This programmed cell death takes place during development and in two critical time windows: first during prenatal development primarily affecting neural progenitors and second during postnatal development affecting differentiating neurons (Kuan et al., 2000; Wong and Marin, 2019).

The relevance of the intrinsic apoptotic pathway in prenatal brain development has been highlighted by the phenotype of mouse embryos carrying null mutations in *Apaf-1*, *caspase-9* or *caspase-3*. These mutants display several brain malformations that include ventricle compression and an enlargement of the proliferative layers that in some cases can provoke exencephaly, a protrusion of the brain outside of the skull due to an overproduction of neural cells, at later embryonic stages (Kuida et al., 1998; Yoshida et al., 1998; Roth et al., 2000).

In the mouse embryonic neocortex, physiological apoptosis is detected in the VZ since E10. During neurogenesis, the percentage of dying cells in the cortical proliferative regions is relatively high at mid-neurogenesis, especially in the SVZ (Blaschke et al., 1996), which is consistent with more recent clonal analysis showing that one of the daughter cells coming from the first division of an IP undergoes cell death (Mihalas and Hevner, 2018). Apoptosis in progenitors is caused by activation of the cell cycle checkpoints or several dysfunctions altering mitotic progression (McKinnon, 2013; Pilaz et al., 2016). Cell death in neocortical progenitors can be caused in a non-autonomous manner by alterations occurring in differentiating neurones (Dhumale et al., 2018).

In the postnatal neocortex, developmental apoptosis is crucial for adjusting the numbers of excitatory projection neurons and inhibitory interneurons to balance the excitability of the circuits. This process takes place during the establishment of neuron connectivity (from postnatal (P)2 to P9 in the mouse) and depends on neuronal activity (Priya et al., 2018; Wong et al., 2018; Wong and Marin, 2019; see **Figure I.11**). Stereology-based studies performed in the mouse estimate that as much as 40% of the interneurons undergo apoptosis (Southwell et al., 2012) and that 13% of projection neurons dye between P2 and P5 (Blanquie et al., 2017). Transient neurons in the CP such as the Cajal-Retzius cells and some subplate neurons are also eliminated through apoptosis (Wong and Marin, 2019; see **Figure I.11**).

Other CNS structures in which developmental apoptosis has been studied are the *striatum* and the retina. In the *striatum*, apoptosis is prominent by the end of the first postnatal week and preferentially affects striosomal and matrix MSN that does not establish contact with nigral structures (Fishell and van der Kooy, 1991). Apoptosis in the retina is also mostly restricted to postnatal stages and occurs in defined temporal waves that specifically affect the distinct types of retinal cells (Young, 1984).

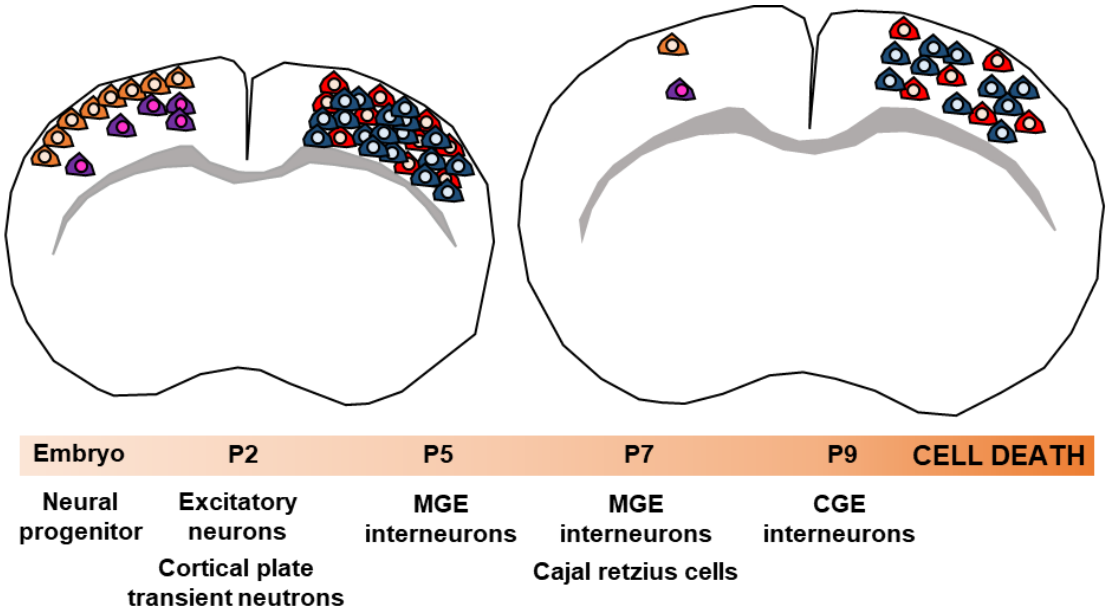

Figure I.11. Developmental cell death in the mouse neocortex. Timescale showing different stages of physiological cell death and the type of cells that are eliminated (Cajal-Retzius cells in orange and cortical plate (CP) transient neurons in purple) or refined in terms of number (excitatory neurons in blue and inhibitory interneurons in red) by physiological cell death in the embryonic and postnatal brain. *From Causeret et al., 2018.*

The regulation of programmed cell death in the developing neocortex and its impact on brain size and final cellular organization of circuits are expected to have important implications in disorders. Aberrant expression of BCL-2 and p53 has been found in

postmortem brain tissues of autistic subjects. Moreover, there are compelling evidence indicating that dysregulation of the apoptosis-related BDNF/AKT/BCL-2 and RAS/RAF/ERK1/2 signalling pathways are contributing to the behavioural deficits in autisms (Wei et al., 2014). PTEN is a phosphatase that negatively regulates AKT-dependent survival. Mutations in *PTEN* are relatively common in patients with autism spectrum disorder (ASD) and macrocephaly (Yehia et al., 2020). Although macrocephaly in patients with *PTEN* mutations is considered the result of an aberrant neurogenesis, experiments in the mouse indicate that PTEN is a critical regulator of developmental apoptosis in differentiating cortical interneurons, suggesting the possibility that abnormal apoptosis may also contribute to the brain size defects in patients with mutations in the *PTEN* gene (Wong and Marin, 2019).

4. DYRK1A

4.1. DYRK proteins

Phosphorylation by protein kinases is the most prevalent post-translational modification of proteins and constitutes a key mechanism for the modification of substrate activity involved in signal transduction and many cellular processes including cell cycle progression, differentiation, apoptosis and cell movement. In humans there are over 500 kinase genes representing 1.7% of the genome. Mutations in these genes and deregulation of kinase activities are causative of several human diseases including cancer (Manning et al., 2002).

Dual-specificity tyrosine-regulated kinases (DYRKs) are present in all eukaryotes and are part of the GMGC group of the eukaryotic kinome. The human GMGC group also comprises cyclin-dependent kinases (CDKs), mitogen-activated protein kinase (MAPKs), glycogen synthase kinase 3 (GSK3) and CDC-like kinases (CLKs) (Varjosalo et al., 2013). DYRK family members phosphorylate in serine, threonine, and tyrosine residues, although the tyrosine phosphorylated activity is restricted to autophosphorylation. DYRK proteins have been implicated in functions related to cell homeostasis and differentiation. From a phylogenetic point of view DYRKs can be classified in two different classes: class I, which among other proteins includes the *D. melanogaster* minibrain and mammalian DYRK1A and DYRK1B proteins, and class II, which includes the mammalian kinases DYRK2, DYRK3 and DYRK4 (Aranda et al., 2011). At the structural level, the conservation among the five mammalian DYRKs is restricted to the kinase domain and to a sequence upstream of this domain known as the DYRK homology (DH)-box (Becker et al., 1998). DYRK1A and DYRK1B have two nuclear localization signals (NLS); one within the N-terminal region and the other at the C-terminal end of the catalytic domain. These two kinases share a proline,

glutamic acid, serine and threonine-rich (PEST) motif located in the protein C-terminal region that is involved in their degradation (Boni et al., 2020).

In most kinases, the transition between the activated and the inactivated state is dynamic and depends on the phosphorylation of a residue within the activation loop. However, in DYRK proteins the activation is irreversible and relies on the autophosphorylation in the second tyrosine residue in the Tyr-X-Tyr motif located within the kinase domain (Himpel et al., 2001). This phosphorylation event occurs in *cis* and is supported by the DH-box sequence (Widowati et al., 2018). Since this process occur during translation, DYRK proteins are considered constitutive active kinases (Lochhead et al., 2005).

4.2. DYRK1A: structural features and expression

DYRK1A gene encodes two protein isoforms of 754 and 763 amino acids generated by alternative splicing events (Aranda et al., 2011). In addition to the characteristic structural domains of mammalian class I DYRKs, DYRK1A has two unique features at the C-terminus: a track of 13 histidine (His) residues, which is involved in the localization of the protein into nuclear speckles (Alvarez et al., 2003), and a serine/threonine (S/T) rich region with an unknown function (Aranda et al., 2011; see **Figure I.12**).

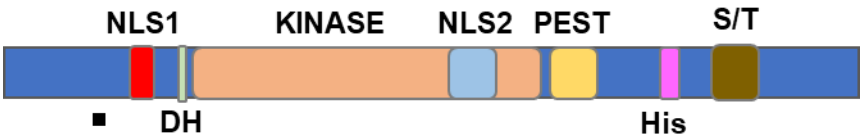

Figure I.12. Structure of the DYRK1A protein. Scheme of DYRK1A showing the different protein motifs. DH, DYRK homology box; KINASE, kinase domain; His, polyhistidine section; NLS1, nuclear localization signal 1; NLS2, nuclear localization signal 2; PEST, peptide sequence rich in proline, glutamic acid, serine and threonine; S/T, serine/threonine enriched region; Black square below indicates the protein regions affected by alternative splicing. *From Aranda et al., 2011.*

DYRK1A is expressed in practically all the tissues and cell types that have been analysed (Aranda et al., 2011; Arbones et al., 2019). Relative to other tissues, the expression of DYRK1A in the brain is high (Guimera et al., 1999; Okui et al., 1999). In the developing brain, the levels of DYRK1A protein peak at the first postnatal week and then progressively decrease until adulthood (Okui et al., 1999). In the mouse developing brain and retina DYRK1A is expressed in pre-neurogenic (neuroepithelial cells) and neurogenic NSCs as well as in differentiated neurons. DYRK1A in all these cell types is predominantly located in the cytoplasm (Hammerle et al., 2008; Laguna et al., 2008; Najas et al., 2015). In differentiating neurons DYRK1A accumulates in the growing axons and dendrites (Hammerle et al., 2003). In the chick neuroepithelial cells, *Dyrk1a* transcripts are

asymmetrically distributed in mitosis and inherited by one neuroepithelial daughter that subsequently divides asymmetrically producing one NSC (RG) and a neuron (Hammerle et al., 2002). This observation suggests that DYRK1A could be an asymmetric determinant for the transition of NSCs between the proliferative (expanding) stage to the neurogenic stage.

In the mouse adult brain, Dyrk1a expression varies depending on the region and it is mostly associated to the neuropil (Marti et al., 2003). In the human brain, DYRK1A localizes in the nucleus and cytoplasm of different neuron types as well as in synaptic terminals (Wegiel et al., 2004), providing evidence of the role of the kinase in synaptic transmission. Biochemical fractionation studies performed in mouse brain samples confirmed the cytoplasmic and nuclear localization of DYRK1A (Aranda et al., 2008), which is consistent with the many putative functions of the kinase in these two cellular compartments (Aranda *et al.*, 2011; Arbones *et al.*, 2019). In addition to neurons, DYRK1A is expressed in other cells of the brain including astrocytes, oligodendrocyte progenitor cells, ependymal cells, and endothelial cells (Marti et al., 2003; Wegiel et al., 2004; Pijuan et al., 2022).

As mentioned before, DYRK1A is a constitutively active kinase and numerous evidences indicate that the enzymatic activity of this kinase is directedly related to the amount of protein (Aranda et al., 2011). DYRK1A activity can be modulated by the autophosphorylation of a serine residue in the PEST domain of the protein (Alvarez et al., 2007) and by the phosphorylation of other kinases, although this has only been reported for LAST2 (Tschop et al., 2011), an effector kinase of the hippo pathway (Ma et al., 2019).

DYRK1A expression can be regulated at the transcriptional and translational levels or by other means including protein stabilization/degradation, binding with scaffolding proteins and by microRNAs (Aranda et al., 2011; Arbones et al., 2019).

In the CNS, *DYRK1A* transcription is downregulated by the binding of the RE1-silencing transcription factor (REST) to the *DYRK1A* promoter (Lu et al., 2011) and upregulated by MEF2D, a member of the myocyte-specific enhancer factor 2 family of transcription factors that is expressed in the developing brain (Wang et al., 2017). In the axons of differentiating neurons, *Dyrk1a* mRNA is locally translated by a ribonucleoprotein complex that comprises the actin-regulatory protein MENA and the RNA-binding proteins PCBP1 and HNRNPK (Vidaki et al., 2017). Furthermore, it has been described that the expression of *DYRK1A* transcripts in the brain is affected by a pathogenic imbalance of CPEB4 (cytoplasmic polyadenylation element binding protein 4) transcript isoforms that results from a decreased inclusion of a neuron-specific microexon and leads to a shortening of the poly(A)-tail length of *DYRK1A* (Parras et al., 2018).

4.3. DYRK1A: substrates and cellular functions

In line with the functional diversity of DYRK1A substrates, DYRK1A is involved in a wide variety of cellular processes including cell cycle progression and cellular senescence, DNA damage response, cell survival and cytoskeletal remodelling.

Cell cycle and senescence:

Compelling evidences indicate that DYRK1A plays a role in G1-S and G2-M transition by phosphorylating different cell cycle regulators. DYRK1A phosphorylates Cyclin D1 and Cyclin D3 in a threonine residue (Thr286 in D1 and Thr283 in D3) promoting Cyclin D exit from the nucleus to the cytoplasm and the subsequent degradation of the protein through the ubiquitin proteasome pathway (Chen et al., 2013; Thompson et al., 2015). This phosphorylating event results in a decreased CDK4/6 activity and therefore into an inhibition of G1-S phase transition. *In vivo* studies indicate that Cyclin D phosphorylation by DYRK1A plays a role in lymphopoiesis (Thompson et al., 2015) and neocortical neurogenesis (Najas et al., 2015). In cultured neural stem cells, DYRK1A can inhibit G1/G0-S phase transition enhancing the transcription of $p21^{CIP1}$ by phosphorylating p53 on Ser15 (Park et al., 2010) or phosphorylating $p27^{KIP1}$ on Ser10, which results in protein stabilization (Soppa et al., 2014). In glioblastoma cells, DYRK1A regulates CDK1 inducing the degradation of mitotic cycling Cyclin B by phosphorylating CDC23 (Recasens et al., 2021). In G0, DYRK1A can phosphorylate a serine (Ser18) in LIN52, a subunit of the MuvB core, promoting p130 binding to the MuvB core and the assembly of the DREAM complex and entry into the quiescent phase (Sadasivam and DeCaprio, 2013). **Figure I.13** summarizes the activities of DYRK1A related to cell cycle progression and senescence.

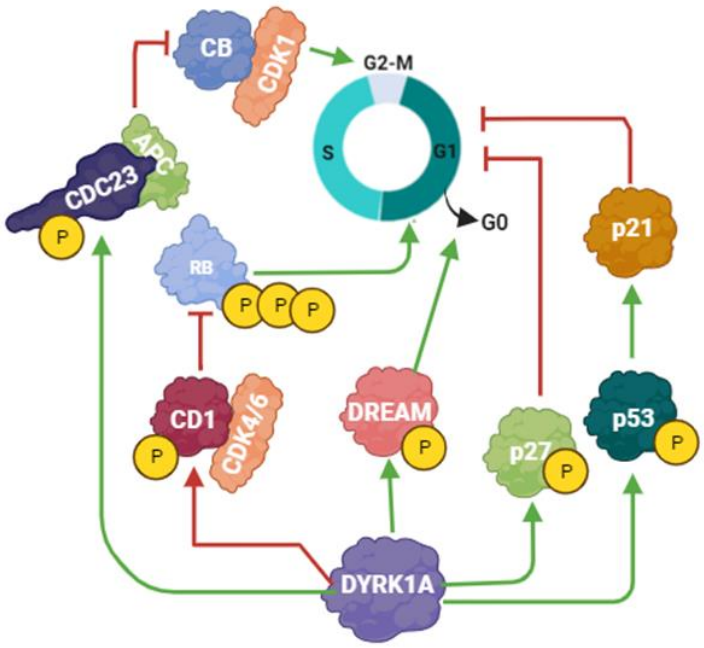

Figure I.13. DYRK1A substrates with cell cycle functions. DYRK1A regulates G1-S transition, promoting the degradation of the G1-S positive regulator Cyclin D1 and the transcription or stabilization of the G1-S negative regulators p21CIP1 and p27KIP1, G2-S transition regulating the activity of Cyclin B-CDK1 complex, and G0, regulating the assembly of the DREAM complex. APC, anaphase promoting complex; CDK1, cyclin-dependent kinase 1; CDK4/6, cyclin-dependent kinase 4/6; CD1, Cyclin D1; CB, Cyclin B; RB, retinoblastoma.

DNA damage repair and cell survival:

Recent studies performed in *C. elegans* and human cells indicate that the DREAM complex represses the expression of several DNA-repair mechanisms limiting DNA-repair capacities. According to the role of DYRK1A in DREAM complex assembly, the pharmacological inhibition of DYRK1A in human quiescent cells increases the expression of DREAM-targeted DNA-repair genes and conferred resistance to distinct types of DNA damage (Bujarrabal-Dueso et al., 2023). DYRK1A can regulate DNA damage repair in different cell lines by phosphorylating RNF169, that as already mentioned is an essential component of the cellular response to DSBs (Roewenstrunk et al., 2019), and Sirtuin 1 (SIRT1), which promotes deacetylation of p53 resulting in inhibition of its activity and resistance to DNA-damage induced apoptosis (Guo et al., 2010). During B cell development, DYRK1A regulates DNA damage response through phosphorylation of its substrate FOXO1 without affecting apoptosis (Bhansali et al., 2021).

DYRK1A can promote cell survival by phosphorylating Thr125 in caspase-9, the upstream caspase in the intrinsic cell death pathway, thus preventing caspase-9 cleavage and the subsequent activation of the pathway (Allan and Clarke, 2009). Caspase-9 phosphorylation by DYRK1A plays a key role in fine-tuning developmental cell death in

differentiating neurons of the retina and the ventral mesencephalon (Laguna et al., 2008, 2013; Barallobre et al., 2014).

Cytoskeletal remodelling:

DYRK1A can regulate the cytoskeletal machinery, thereby contributing to the development and maintenance of neurites and dendritic spines, and ultimately neuronal function (Arbones et al., 2019).

DYRK1A negatively regulates the actin cytoskeleton by phosphorylating the GTPase binding domain of Neural Wiskott–Aldrich syndrome protein (N-WASP) in three threonine residues. DYRK1A phosphorylation of N-WASP leads to the inhibition of Arp2/3-complex-mediated actin polymerization (Park et al., 2012). DYRK1A is also implicated in the assembly of microtubules phosphorylating ß-tubulin (Ori-McKenney et al., 2016) and the microtubule-associated protein Tau (Liu et al., 2022).

4.4. DYRK1A in neurodevelopmental syndromes

DYRK1A has been involved in different human disorders including diabetes (Rachdi et al., 2014; Shen et al., 2015), different types of cancers (Luna et al.,2019; Laham et al., 2022; Li et al., 2022), cardiac pathologies (Kuhn et al., 2009), neurodegenerative diseases such as Alzheimer's and Parkinson diseases (Demuro et al., 2021), and syndromic forms of ID (Arbones et al., 2019).

Since the identification of the human *DYRK1A* gene in the Down syndrome critical region of chromosome 21 (Guimera et al., 1997) many laboratories, including ours, have studied the contribution of DYRK1A overexpression in ID and other clinical characteristic features associated to Down syndrome using mice that overexpress the *Dyrk1a* gene alone (Altafaj et al., 2001; Guedj et al., 2012) or have in trisomy all or part of human chromosome 21 or orthologous mouse genomic regions (Herault et al., 2017; Antonarakis et al., 2020). Collectively, these studies show that DYRK1A contributes to the characteristic ID and Alzheimer-like neuropathology in Down syndrome (Herault et al., 2017; Arbones et al., 2019; Antonarakis et al., 2020). Indeed, DYRK1A has long been proposed as a therapeutic target to ameliorate cognitive deficits in Down syndrome (Becker et al., 2014).

In a transgenic mouse that carries 3 functional copies of *Dyrk1a* (tgBac*Dyrk1a*) and in the Ts65Dn mouse which contains around 100 chromosome 21 gene in trisomy including *DYRK1A*, the cellularity of the retina is increased due to an inhibition of developmental caspase-9 mediated apoptosis. The retina phenotype in the Ts65Dn mouse is completely rescued by genetic normalization of *Dyrk1a,* indicating that trisomy of *Dyrk1a* is the cause of retinal cellular defects in the Ts65Dn mouse model. Interestingly, people with Down syndrome have thicker retinas suggesting that similar developmental alterations occur in

patients and trisomic mice (Laguna et al., 2013). Defects in cortical neurogenesis and deficits in neocortical projection neurons have been observed in human trisomy-21 tissue samples and in the Ts65Dn mouse model (Haydar and Reeves, 2012). Experiments performed in the tgBac*Dyrk1a* mouse model provide evidence that DYRK1A overexpression is likely responsible to the cell cycle alterations and defects in neurogenesis previously observed in the developing neocortex of Ts65Dn embryos (Najas et al., 2015). Remarkably, the developing neocortex in the Ts65Dn model shows increased astrogliogenesis, which seems to be caused by the effect of DYRK1A overexpression on the activity of the pro-astrogliogenic transcription factor STAT3 (Kurabayashi et al., 2015). Neural progenitors derived from Down syndrome induced pluripotent stem cells have also proliferative defects and produce less neurons and more astrocytes, defects that are partially corrected by targeting DYRK1A pharmacologically or by shRNA (Hibaoui et al., 2014). These data and mice behavioural studies provide compelling evidence of the contribution of DYRK1A overexpression in Down syndrome neuropathology (Haydar and Reeves, 2012; Arbones et al., 2019).

More recently a new syndromic form of ID and ASD known as DYRK1A-related intellectual disability syndrome or DYRK1A syndrome has been defined. This syndrome is caused by *de novo* mutations in one allele of the *DYRK1A* gene and has an estimated prevalence of 1:1.000.000 in the general population (van Bon et al., 2016). Mutations in *DYRK1A* are loss-of function mutations and include chromosomal rearrangements and deletions affecting the *DYRK1A* locus as well as small insertions and deletions and nonsense and missense mutations (van Bon et al., 2016). Characteristic features of the DYRK1A syndrome include general developmental delay, microcephaly, moderate to severe ID, speech delay or complete absence of communicative language, motor difficulties, feeding problems, genito-urinary anomalies, and a distinctive facial gestalt. Visual problems and febrile and non-febrile seizures are also frequent traits of this syndrome. Patients with DYRK1A syndrome present autism-like behaviours or autism (Bronicki et al., 2015; Ji et al., 2015; Luco et al., 2016; van Bon et al., 2016; Blackburn et al., 2019). Indeed, large-scale genomic studies have identified *DYRK1A* as one of the susceptibility genes for ASD (De Rubeis et al., 2014; Stessman et al., 2017). A systematic study of the brain morphology in DYRK1A syndrome has not been performed, but the most frequent magnetic resonance imaging findings among the reported cases are cortical atrophy, large ventricles, and hypoplasia of the *corpus callosum* indicating defects in the development of the cerebral cortex (Bronicki et al., 2015; Ji et al., 2015; Luco et al., 2016).

The *Dyrk1a* knockout mouse is embryonically lethal. *Dyrk1a* heterozygous mice (*Dyrk1a*$^{+/-}$) are viable but present most of the characteristic traits in DYRK1A syndrome including developmental delay, microcephaly, motor gait dysfunctions, cognitive defects,

epilepsy, and autistic-like behaviours (Fotaki et al., 2002, 2004; Arque et al., 2008; Arranz et al., 2019). Flies with hypomorphic mutations in the *minibrain* gene, the orthologous gene of *DYRK1A* in *Drosophila melanogaster*, also present small brains (Tejedor et al., 1995) indicating that DYRK1A/Mnb has conserved functions in brain growth across evolution.

4.5. Morphological brain alterations in *Dyrk1a*$^{+/-}$ and tgBac*Dyrk1a* mice

The brain in adult *Dyrk1a*$^{+/-}$ and tgBac*Dyrk1a* mice show a direct correlation between DYRK1A dosage and brain size. In these two mice, brain size alterations are region specific and predominantly affect the tectum (superior and inferior *colliculi*) and ventral structures such as the ventral posterolateral and posteromedial thalamic nuclei. The neocortex in these mutants present a normal lamination but an abnormal thickness: reduced in the *Dyrk1a*$^{+/-}$ mouse and augmented in the tgBac*Dyrk1a* mouse (Fotaki et al., 2002; Guedj et al., 2012). The *Dyrk1a*$^{+/-}$ mouse presents an increased density of excitatory neurons in all neocortical layers and of inhibitory neurons in layers V and VI. Increased numbers of astrocytes have been reported in the neocortex of postnatal *Dyrk1a*$^{+/-}$ mice (Arranz et al., 2019; Pijuan et al., 2022). Astrocytes are also more abundant in the hippocampus and other regions of *Dyrk1a*$^{+/-}$ brains (Fotaki et al., 2002; Guedj et al., 2012; Pijuan et al., 2022). Conversely, tgBac*Dyrk1a* mice have less excitatory neurons in the neocortex and less astrocytes in the hippocampus than control mice (Guedj et al., 2012). The number of inhibitory neurons in the neocortex of tgBac*Dyrk1a* mutants is preserved but the proportion of Parvalbumin and Somatostatin inhibitory neurons is altered (Najas doctoral thesis, 2015).

Studies performed in *Dyrk1a*$^{+/-}$ and tgBac*Dyrk1a* mutants during embryonic and postnatal development show that the defects in neocortical excitatory neurons arise early in development and is likely due to an alteration in the mode of division of the dorsal RG at the onset of neurogenesis. In tgBac*Dyrk1a* embryos dorsal RG produces more IP at the expense of neurons while the opposite occurs in the dorsal telencephalon of *Dyrk1a*$^{+/-}$ embryos (Najas et al., 2015). The defects in neurogenesis in the tgBac*Dyrk1a* mutant correlate with an increase in the cell cycle length of RG cells, which is due to an enlargement of the G1 and S phases. The nuclear levels of Cyclin D1 in tgBac*Dyrk1a* dorsal RG cells is significantly decreased due to the action of DYRK1A on Cyclin D1 nuclear export and degradation of the protein throughout the ubiquitin-proteasome pathway, thereby providing a mechanistic explanation for the cell cycle defects observed in this mutant (Najas et al., 2015). The defects in neurogenesis observed in tgBac*Dyrk1a* and *Dyrk1a*$^{+/-}$ mutants affect the numbers and proportions of excitatory neuron types, thereby altering brain wiring and functionality (Najas et al., 2015; Arranz et al., 2019).

4.6. Brain phenotypes of conditional *Dyrk1a* mutant mice

Throughout the development of this thesis two articles published the brain phonotype of two different *Dyrk1a* conditional knockout mouse models generated by the Cre-loxP system. In the first knockout model, the expression of Cre-recombinase was driven under the control of the *Emx1* promoter abrogating DYRK1A expression in the dorsal telencephalon before neurogenesis. The *Emx1:Dyrk1a* knockout mouse die at birth. At the end of gestation, the brains of mutant embryos present a striking size reduction and a disorganized cerebral cortex. *Emx1:Dyrk1a* mice with the mutation in heterozygosity survive until adulthood. These mice present altered size and cellularity in the neocortex and an abnormal morphology of the excitatory neurons and their axonal projections. Remarkably, *Emx1:Dyrk1a* heterozygous mutants exhibit autism-like behaviours (Levy et al., 2021). These results confirm previous data showing that DYRK1A plays a role in cortical neurogenesis and that lowering the DYRK1A dose has a detrimental impact on the morphological differentiation of cortical projection neurons affecting the connectivity of brain circuits, thus contributing to the neurological dysfunctions associated to DYRK1A syndrome (Arbones et al., 2019).

The second conditional *Dyrk1a* mutant was generated expressing Cre-recombinase driven by the *Camk2* promoter. In the *Camk2a:Dyrk1a* mutant, DYRK1A expression is abrogated in all the excitatory neurons of the neocortex and hippocampus from the third postnatal week. The neocortex of *Camk2a*:*Dyrk1a* knockout mice is thinner than normal. As in the *Dyrk1a*$^{+/-}$ mouse, neuronal densities in the neocortex of *Camk2a*:*Dyrk1a* mice are increased, suggesting a reduction of the neuropil. Moreover, *Camk2a*:*Dyrk1a* knockout mice present alterations in motor and cognitive activities (Brault et al., 2021), which is consistent with the role of DYRK1A in the structural maturation and functionality of cortical excitatory neurons.

The phenotypes of tgBac*Dyrk1a* and *Dyrk1a*$^{+/-}$ mutant mice with an imbalance dosage of DYRK1A and of the two conditional *Dyrk1a* mutants described above indicate that DYRK1A is critical for the normal development of the neocortex, regulating neurogenesis in the embryo and morphological differentiation and probably synaptogenesis in postnatal stages. The knowledge of the distinct molecular functions of DYRK1A in brain growth and neuronal differentiation is still limited.

OBJECTIVES

The general objective of my thesis was to give new insights into the functions regulated by DYRK1A in the neurogenesis of the embryonic telencephalon in physiological condition as well as in the DYRK1A syndrome using the mouse as an animal model.

When I started this PhD thesis, there were no mouse models to study the impact of a *Dyrk1a* null mutation in the central nervous system. Thus, to provide evidence on the role of DYRK1A in neurodevelopment, the **first objective** of the thesis was to generate the mouse *Nestin*Cre:*Dyrk1a* conditional mutant, which carries a *Dyrk1a* null mutation in all neural progenitors before the onset of neurogenesis and characterise the prenatal development of the telencephalon in this model.

Given the severity and early onset of the brain phenotype in the *Nestin*Cre:*Dyrk1a* null mutant, the **second objective** of the PhD thesis was to generate the *Sox2*Cre*ERT2*:*Dyrk1a* conditional mutant mouse and analyse the effect of a *Dyrk1a* null mutation in the prospective neocortex at different developmental times.

METHODS

1. Animals

1.1. Mouse strains and housing conditions

To introduce a null *Dyrk1a* mutation in neural progenitors of the mouse embryo, we used the Cre-loxP conditional deletion strategy (Hoess et al., 1984). We generated and analysed two *Dyrk1a* conditional mutants: the *Nestin*Cre:*Dyrk1a* mutant and the *Sox2*Cre*ERT2:Dyrk1a* mutant.

To generate the conditional *Nestin*Cre:*Dyrk1a* mutant model, we used a *Dyrk1a*$^{Fl/Fl}$ mouse (Thompson et al., 2015) and the transgenic *NestinCre* (*NesCre*8) mouse generated in Zhong's laboratory (Petersen et al., 2002). In this transgenic line, the expression of Cre-recombinase, which is under the control of the *Nestin* promoter, takes place in all neural progenitor and starts at pre-neurogenic stages (E8.5). To generate the conditional *Sox2*Cre*ERT2:Dyrk1a* mutant model, we used the same *Dyrk1a*$^{Fl/Fl}$ mutant as for the *Nestin*Cre:*Dyrk1a* model and the *Sox2*Cre*ERT2* mouse generated in Nicoli's laboratory (Favaro et al., 2009). In this mouse, Cre-recombinase expression is induced by tamoxifen and is driven by an upstream enhancer of the *SOX2* gene that directs the expression of the transcription factor SOX2 to neural progenitors of the dorsal telencephalon (Zappone et al., 2000). To assess Cre-recombinase expression in *Sox2*Cre*ERT2:Dyrk1a* mutants, we first crossed *Sox2*Cre*ERT2* mice with the tdTomato loxP reporter mouse mB6.Cg-Gt (ROSA) 26Sortm14 (CAG-tdTomato) Hze/J (tdTomato from now on) from Jackson Laboratories (#007914). The mating strategy to generate the *Nestin*Cre:*Dyrk1a* and *Sox2*Cre*ERT2:Dyrk1a* conditional mutants and the genotypes of littermate embryos that we have analysed are summarized in **Figure M.1**.

To collect embryos of a particular developmental stage, we set up controlled matings. To this end, we crossed two to three *Dyrk1a*$^{Fl/Fl}$ females (2 to 4 months of age) with either one *Nestin*Cre*:Dyrk1a*$^{Fl/+}$ or one *Sox2*Cre*ERT2*+:*Dyrk1a*$^{Fl/+}$:tdTomato male. Females were checked for the presence of a copulation vaginal plug the following morning. Embryonic stage (E) 0.5 was considered the day of the vaginal plug.

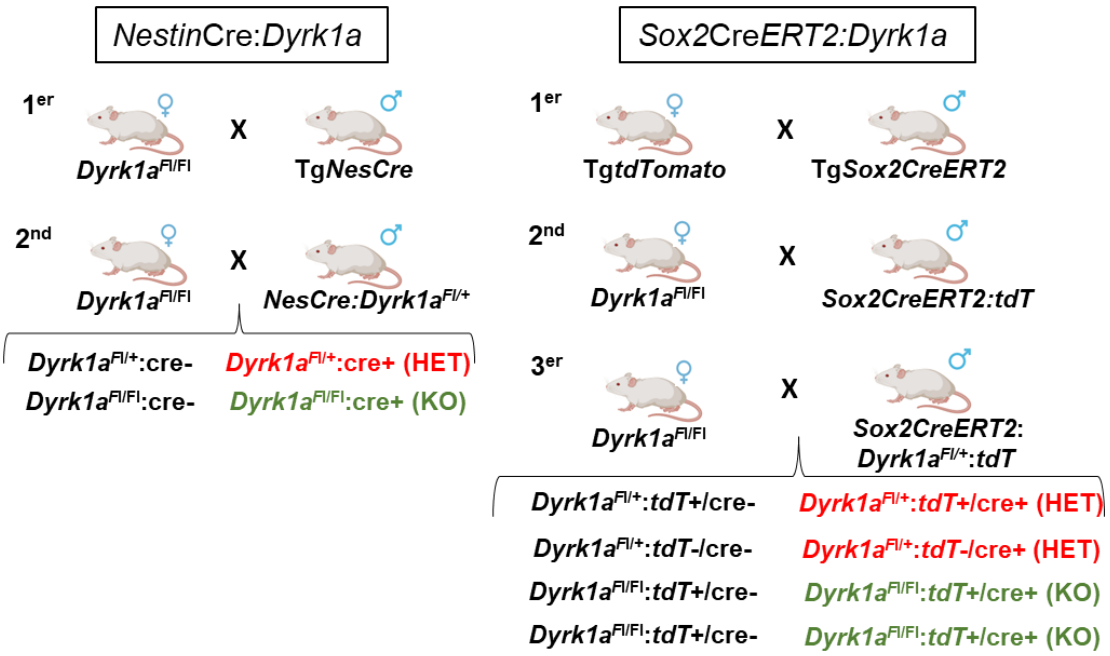

Figure M.1. Mating strategy for the generation of *NestinCre*:*Dyrk1a* and *Sox2CreERT2*:*Dyrk1a* mutant embryos. The genotypes of embryos with the *Dyrk1a* mutation in heterozygosity (HET) are in red and with the mutation in homozygosity (KO) in green. Genotypes of embryos used as controls are in black. Double *Sox2CreERT2*:tdTomato (tdT) transgenic mice were used for the generation of *Sox2CreERT2*:*Dyrk1a* mutants.

In the *Nestin*Cre:*Dyrk1a* model, Cre-recombinase expression was checked by immunoblotting using total brain extracts prepared from E11.5 control (*Dyrk1a*$^{Fl/Fl}$:cre-) and homozygous *Nestin*Cre:*Dyrk1a* (*Dyrk1a*$^{Fl/Fl}$:cre+) mutant embryos (*NesCre*:*Dyrk1a*-KO embryos from now on). As shown in **Figure M.2A**, DYRK1A was not detected in extracts that were immunopositive for Cre-recombinase. To determine the developmental time in which DYRK1A expression declines in the conditional *Nestin*Cre:*Dyrk1a* mutant, we performed immunoblots with brain extracts from E10.5 and E11.5 control, heterozygous (HET) (*Dyrk1a*$^{Fl/+}$:cre+, *NesCre*:*Dyrk1a*-HET from now on) and *NesCre*:*Dyrk1a*-KO littermate embryos. At E10.5 the levels of Dyrk1a in *NesCre*:*Dyrk1*-HET and *NesCre*:*Dyrk1a*-KO brains were reduced 20% and 50% with respect to the controls, respectively. At E11.5, brain Dyrk1a levels decreased to 50% in *NesCre*:*Dyrk1a*-HETs and to more than 80% in *NesCre*:*Dyrk1a*-KOs with respect to the controls (**Figure M.2B**), thus correlating with the number of functional *Dyrk1a* alleles. These immunoblots indicate that despite *Cre-recombinase* expression in the *NesCre*8 transgenic line starts at E8.5 (Petersen et al., 2002), Dyrk1a activity in the KO brains is not abrogated until E11.5.

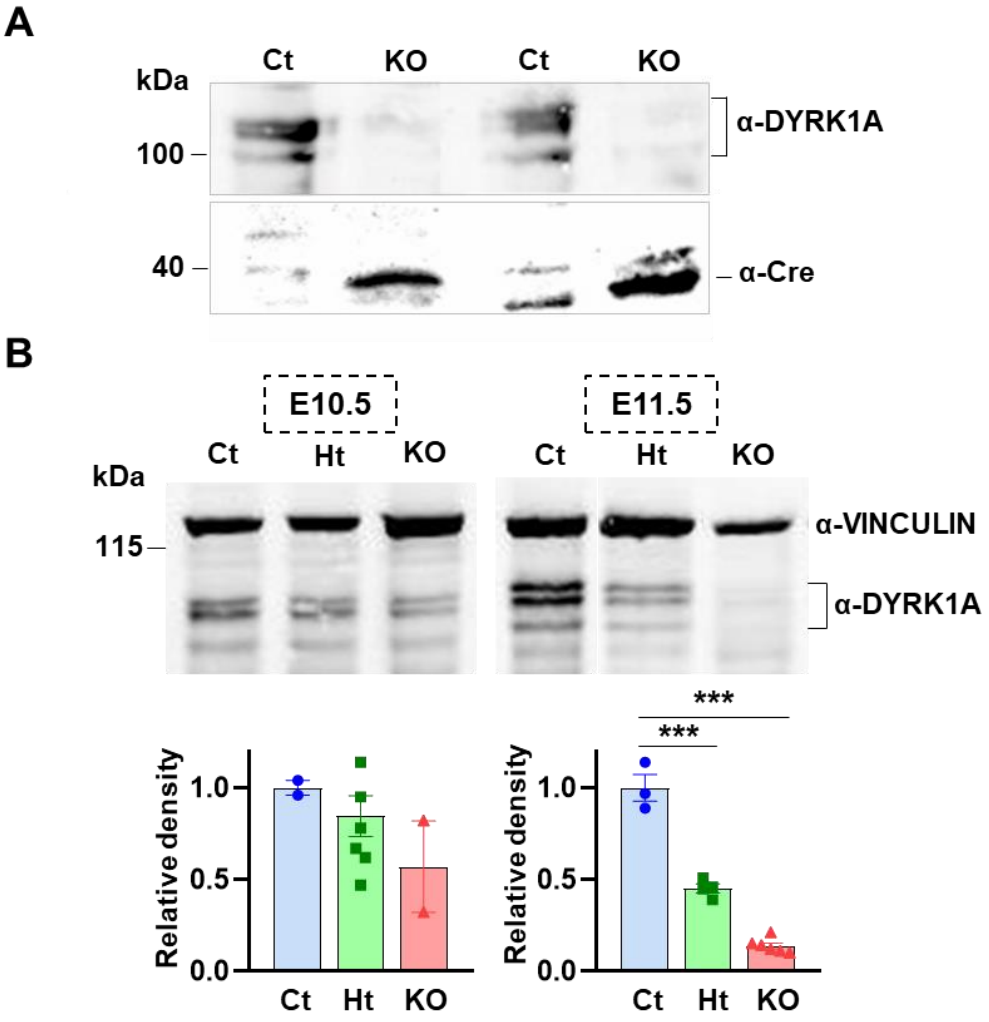

Figure M.2. Dyrk1a protein levels in control, *NesCre*:*Dyrk1a*-HET and *NesCre*:*Dyrk1a*-KO brain extracts. (A) Representative immunoblots of control (Ct) and *NesCre*:*Dyrk1a*-KO (KO) extracts prepared from E11.5 brains and probed with anti-DYRK1A and Cre-recombinase (Cre) antibodies. (B) Representative immunoblots of Ct, *NesCre*:*Dyrk1a*-HET (Ht) and KO extracts prepared from E10.5 and E11.5 brains and probed with the indicated antibodies. The histograms show the level of DYRK1A normalized to Vinculin and expressed relative to the controls. The values (mean ± SEM) correspond to individual littermate embryos. ***P<0.001 in a two-tailed Student t-test.

To induce Cre-recombinase expression in embryos carrying the *Sox2CreERT2* transgene, we injected tamoxifen in pregnant mice (0.1 mg tamoxifen/gr body weight).

All mice were maintained in conventional cages in the animal facilities of the Centre d'Investigació i Desenvolupament (CID-CSIC). Housing conditions were 12 h light/dark cycles in controlled environmental conditions of humidity (60%) and temperature (22ºC±2ºC). Food and water were provided *ad libitum*. The experimental procedures were carried out in accordance with the European Union guidelines (Directive 2010/63/UE) following protocols approved by the Ethics Committees of the CID and the CSIC and by the Generalitat de Catalunya.

1.2. Genotyping

Genotyping was performed by polymerase chain reaction (PCR) using genomic DNA obtained from embryonic tissue or tail biopsies. DNA extraction from fresh or frozen tissue samples was done in a solution of 25 mM NaOH containing 0.2 mM EDTA by heating at 95ºC for 30 min. The incubation volume was adjusted according to the type of tissue and the size of the sample. The solution was neutralized by adding 1:1 volume of 40 mM Tris-HCl pH 5, and the supernatant transferred into a 0.5 ml Eppendorf tube. One to two μl of the supernatant was used for PCR with the primers and conditions indicated in **Table M1** (in the Annex)**.** Considering previous data that reports germline recombination of floxed alleles in *Nestin*Cre lines (Luo et al., 2020), *NesCre*:*Dyrk1a*-KO and HET embryos were genotyped using 3 PCR primers that amplify the *Dyrk1a* wild-type and floxed alleles and the recombinant floxed allele (*Dyrk1a*-Δ). To identify the *NestinCre* and *Sox2CreERT2* transgenes in the genomic DNA samples, we used two sets of PCR primers, one that amplifies a fragment of the Cre-recombinase cassette and another that amplifies an unrelated fragment of the genome and serves as control of the reaction. The same strategy was used to genotype mice and embryos carrying the *td*Tomato reporter cassette. Electrophoresis of the PCR products was done in either 1.5% or 2% agarose gel containing Sybr® Safe DNA gel stain (Thermofisher).

1.3. Treatments

For some experiments 5-bromo-2'-deoxyuridine (BrdU, Sigma-Aldrich) and 5-ethynyl-2'-deoxyuridine (EdU, Life Technologies) were injected in pregnant mice to label cells in S phase. For BrdU treatment, a solution of 10 mg of BrdU diluted in 1 ml sterile water was injected intraperitoneally to a final dosage of 100 mg BrdU/kg body weight. For EdU treatment, a solution of 1 mg of EdU in 1 ml sterile water was injected peritoneally to a finale dosage of 10mg EdU/kg body weight. Injection times of BrdU and EdU are detailed in section 3.3.

For tamoxifen treatment, a solution of 20 mg of tamoxifen (Sigma-Aldrich) diluted in 1 ml of pre-heated (55ºC) Ethanol/Corn Oil 1:10 solution, was injected intraperitoneally in pregnant females in a finale dosage of 0.1 mg tamoxifen/gr body weight.

2. Protein expression analysis

2.1. Brain lysates

Mouse brains were collected after decapitation of the embryo and immediately frozen in dry ice. For certain experiments, dorsal and ventral telencephalon were dissected out under a binocular microscope and frozen independently. Total protein extracts were prepared by resuspension of the frozen tissue in 25 mM Tris-HCl pH 7.4 buffer containing 1% (w/v) SDS, 1mM EDTA, 10 mM sodium pyrophosphate, 20 mM glicerol-2-phosphate, 2 mM sodium orthovanadate and 2mM phenylmethylsulfonyl fluoride (PMSF). This buffer was additionally supplemented with a protease inhibitor cocktail (Roche) to avoid protein degradation. Samples were homogenised mechanically using a pipette tip and then sonicated with 5 pulses of 30 sec each in a Diagenode UCD-200TM Bioruptor. Resultant supernatants were boiled at 95ºC and stored at -80ºC.

Protein concentration was determined using a colorimetric assay (BCA Protein Assay Kit from Pierce, according to the manufacturer's indications). Absorbances were read in a Power Wave XS (Biotek).

2.2. Immunoblotting

Protein extracts (20 to 80 µg) were mixed with Laemmli buffer (83 mM Tris-HCl pH 6.8, 2% w/v SDS, 10% v/v glicerol-2-phosphate, 100 mM Dithiothreitol and 0.01% bromophenol blue (Sigma-Aldrich). After mixing, samples were heated for 5 min at 95ºC and resolved on an SDS-PAGE gel (8 to 12% acrylamide depending on the molecular weight of the protein of interest) at 125 V in running buffer (25 mM Tris-base pH 10.2, 200 mM glycine (Sigma-Aldrich)). Proteins on the gel were transferred onto a nitrocellulose membrane (Hybond-ECL, Amersham) in transfer buffer (25 mM Tris-HCl pH 8.3 containing 200 mM glycine and 20% v/v methanol). Transfer conditions were set up at 240 mA for 60 min at 4ºC.

Correct protein transfer was checked by Ponceau staining (Sigma-Aldrich-Aldrich). Transferred membranes were washed in PBS-T (phosphate buffer saline (PBS) containing 0.1% (v/v) Tween (Sigma-Aldrich)) and blocked in PBS-T with 5% non-fat milk (w/v). Then, membranes were incubated overnight (ON) at 4ºC with the corresponding primary antibody diluted in the same blocking solution. The list of the primary antibodies used in this work are in the Annex (**Table M2**). Membranes were washed in PBS-T and incubated for 1 h at room temperature (RT) with the fluorescent secondary antibodies anti-mouse IgG IRDye-800CW and/or anti-rabbit IgG IRDye-680RD (LICOR Biosciences) diluted in PBS-T with

0.25% bovine serum albumin (BSA). After three washes in PBS-T, infrared fluorescence was visualized in the LI-COR Odyssey IR Imaging System V3.0 (LI-COR Biosciences).

Quantification of protein levels was done using the Odyssey software version 3.0. We used Actin or Vinculin as loading control for the normalization of protein levels. Protein quantifications were done in a minimum of three independent lysates per experimental condition (genotype or developmental stage).

3. Histology and cell counts

3.1. Tissue preparation

To prepare brain sections, the head of the embryo was dissected and fixed in paraformaldehyde (PFA) solution (4% (w/v) PFA in PBS pH 7.4) ON at 4ºC. Embryo heads were then rinsed in PBS and cryoprotected by immersion in PSB with 30% (w/v) sucrose at 4ºC for 1 day until the head sunk indicating that it has absorbed enough to be isotonic to the sucrose. For cryostat sectioning, heads from E11.5, E12.5 and E13.5 embryos were embedded in Tissue-Tek OCT (Sakura Finetek) and frozen at -30ºC in isopentane (Panreac). In the case of E15.5, E17.5 and E19.5 brain embryos, cryoprotected heads were directly immersed in isopentane at -30ºC. Head sections (20 µm) were obtained using a Leica CM3050S cryostat and collected serially on SuperFrost® slides (VWR). Slides were maintained at -20ºC until usage.

3.2. Immunofluorescence

Brain sections used for immunofluorescence were washed in PBS. For antibodies that required an antigen retrieval, treatment consisted in boiling the sections for 10 min in sodium citrate buffer pH 6.0. For BrdU detection, we used an additional treatment to denaturate the DNA. The treatment consisted in an incubation with 2N HCl at 37ºC for 30 min followed by pH reestablishment by a 15 min incubation in 0.1 M boric acid at RT. After these treatments (if needed), tissue slides were permeabilized for 30 to 90 min with PBS containing 0.2% (v/v) Triton-X100 and incubated for 60 min at RT in blocking solution (PBS containing 0.2% (v/v) Triton-X100 and 10% (v/v) fetal bovine serum (FBS)). Then, samples were incubated for 72h at 4ºC with the corresponding primary antibody (or antibodies) diluted in antibody incubation solution (PBS containing 0.2% (v/v) Triton-X10 and 5% (v/v) FBS). After washing, samples were incubated with the secondary antibodies diluted in incubating solution for 2 h at RT. In some cases, an incubation with biotinylated secondary antibody followed by a 45 min incubation with Alexa fluor 488- or 568-conjugated Streptavidin were

done to amplify the staining signal. Cell nuclei were stained with 4′,6-diamidino-2-phenylindole, dihydrochloride (DAPI) (0.1 µg/ml; Vector Labs) and the samples mounted in Vectashield (Vector Labs). Some samples were mounted in an 80% glycerol solution.

The primary and secondary antibodies used in immunofluorescences are in **Tables M.3 and 4** (in the Annex).

3.3. Cell cycle length

To estimate the length of the cell cycle and S phase we used the method described in Martynoga et al., 2005. Briefly, pregnant females were treated with one pulse of EdU and 15 min latter with one pulse of BrdU. Animals were sacrificed 30 min after BrdU treatment, and the embryos collected and processed as describe in section 3.1. Sections were immunostained for BrdU and SOX2 and EdU detected using the Click-iT EdU Alexa Fluor 647 kit (Life Technologies). The number of SOX2+, BrdU+ EdU+ and Edu+ BrdU- cells were counted to calculate the duration of the S phase and the total cell cycle as indicated in Results (**Figure R.10A**).

3.4. Image acquisition and analysis

Image acquisition was performed with the equipment of the Molecular Imaging Platform Unit (http://www.ibmb.csic.es/groups/molecular-imaging-platform) of the IBMB-CSIC. Wide-field images were collected either in a Leica AF7000 motorized microscope or in a Leica light microscope Thunder imager. Confocal images were taken either in a confocal SP5 microscope using the Leica Confocal Software (LCS) or in a Zeiss LSM-780 microscope controlled under the LSM Software ZEN 2.1. Samples from the same experiment were imaged with the same microscope and the same settings to reduce technical variability. Images were analyzed with the Fiji software (Schindelin et al., 2012).

Measurements in brain slices were done in images obtained from coronal brain sections. Quantifications in sections were performed in a minimum of two sections per animal and a minimum of three animals per experimental condition.

3.5. Morphometry and cell counts

The area of the dorsal and ventral telencephalon and the thickness of the germinal and neurone layers were measured in Thunder images obtained with the 10x objective using the *Measurement tool* and the polygon selection tool of Fiji. For the analysis of *Sox2CreERT2:Dyrk1a* embryos, these measurements were performed in images obtained in the Zeiss confocal microscope with a 25x immersion objective using the same Fiji tools.

The area and circularity of nuclei were measured in images obtained with a 20x objective in the Leica SP5 microscope using the *oval* tool of Fiji. In the case of nuclei expressing tdTomato, the area and circularity were measured in images obtained with the 25x immersion objective in the Zeiss confocal microscope using the same Fiji tool.

Cells from the region of interest were counted on images obtained in the confocal Zeiss microscope using a 25x objective or in the Thunder Imager with a 10x objective. SOX2+, TBR2+, TBR1+, SATB2+ and CTIP2+ cells of the dorsal telencephalon were counted on confocal images in columns of a defined width at the level of the somatosensory cortex. In the *NesCre*:*Dyrk1a*-KO, these cells were counted in an equivalent region. SOX2+ cells of the ventral telencephalon were counted in a 150 µm width column within the middle of the LGE. Active-caspase3 immunopositive cells were counted in the whole dorsal telencephalon and in a column in the middle of the LGE in Thunder images. Cells immunopositive for ɣ-H2AX and p53 and pyknotic nuclei were counted in the whole dorsal telencephalon and LGE territory on confocal images. Cells in mitosis were as well counted in the whole dorsal telencephalon and LGE but, in this case, on Thunder images. To calculate cell cycle parameters, we counted cells in a 200 µm or 100 width columns in the central region of the dorsal telencephalon on confocal images.

4. Cell cycle profile by flow cytometry

Cell cycle profiles were performed in cell samples obtained from the dorsal telencephalon of E11 embryos. Briefly, the telencephalon was dissected in PBS and incubated in a DMEM solution containing papain (final concentration 0.52 µg/µl) at 37ºC for 10 min. Then, the tissue was disaggregated mechanically, and cells were centrifuged at 250 g for 10 min and fixed with 100% methanol at 4ºC for 2 h. After fixation, cells were centrifuge, resuspended in a solution of propidium iodide (0.027 µg/µl) and incubated for 1.5 h at RT. Cells from individual embryos (around 15,000 cells) were analyzed on a Beckman Coulter flow cytometer and the data processed using the FlowJo software from BD Bioscience.

5. Statistical Analysis

Normal distribution of the data was assessed by the Shapiro-Wilk normality test using GraphPad Prism 8 software. Once normal distribution of the data was confirmed, the *P* value was calculated by the parametric test two-tailed Student's t-test. A minimum of three embryos per genotype was analysed in each experiment, except for the quantification of

cells expressing Ki-67 or SOX2 in the dorsal telencephalon of E11.5 and E15.5 embryos, respectively. Differences were considered significant at *P<0.05, ** P<0.01, *** P<0.001. Mean, SEM (standard error of the mean) and P values were calculated using Excel. Histograms and violin plots were plotted using GraphPad.

RESULTS

1. General phenotype of the *NesCre*:*Dyrk1a* conditional mutant

At the onset of neurogenesis, constitutive null *Dyrk1a*$^{-/-}$ embryos show a notable developmental delay and reduced number of neurons. These embryos die between E10.5 and E13.5 (Fotaki et al., 2002). The genotype of postnatal mice obtained from *NesCre*:*Dyrk1a*$^{Fl/+}$ x *Dyrk1a*$^{Fl/Fl}$ crosses (**Figure M.1**) indicated that *NesCre*:*Dyrk1a*-KO mice are lethal, since we could not recover a single alive conditional null mutant from several litters genotyped at different postnatal stages (from P0 to weaning (around P21)). However, the embryos from 7 litters obtained by the same type of crosses at E17.5 followed the expected mendelian proportions (control (Cre-): n=38 embryos (48%); *NesCre*:*Dyrk1a*-HET: n=21 embryos (26%); *NesCre*:*Dyrk1a*-KO: n=21 embryos (26%)) indicating that *NesCre*:*Dyrk1a*-KO embryos/pups die around birth. At E17.5, *NesCre*:*Dyrk1a*-KO brains showed a significant size reduction that appeared more prominent in the midbrain than in the telencephalic vesicles (68% reduction in the midbrain; 35% reduction in the telencephalic vesicles). *NesCre*:*Dyrk1a*-HET embryos also showed smaller telencephalic vesicles than the controls, but the differences between *NesCre*:*Dyrk1a*-HET and control embryos did not reach statistical significance (**Figure R.1**). Brain weight in *NesCre*:*Dyrk1a* mutants was also decreased, being the decrease with respect to the controls more important in the *NesCre*:*Dyrk1a*-KO embryo than in the heterozygous mutant (61% weight reduction in *NesCre*:*Dyrk1a*-KO brains, P=1x10^{-5} in a two-tailed Student *t*-test; 13% weight reduction in *NesCre*:*Dyrk1a*-HET brains, P=0.012 in a two-tailed Student *t*-test. n=3-4 embryos each genotype). These results are in accordance with the conserved role of DYRK1A/minibrain protein in brain growth (Arbones et al., 2019).

NesCre:*Dyrk1a*-HET mice are viable throughout postnatal life and do not display any major alterations except for the reduction of their body weight at P7 (28.8% reduction with respect to controls, P=3.5 x 10^{-6} in a two-tailed Student *t*-test. n=6 to 10 animals each genotype) and at age 2-months (males: 23% reduction with respect to the control, P=0.033 in a two-tailed Student *t*-test. n=2 to 4 animals each genotype; females: 31% reduction with respect to the control, P=3.5 x 10^{-6} in a two-tailed Student *t*-test. n=6 to 10 animals each genotype). The reduction in body size and weight in postnatal *NesCre*:*Dyrk1a*-HET mice is similar than in *Dyrk1a*$^{+/-}$ mice (Fotaki et al., 2002), indicating that the small body of young haploinsufficient *Dyrk1a*$^{+/-}$ mice results from neurodevelopmental dysfunctions. Of note, *Dyrk1a*$^{+/-}$ mice are obese in the adulthood due to a severe glucose intolerance (Rachdi et al., 2014).

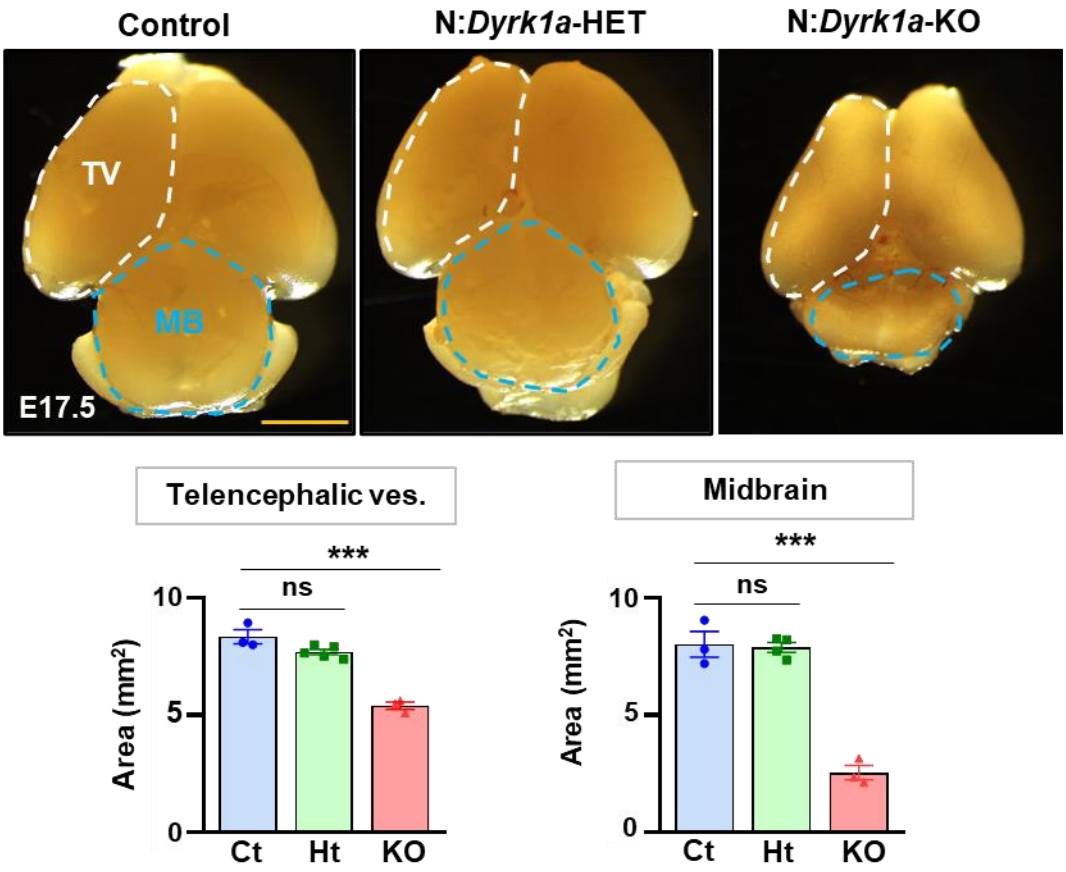

Figure R.1. Brain size in *NesCre*:*Dyrk1a*-HET and *NesCre*:*Dyrk1a*-KO embryos at late neurogenesis. Dorsal view of E17.5 control and Dyrk1a mutant brains. One telencephalic vesicle (TV) and the midbrain (MB) are limited with white and blue dashed lines, respectively. Values in the histograms correspond to the area (mean ± SEM) of one telencephalic vesicle and the midbrain measured in control (Ct) and *NesCre*:*Dyrk1a*-KO (KO) embryos (n=3 each genotype), and *NesCre*:*Dyrk1a*-HET (Ht) embryos (n=5). ns, not significant; ***P<0.001 in a two-tailed Student t-test. Scale bar: 1.5 mm.

2. Structural brain alterations in the *NesCre*:*Dyrk1a* conditional mutant

The comparative morphological analysis of coronal brain sections from E17.5 control, *NesCre*:*Dyrk1a*-HET and *NesCre*:*Dyrk1a*-KO embryos at different levels of the anterior-posterior axis revealed important anomalies in *NesCre*:*Dyrk1a*-KO brains. These include an almost complete absence of ventral structures such as the caudate putamen, the pre-thalamus, and the pre-thalamic and hypothalamic nuclei surrounding the third ventricle. The dentate gyrus in the dorsal telencephalon of *NesCre*:*Dyrk1a*-KO embryos was also severely affected. The thickness of the dorsal telencephalon in the *NesCre*:*Dyrk1a*-KO brain was normal, but its laminar organization was slightly altered, especially in the IZ and the CP (see

Figure R.2). Ventral telencephalic structures in the two *NesCre*:*Dyrk1a*-KO embryos recovered before birth (E19.5) were completely absent (**Figure R.3**). Moreover, the anatomical disorganization of the dorsal telencephalon in E19.5 *NesCre*:*Dyrk1a*-KO embryos was more evident (**Figure R.3**) than at E17.5 (**Figures R.2**). At birth, both the dorsal and ventral telencephalon of *Emx1:Dyrk1a* conditional null mutants are smaller than normal (Levy et al., 2021), despite the fact that *Emx1* expression in the developing brain is restricted to dorsal progenitors (Gorski et al., 2002). Therefore, it is possible that the absence of DYRK1A in the dorsal telencephalon of *NesCre*:*Dyrk1a*-KO embryos has a negative impact in the development of ventral structures. The brain phenotype of the *NesCre*:*Dyrk1a* conditional null mutant reported here suggest a fundamental role for DYRK1A in brain neurogenesis, both in dorsal and ventral territories.

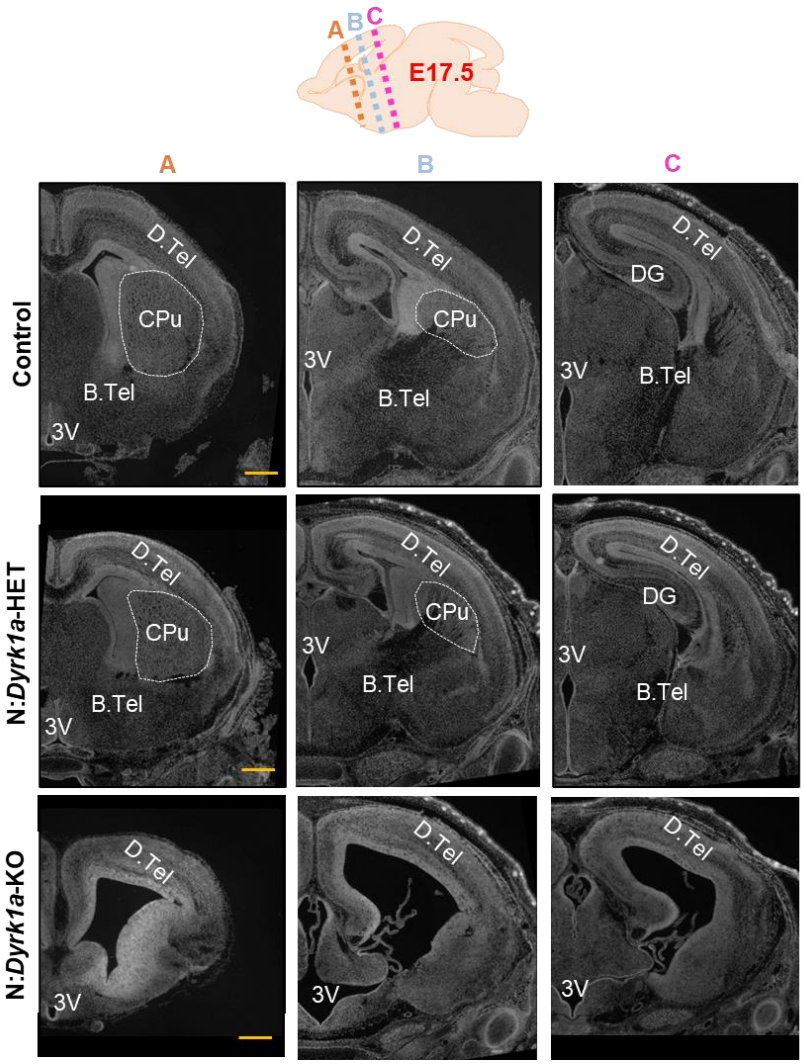

Figure R.2. Morphological brain alterations in *NesCre*:*Dyrk1a*-HET and *NesCre*:*Dyrk1a*-KO embryos at late neurogenesis. Representative images of a coronal section with the nuclei stained with DAPI from E17.5 control, *NesCre*:*Dyrk1a*-HET and *NesCre*:*Dyrk1a*-KO littermate embryos showing one brain hemisphere. The sections correspond to the rostro-caudal position (A, B or C) indicated in the cartoon by dashed lines. B.Tel, basal telencephalon; CPu, caudate putamen; DG, dentate gyrus; D.Tel, dorsal telencephalon; 3V, third ventricle. Scale bar: 500 μm.

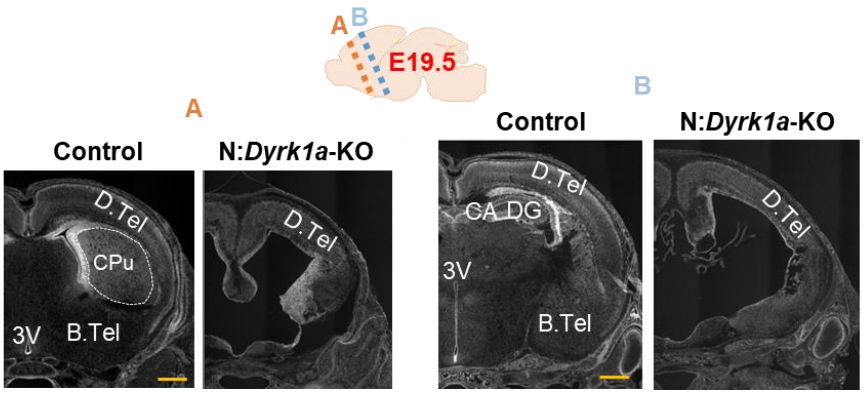

Figure R.3. Morphological brain alterations in *NesCre*:*Dyrk1a*-KO embryos before birth. Representative images of coronal sections with the nuclei stained with DAPI from E19.5 control and *NesCre*:*Dyrk1a*-KO embryos showing one brain hemisphere. The sections correspond to the rostro-caudal position (A or B) indicated in the cartoon by dashed lines. B.Tel, basal telencephalon; CA, cornu ammonis; CPu, caudate putamen; DG, dentate gyrus; D.Tel, dorsal telencephalon; 3V, third ventricle. Scale bar: 500 µm.

Structural abnormalities in *NesCre*:*Dyrk1a*-HET brains were more subtle and mostly restricted to the ventral telencephalon. At E17.5, heterozygous brains presented a significant size reduction (12% reduction with respect to the control, P=0.042 in a two-tailed Student t-test. n=3 embryos per genotype; see images in **Figure R.2**). The caudate-putamen of *NesCre*:*Dyrk1a*-HET embryos also seemed smaller than normal (**Figure R.2**). This structure is the major component of the *striatum*, a subcortical region involved in the development of characteristic behaviours in ASD (Langen et al., 2009). Using the Cavalieri method (Mayhew and Olsen, 1991), we measured the volume of the caudate-putamen in coronal brain sections of E17.5 *NesCre*:*Dyrk1a*-HET and control littermate embryos immunolabeled for CITP2, a marker of striatal MSNs (Molyneaux et al., 2007). As shown in **Figure R.4**, the volume of the striatum was 25% smaller in *NesCre*:*Dyrk1a*-HET embryos than in the controls indicating defects in the production and/or differentiation of MSNs in the heterozygous mutant.

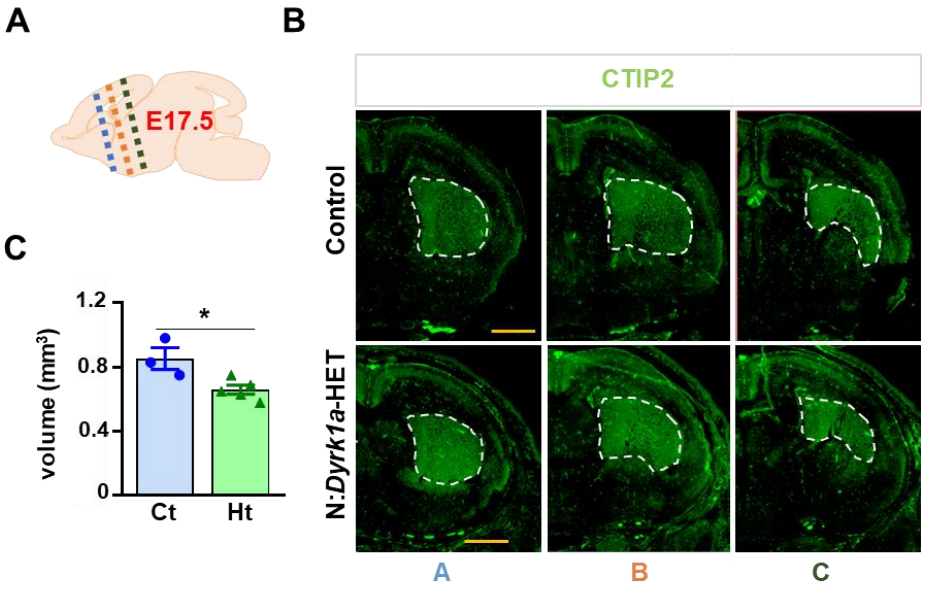

Figure R.4. Size of the *striatum* in *NesCre*:*Dyrk1a*-HET embryos at late neurogenesis. (A) Cartoon of a E17.5 brain. The dashed lines indicate the position in the rostro-caudal axis (A, B or C) of the sections analysed. (B) Representative sections from E17.5 control and *NesCre*:*Dyrk1a*-HET embryos stained for CTIP2. The white dashed lines delimit the *striatum*. (C) Values in the histogram correspond to the striatum volume (mean ± SEM) measured in 3 control and 5 *NesCre*:*Dyrk1a*-HET embryos at rostro-caudal level B. *P<0.05 in a two-tailed Student t-test. Scale bar: 700 µm.

At E13.5 we did not detected any gross morphological alteration in *NesCre*:*Dyrk1a*-HET embryos (**Figure R.5A**). By contrast, the morphology of *NesCre*:*Dyrk1a*-KO brains at this developmental stage was significantly affected, especially in the ventral telencephalon, that showed an important reduction of the parenchyma (44% reduction with respect to the controls, *P*=0.005 in a two-tailed Student t-test. n=4-5 embryos each genotype. Measures performed in sections at the anterior-posterior position B in **Figure R.5A**). The examination of sections stained with DAPI at higher magnifications revealed the presence of pyknotic nuclei in the MZ of the LGE and MGE in *NesCre*:*Dyrk1a*-KO brains (**Figure R.5B**). This observation suggests that cell death may be the cause of the severe reduction of ventral brain parenchyma in *NesCre*:*Dyrk1a*-KO embryos.

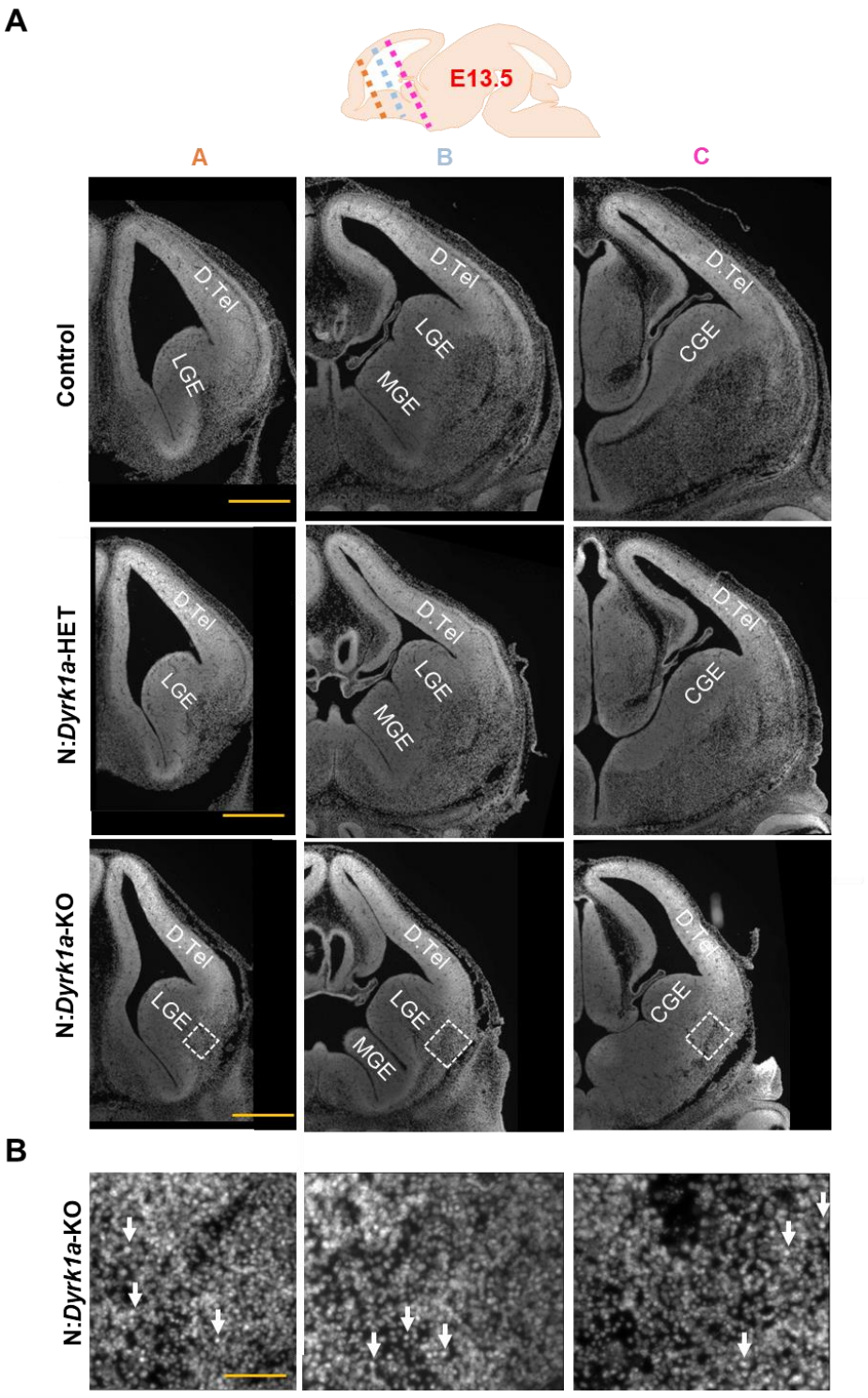

Figure R.5. Presence of pyknotic nuclei in *NesCre*:*Dyrk1a*-KO brains at mid-neurogenesis. (A) Representative images of coronal sections with the nuclei stained with DAPI from E13.5 control, *NesCre*:*Dyrk1a*-HET and *NesCre*:*Dyrk1a*-KO embryos showing one brain hemisphere. The sections correspond to the rostro-caudal position (A, B or C) indicated in the cartoon by dashed lines. White dashed boxes in the mantle zone of N-Dyrk1a-KO brains are amplified in the images shown in B. (B) Notice that many of the nuclei in the mantle zone of *NesCre*:*Dyrk1a*-KO brains are pyknotic. The white arrows point to some of these nuclei. CGE, caudal ganglionic eminence; LGE, lateral ganglionic eminence; MGE, medial ganglionic eminence; D. Tel, dorsal telencephalon. Scale bar: 500 μm (A) and 100 μm (B).

3. DNA damage in the *NesCre*:*Dyrk1a* conditional mutant brain

To assess the onset of pyknotic nuclei appearance in the *NesCre*:*Dyrk1a*-KO telencephalon, we examined coronal brain section from control and *NesCre*:*Dyrk1a*-KO embryos starting at E11.5. At this developmental stage, pyknotic nuclei were already present in the ventral telencephalon of *NesCre*:*Dyrk1a*-KO embryos (data not shown). We then examined the possibility that pyknotic cells in the *NesCre*:*Dyrk1a*-KO brains were dying by apoptosis by performing immunostainings for the active form of caspase-3 and counting the number of caspase-3+ cells in control and *NesCre*:*Dyrk1a*-KO brain sections. Cell quantifications were done in the whole dorsal telencephalon or in an area of $6.0x10^4$ μm^2 of the LGE (see **Figures R.6, R.7A and R.8A**). At E11.5, control brains showed very few apoptotic cells (active caspase-3+ cells/hemisphere: 0.7±0.21 dorsal telencephalon; 1.9±0.2 in the LGE. n=23 brain sections from 3 embryos). In the mutant littermates, caspase-3+ cells were more abundant than in the control (**Figure R.6)**, particularly in the ventral telencephalon.

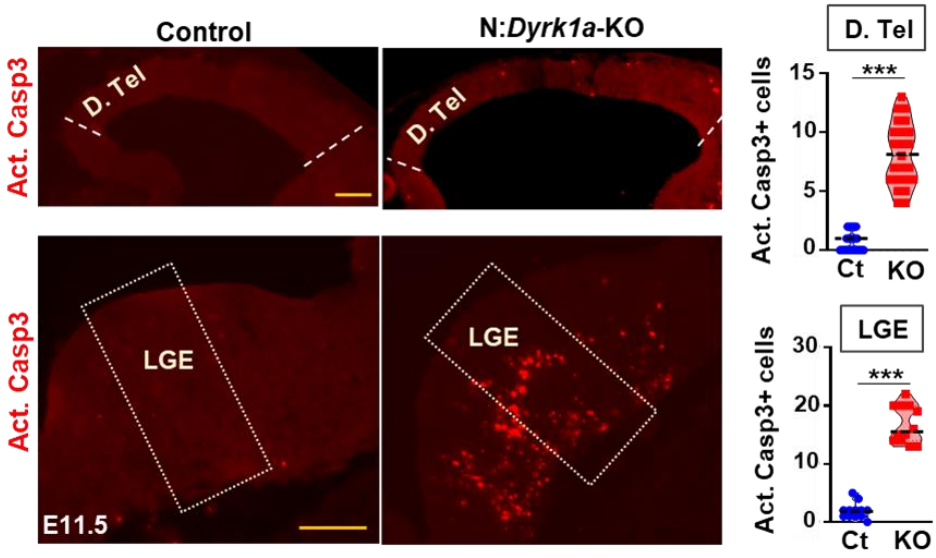

Figure R.6. Cell death in *NesCre*:*Dyrk1a*-KO brains at the onset of neurogenesis. Representative coronal sections of a dorsal telencephalon (D. Tel) and lateral ganglionic eminence (LGE) of E11.5 control (Ct) and *NesCre*:*Dyrk1a*-KO (KO) littermate embryos immunostained for the active form of caspase-3 (Act. Casp3). White dashed lines indicate the limits of the D. Tel territory and the rectangles in the LGE the area where Casp3+ cells where counted. Points in the violin plots correspond to the number of Act. Casp3+ cells measured in the whole D. Tel (n=23 hemispheres from 3 embryos per genotype) or in an area of 6.0x104 µm2 of the LGE (n=12 hemispheres from 3 embryos per genotype) of Ct and KO brains. Mean values are indicated by black dashed lines. ***P<0.001 in a two-tailed Student t-test. Scale bar: 100 µm.

As for pyknotic nuclei, the region of the ventral telencephalon with the highest cell death was the LGE. At E13.5, *NesCre*:*Dyrk1a*-KO embryos showed a significant increase in caspase-3+ apoptotic cells with respect to the controls both in the whole dorsal telencephalon and in an area of $5.8x10^4$ μm^2 within the LGE (**Figure R.7**). Apoptotic cells in the *NesCre*:*Dyrk1a*-KO LGE were concentrated in the MZ, where neurons and progenitors are intermingled, and in the prospective *striatum* (**Figure R.7A**). At this developmental stage, apoptotic cells in the dorsal telencephalon of control and *NesCre*:*Dyrk1a*-KO embryos were located in the VZ-SVZ (**Figures R.7** and data not shown). Later in development, at E15.5, we did not detect active caspase-3+ cells in the dorsal telencephalon of control embryos. However, these cells were very abundant in the same region of *NesCre*:*Dyrk1a*-KO embryos, especially in the territory occupied by neurons (IZ and CP; see **Figure R.8**). At this developmental stage, apoptosis was still present in the ventral regions of *NesCre*:*Dyrk1a*-KO brains, where there was a prominent reduction of the parenchyma (data not shown).

The observations presented so far suggest that aberrant apoptosis in *NesCre*:*Dyrk1a*-KO brains mainly affects progenitor cells at the first steps of neurogenesis, also affecting neurons as neurogenesis advances. The fact that the increase in caspase-3+ cells in *NesCre*:*Dyrk1a*-KO brains was more prominent and started earlier in ventral than in dorsal regions (**Figure R.6 and R.7**) strongly suggests that cell death is the cause of the massive loss of cells observed in the *NesCre*:*Dyrk1a*-KO brains by the end of neurogenesis (E17.5 and E19.5; **Figures R.2 and 3**).

Apoptosis in the developing brain is mediated by the intrinsic (caspase-9 dependent) cell death pathway (Hakem et al., 1998). To assess whether increased cell death in *NesCre*:*Dyrk1a*-KO embryos could be the consequence of an aberrant activation of the intrinsic pathway, we immunostained E13.5 *NesCre*:*Dyrk1a*-KO brain sections for the active form of caspase-9. The immunostaining pattern of active caspase-9 in the *NesCre*:*Dyrk1a*-KO brains was very similar to that of active caspase-3, as shown in the LGE in **Figure R.7C**, indicating that aberrant apoptosis in the brain of *NesCre*:*Dyrk1a*-KO embryos is mediated by caspase-9 activation.

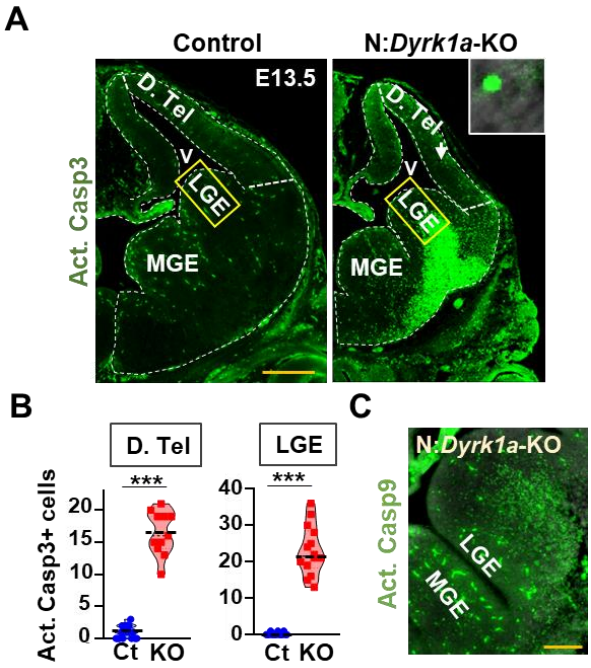

Figure R.7. Cell death in *NesCre*:*Dyrk1a*-KO brains at mid-neurogenesis. (A) Representative coronal sections immunostained for the active form of caspase-3 (Act. Casp3) showing one brain hemisphere of a E13.5 control (Ct) and *NesCre*:*Dyrk1a*-KO (KO) littermate embryo. White arrowhead in the KO dorsal telencephalon points to an Act. Casp3+ cell that is magnified in the white square. (B) Points in the violin plots correspond to the number of Act. Casp3+ cells measured in the whole D. Tel (n=11-20 hemispheres from 3 embryos each genotype) or in an area of 5.8x104 µm2 (yellow rectangle in A) of the lateral ganglionic eminence (LGE) (n=11-14 hemispheres from 3 embryos each genotype). Mean values are indicated by black dashed lines. (C) Coronal section of the ventral telencephalon of an E13.5 KO embryo immunostained for the active form of caspase-9 (Act. Casp9). ***P<0.001 in a two-tailed Student t-test. MGE, medial ganglionic eminence; V, ventricle. Scale bar: 500 µm (A) and 100 µm (C).

Previous data indicate that DYRK1A phosphorylates caspase-9 at Thr125 in retinal and ventral midbrain neurons during development, thereby inhibiting physiological apoptosis (Laguna et al., 2008) (see scheme in **Figure R.9A**). We therefore checked by immunoblotting the levels of caspase-9 phosphorylated in Thr125 in extracts from the ventral telencephalon of control and *NesCre*:*Dyrk1a*-KO embryos at E11.5, when aberrant apoptosis in this region was already evident (**Figure R.6**). As shown in **Figure R.9B**, at E11.5 the levels of phosphorylated caspase-9 relative to total a caspase-9 were similar in control and *NesCre*:*Dyrk1a*-KO brain extracts, suggesting that kinases other than DYRK1A are phosphorylating caspase-9 in the inhibitory residue Thr125. Therefore, an aberrant caspase-9 activity does not seem to be the cause of the increased apoptosis displayed by *Dyrk1a* KO brains.

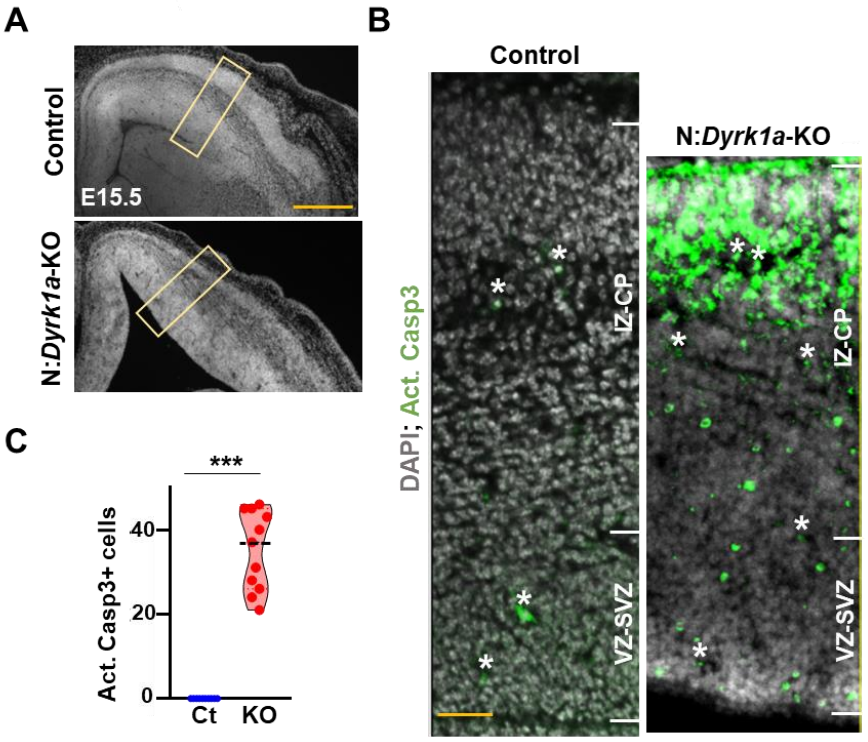

Figure R.8. Cell death in the dorsal telencephalon of *NesCre*:*Dyrk1a*-KO mutants at late neurogenesis. (A) Representative images of the dorsal telencephalon of E15.5 control (Ct) and *NesCre*:*Dyrk1a*-KO (KO) mutant brains with the nuclei labelled with DAPI. (B) Magnifications of the area delimited by the rectangle in A showing the immunostaining for the active form of caspase-3 (Act. Casp3). White asterisks point to autofluorescent signal from blood vessel cells. (C) Points in the violin plot correspond to the number of Act. Casp3+ cells measured in a 150 µm wide column (rectangle in A) of the dorsal telencephalon of Ct and KO brains. n=10-11 columns from two embryos each genotype. Mean values are indicated by black dashed lines. ***P<0.001 in a two-tailed Student t-test. CP, cortical plate; IZ, intermediate zone; SVZ, subventricular zone; VZ, ventricular zone. Scale bar: 300 µm (A) and 50 µm (B).

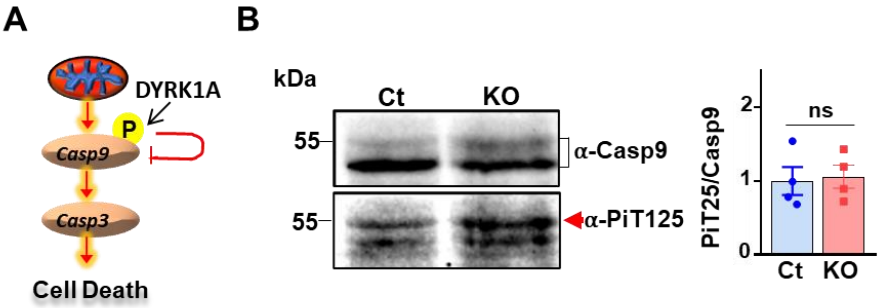

Figure R.9. Phosphorylation levels of the DYRK1A substrate caspase-9 in *NesCre*:*Dyrk1a*-KO embryos. (A) Scheme showing DYRK1A regulation of apoptotic cell death. (B) Representative western blot of extracts prepared from the ventral telencephalon of E11.5 control (Ct) and *NesCre*:*Dyrk1a*-KO (KO) embryos probed for caspase-9 (Casp9) and the phosphorylated form of the protein (PiT125, pointed by red arrow). Values (mean ± SEM) in the histogram correspond to the phosphorylation levels of PiT125 relative to the total amount of Casp9 in brain extracts from Ct and KO embryos. n=4 embryos per genotype. ns, not significant.

During neurogenesis, neural progenitors divide fast, especially in the ventral ganglionic eminences (Turrero Garcia and Harwell, 2017). Due to this fact, neural progenitors are very sensitive to replicative stress (McKinnon, 2017). Thus, it is possible that persistent DNA damage due to replicative stress causes or contributes to the increased apoptosis in *NesCre*:*Dyrk1a*-KO brains (see scheme in **Figure R.10A**). To test this possibility, we immunostained E11.5 control and *NesCre*:*Dyrk1a*-KO brain sections for γH2AX, a marker of the activation of the ATM and ATR kinase pathways involved in DDR (Rogakou et al., 1998). The number of γH2AX+ cells in control brains was very low (cells/hemisphere: 0.42±0.30 in the dorsal telencephalon; 0.85±0.16 in the LGE. n=8 hemispheres from 3 embryos) and restricted to the proliferative layer (labelled for SOX2; **Figure R.10B, C**). In *NesCre*:*Dyrk1a*-KO brains, the number of γH2AX cells increased 2.8 times in the dorsal telencephalon and 5.1 times in the LGE (**Figure R.10D**). As in the controls, most γH2AX+ cells in the *Dyrk1a* mutant LGEs were in the SOX2 territory (**Figure R.10C**). The positive correlation between the number and distribution of active caspase-3+ cells and γH2AX+ cells (**Figures R.6 and R.10B-D**) in E11.5 *NesCre*:*Dyrk1a*-KO brains suggests that apoptosis in these brains is caused by unresolved lesions in the DNA, likely because of replicative stress. To provide more evidence on this notion, we repeated the same immunostaining in E13.5 brains from control and *NesCre*:*Dyrk1a*-KO littermates. As in E11.5, γH2AX+ cells in the dorsal telencephalon and LGE of 13.5 mutant embryos were similarly increased and showed a similar distribution pattern than active caspase-3+ cells (**Figures R.7 and R.11**).

DDR-dependent apoptosis requires activation of the tumour suppressor p53 (Williams and Schumacher, 2016). Thus, we immunostained control and *NesCre*:*Dyrk1a*-KO brain sections for p53 24 h after we started to detect active caspase-3+ and γH2AX+ cells in the KO brains (**Figures R.6 and R.10**). As shown in **Figure R.12**, at E12.5 there were more p53+ nuclei in the dorsal telencephalon and in the LGE of *NesCre*:*Dyrk1a*-KO embryos than in the controls. Remarkably, the increase in active p53 cells was more significant in the LGE than in the dorsal telencephalon (350% increase over the controls in the LGE and 100% increase in the dorsal telencephalon; see **Figure R.12C**). Moreover, p53+ nuclei in both control and *NesCre*:*Dyrk1a*-KO brains were located almost exclusively in the proliferative regions (immunonegative for the pan-neuronal marker TUJ1; **Figure R.12A and B**). This result is in line with the notion that apoptosis in *NesCre*:*Dyrk1a*-KO brains is caused by persistent activation of DDR pathways.

Collectively, the results presented so far suggest that DYRK1A is necessary to cope with the replicative stress in brain progenitors during embryonic neurogenesis.

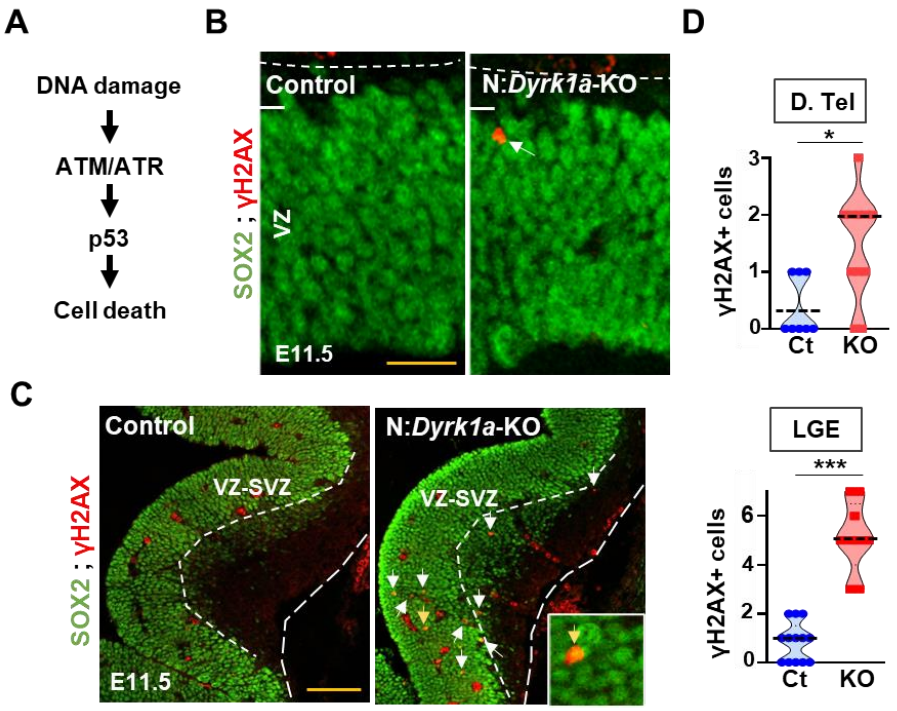

Figure R.10. DNA damage response in *NesCre*:*Dyrk1a*-KO brains at the onset of neurogenesis. (A) Scheme of p53-mediated cell death in response to DNA damage. (B, C) Representative images of the dorsal telencephalon (D. Tel) (B) and the lateral ganglionic eminence (LGE) (C) of E11.5 control (Ct) and *NesCre*:*Dyrk1a*-KO (KO) mutant brains immunostained for γH2AX and SOX2. The white arrows in B and C point to γH2AX+ nuclei. The γH2AX+ nuclei pointed by the yellow arrow in C is magnified in the white square. Autofluorescent signal from blood vessel cells (in red) is detected in the LGEs of Ct and KO brains. (D) Points in the violin plots correspond to the number of γH2AX+ cells counted in the D. Tel (n=8-11 hemispheres from 3 embryos each genotype) and LGE (n=9-13 hemispheres from 3 embryos each genotype) of Ct and KO brains. Mean values are indicated by black dashed lines. *P<0.05, ***P<0.001 in a two-tailed Student t-test. SVZ, subventricular zone; VZ, ventricular zone. Scale bar: 50 μm (A) and 100 μm (B).

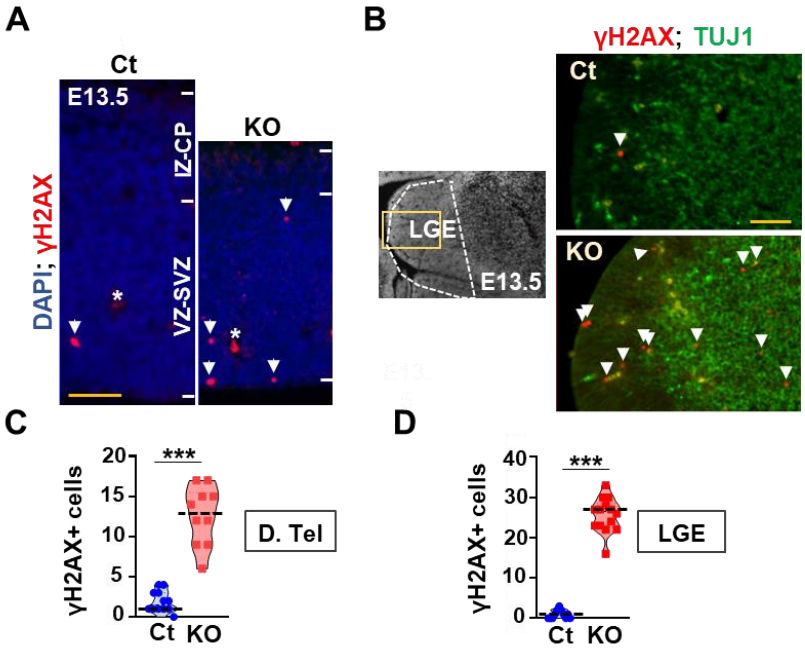

Figure R.11. DNA damage response in *NesCre*:*Dyrk1a*-KO brains at mid-neurogenesis. (A) Representative images of the dorsal telencephalon (D. Tel) of E13.5 control (Ct) and *NesCre*:*Dyrk1a*-KO (KO) brains immunostained for γH2AX and the nuclei labelled with DAPI. Arrows point to γH2AX+ nuclei and asterisks to autofluorescent signal from blood vessel cells. (B) Coronal brain section showing the lateral ganglionic eminence (LGE) of an E13.5 embryo. The dashed line delimits the LGE where γH2AX+ cells were counted and the rectangle the region of the images shown from Ct and KO sections immunostained for γH2AX and TUJ1. Arrowheads in these images point to γH2AX+ nuclei. (C, D) Each point in the violin plots corresponds to the number of γH2AX+ cells counted in the D. Tel (C) or the LGE (D) of Ct and KO brains. n=11-12 hemispheres from 5-6 Ct and KO embryos in C; n=12-14 hemispheres from 5 embryos each genotype in D. Mean values are indicated by black dashed lines. ***P<0.001 in a two-tailed Student t-test. CP, cortical plate; IZ, intermediate zone; SVZ, subventricular zone; VZ, ventricular zone. Scale bar: 50 μm (A) and 100 μm (B).

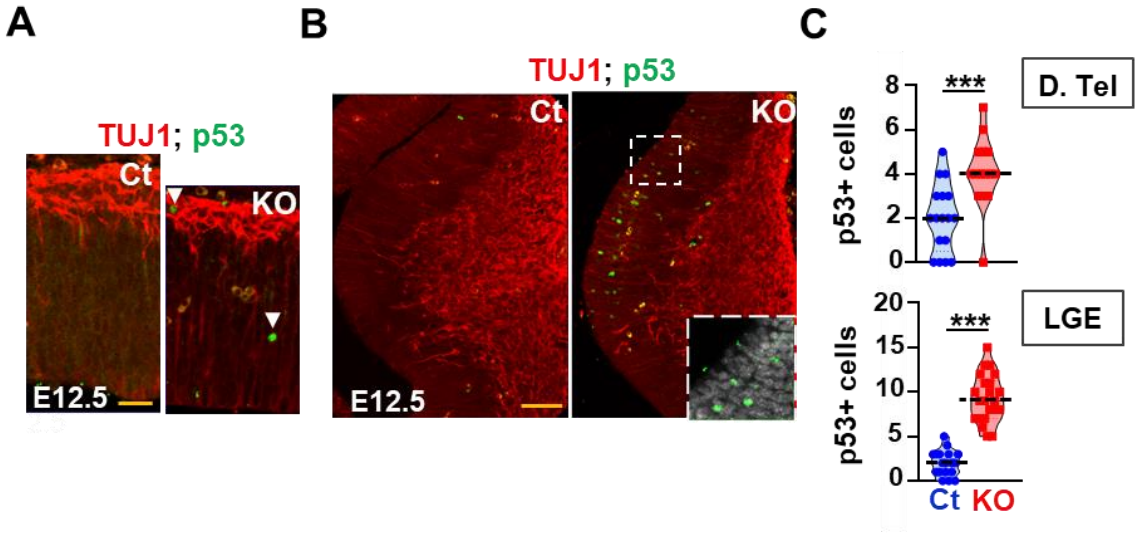

Figure R.12. p53 immunostaining in *NesCre*:*Dyrk1a*-KO brains at early-neurogenesis. (A, B) Representative images of the dorsal telencephalon (D. Tel) (A) and the lateral ganglionic eminence (LGE) (B) of E12.5 control (Ct) and *NesCre*:*Dyrk1a*-KO (KO) brain sections immunostained for p53 and TUJ1. White arrows in A point to p53+ nuclei. The white square in the KO section in B is magnified to better illustrate p53 immunostaining. (C) Points in the violin plots correspond to the number of γH2AX+ cells counted in the D. Tel (n=15-17 hemispheres from 3 embryos each genotype) or the LGE (n=18-22 hemispheres from 3 embryos each genotype) of Ct and KO brains. Mean values are indicated by black dashed lines. ***P<0.001 in a two-tailed Student t-test. Scale bar: 30 μm (A) and 100 μm (B).

4. Cell cycle parameters in the radial glia of dorsal *NesCre*:*Dyrk1a* mutant brains

DNA damage repair in neural progenitors takes place mainly by HR during S and G2 phases of the cell cycle, when sister chromatid is available. Thus, defects in DNA damage repair can impact on cell cycle progression and vice-versa (Jackson and Bartek, 2009). Previous literature indicates that DYRK1A participates in DNA repair and regulates cell cycle progression (Chen et al., 2013; Guard et al., 2019; Roewenstrunk et al., 2019).

Therefore, we carried out experiments to check for possible cell cycle alterations in the RG (apical progenitors) of *NesCre*:*Dyrk1a*-KO embryos and their control littermates.

In neural progenitors, DYRK1A can inhibit G1-S transition by phosphorylating the positive regulator Cyclin D1, promoting Cyclin D1 nuclear export and its degradation through the ubiquitin-proteasome pathway, and the negative regulator $p27^{KIP1}$, promoting its stabilization (Soppa et al., 2014; Najas et al., 2015) (**Fig R.13A**). Therefore, we determined the levels of Cyclin D1 and $p27^{KIP1}$ in brain extracts of E11.5 *NesCre*:*Dyrk1a*-KO and control embryos by immunoblotting. For this experiment we used extracts obtained from the dorsal telencephalon because at this developmental stage most of the cells in the dorsal brain are apical progenitors and CDK4/6 activity in these progenitors is Cyclin D1-dependent (Lange et al., 2009; Pilaz et al., 2009). In accordance with previous data obtained in the tgBac*Dyrk1a* and *Dyrk1a*$^{+/-}$ mouse models (Najas et al., 2015), the levels of Cyclin D1 in the *NesCre*:*Dyrk1a*-KO dorsal telencephalon were much higher than in the controls (**Figure R.13B**). A significant increase in nuclear Cyclin D1 levels in dorsal and ventral VZ progenitors was also observed by immunofluorescence in E11.5 *NesCre*:*Dyrk1a*-KO brain sections (data not shown). At E12.5, the levels of Cyclin D1 in extracts from the dorsal telencephalon of *NesCre*:*Dyrk1a*-KO embryos were also increased (data not shown), but the increase was less severe than at E11.5 (5.32 ± 0.66 and 3.48 ± 0.57 times with respect to the controls at E11.5 and E12.5, respectively). This is in line with previous data suggesting that DYRK1A regulation of Cyclin D1 protein levels in dorsal apical progenitors is key at the onset of neurogenesis, when nuclear Cyclin D1 levels in this progenitor type is high (Najas et al., 2015). Despite the fact that DYRK1A can regulate $p27^{KIP1}$ levels in cultured cells (Soppa et al., 2014), no differences in $p27^{KIP1}$ protein levels were detected in the dorsal telencephalon of E11.5 *NesCre*:*Dyrk1a*-KO embryos when compared to control littermates (**Figure R.13B**). Again, this is in line with the normal levels of $p27^{KIP1}$ detected in the dorsal telencephalon of E11.5 tgBac*Dyrk1a* and *Dyrk1a*$^{+/-}$ embryos (Najas et al., 2015). These results indicate that the effect of DYRK1A on Cyclin D1 and $P27^{KIP1}$ is probably dependent on the cellular context and the developmental stage.

Cyclin D1 bound to CDK4/6 activates CDK4/6, leading to Retinoblastoma (Rb) phosphorylation (Weinberg, 1995). Thus, as a readout of CDK4/6 activity, we next checked by immunoblotting the phosphorylation status of Rb in the dorsal telencephalon of E11.5 *NesCre*:*Dyrk1a*-KO embryos and control littermates. In agreement with the increased levels of nuclear Cyclin D1, the levels of hyperphosphorylated Rb were also augmented in extracts obtained from *NesCre*:*Dyrk1a*-KO brains (**Figure R.13C**), suggesting that cell cycle progression in dorsal *NesCre*:*Dyrk1a*-KO RG cells is likely affected, at least at the onset of neurogenesis. The majority of VZ cells in the dorsal telencephalon of control and *NesCre*:*Dyrk1a*-KO embryos expressed the RG marker PAX6 (Gotz et al., 1998). In both

genotypes, 99% of PAX6 progenitors expressed the proliferation marker Ki67 (**Figure R.14**), indicating that the entire set of dorsal progenitors is cycling.

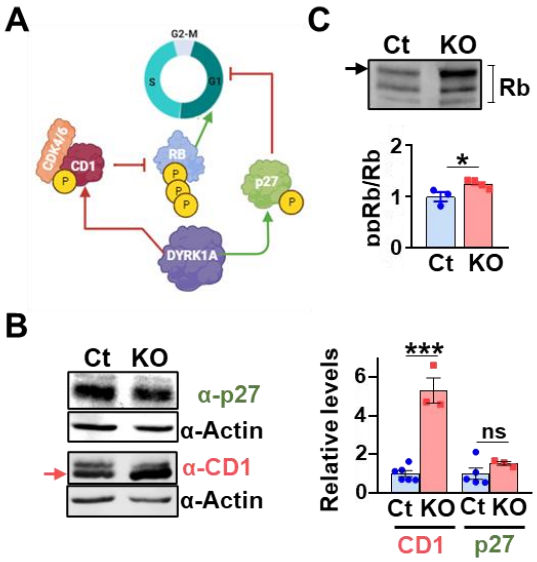

Figure R.13. Protein levels of cell cycle regulators in the dorsal telencephalon of *NesCre*:*Dyrk1a*-KO embryos. (A) Scheme showing the regulation of G1 to S phase transition throughout the phosphorylation of Cyclin D1 (CD1) and p27KIP1 (p27) by DYRK1A. (B) Representative immunoblots of dorsal telencephalic extracts from E11.5 Ct and KO embryos probed for Cyclin D1 and p27. Arrow points to the Cyclin D1 (CD1) isoform that is phosphorylated by DYRK1A. Data in the histogram corresponds to the levels (mean ± SEM) of CD1 and p27 in Ct and KO samples normalized to actin and expressed relative to controls. (C) Representative immunoblot of dorsal brain extracts from E11.5 control (Ct) and *NesCre*:*Dyrk1a*-KO (KO) embryos probed for retinoblastoma (Rb). Arrow points to the hyperphosphorylated form of retinoblastoma (ppRb). Data in the histogram corresponds to the proportion of Rb that is hyperphosphorylated in KO samples (mean ± SEM) relative to the levels in controls. n=3-5 embryos per genotype. ns, not significant; *P<0.05; ***P<0.001 in a two-tailed Student t-test.

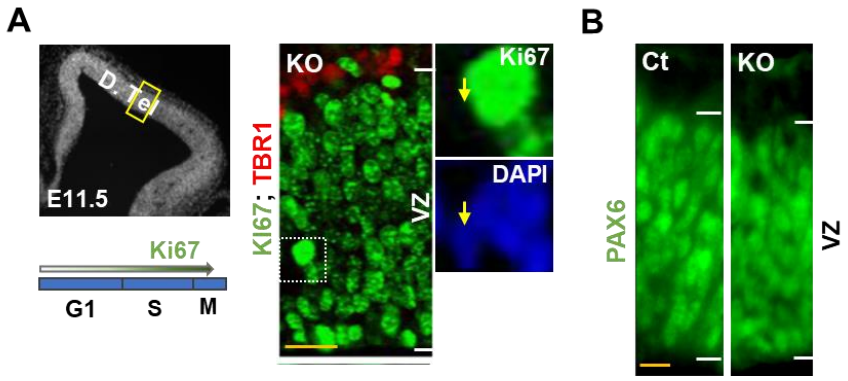

Figure R.14. Ki67 and PAX6 expression in the dorsal telencephalon of *NesCre*:*Dyrk1a*-KO embryos at the onset of neurogenesis. (A) Coronal section of an E11.5 control brain and representative image of the dorsal telencephalon (position indicated by the yellow rectangle in A) immunolabelled for Ki67 and TBR1 and the nuclei labelled with DAPI. Magnifications of the area delimited by the white square are on the right. Yellow arrowheads point to a nucleus in the ventricular zone (VZ) that is negative for Ki67. The expression levels of Ki67 during the cell cycle are indicated. (B) Images of the dorsal telencephalon of control (Ct) and *NesCre*:*Dyrk1a*-KO (KO) embryos immunolabeled for PAX6. Scale bars: 10 µm.

To detect possible alterations in the cell cycle progression of *NesCre*:*Dyrk1a*-KO RG cells, we next isolated cells from the dorsal telencephalon of E11.5 *NesCre*:*Dyrk1a*-KO and control embryos and estimated the percentages of cells that were in G0-G1, S or G2-M

phases by flow cytometry. The results showed that the dorsal proliferative region of *NesCre*:*Dyrk1a*-KO brains had more cells in S phase and less cells in G0-G1 than the controls, whereas the percentage of cells in G2-M was very similar in both genotypes (**Figure R.15**). These cell cycle profiles suggest that dorsal telencephalic *NesCre*:*Dyrk1a*-KO progenitors display an altered replication phase. To explore this possibility, we calculated the total cell cycle length and S phase length in dorsal VZ progenitors immunostained for SOX2 (**Figure R.16B**) in *NesCre*:*Dyrk1a*-KO and control embryos using the EdU-BrdU double labelling approach previously described (Martynoga et al., 2005). Cell cycle parameters were calculated at two developmental stages, at E11.5 and 24 h later (see experimental design and the equations to calculate these parameters in **Figure R.16A**). Quantifications of VZ SOX2+, BrdU+ and EdU+ cells were performed in the middle of the dorsal telencephalon (**Figure R.16B**). In agreement with the PAX6 immunostainings (**Figure R.14A**), most VZ cells in the dorsal telencephalon of control and *NesCre*:*Dyrk1a*-KO brains expressed high levels of the transcription factor SOX2. At E11.5, the numbers of dorsal SOX2+ cells were similar in both genotypes. However, these progenitors significantly increased in the *NesCre*:*Dyrk1a*-KOs at E12.5 (**Figure R.16B, C**) and at E13.5 (data not shown). In accordance with the cell sorting experiment shown in **Figure R.15**, E11.5 *NesCre*:*Dyrk1a*-KO SOX2+ progenitors showed longer S phases (40% increase with respect to controls). At E12.5, the duration of the S phase in the mutant dorsal SOX2+ progenitors was also increased, but the differences with respect to the controls (14% increase) were much subtle than at E11.5 (**Figure R.16D**). Similarly, SOX2+ *NesCre*:*Dyrk1a*-KO progenitors had longer cell cycles than the controls at E11.5 and E12.5, but the differences between genotypes were more subtle as neurogenesis advances (27% increase at E11.5 and 13% increase at E12.5; see **Figure R.16D**). At both developmental stages, the lengthening of the total cell cycle (5.4 h increase at E11.5 and 3.3 h at E12.5) was greater than the lengthening of the S phase (4.1 h increase at E11.5 and 1.4 h at E12.5), suggesting that G1 to S phase transition is delayed in the dorsal *NesCre*:*Dyrk1a*-KO RG cells. This delay is likely the consequence of the dysregulation of DYRK1A substrates, acting in G1 such as Cyclin D1.

Together, these results are in accordance with previous data showing a role of DYRK1A in G1 to S transition (Chen et al., 2013) and DNA repair involving HR (An et al., 2018; Guard et al., 2019; Roewenstrunk et al., 2019), which is consistent with the expression of the DDR marker γH2AX observed in the proliferative regions of *NesCre*:*Dyrk1a*-KO brains at the beginning of neurogenesis (**Figures R.10 and 11**).

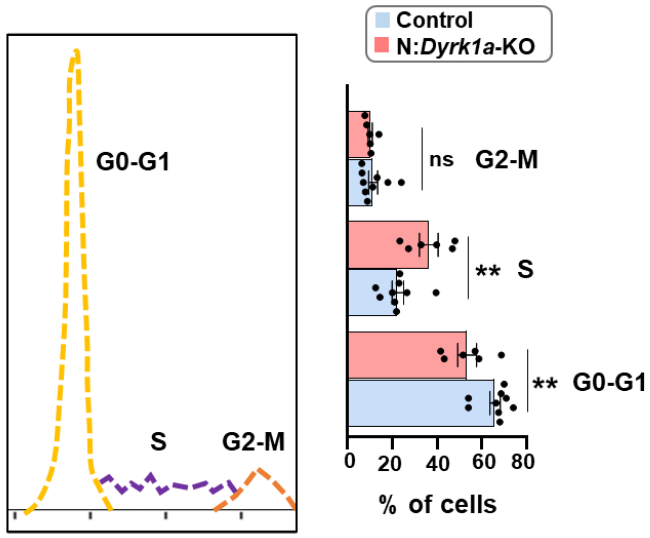

Figure R.15. Cell cycle profile of dorsal neural progenitors in *NesCre*:*Dyrk1a*-KO embryos. Representative cell cycle profile of wild-type cells obtained from the dorsal telencephalon of E11.5 embryos showing the peaks of the cells in G0-G1, S or G2-M. Histogram corresponds to the percentage of cells (mean ± SEM) that are in G0-G1, S or G2-M in control and *NesCre*:*Dyrk1a*-KO embryos. Each point in the graph corresponds to the data obtained from one embryo. n=9 control embryos; n=6 *NesCre*:*Dyrk1a*-KO embryos. ns, not significant; **P<0.01 in a two-tailed Student t-test.

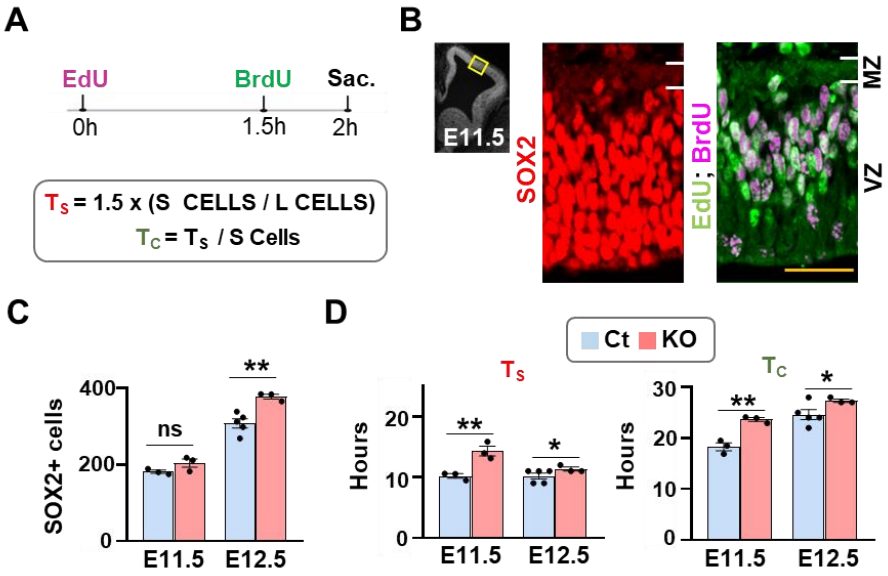

Figure R.16. Cell cycle parameters of dorsal neural progenitors in *NesCre*:*Dyrk1a*-KO embryos. (A) Scheme indicating the time of EdU and BrdU injections and embryo sacrifice for the quantification of S phase length (Ts) and total cell cycle length (Tc) in E11.5-E12.5 SOX2+ (apical) progenitors. L CELLS = EdU+ BrdU- cells/SOX2+ cells; S CELLS = EdU+ BrdU+ cells/SOX2+ cells. (B) Images of the dorsal telencephalon of an E11.5 wild-type embryo showing SOX2 and BrdU and EdU labelled cells. (C, D) Data in the histograms corresponds to the number of SOX2+ progenitors (C) and the duration of the S phase (Ts) and the total cell cycle (Tc) (mean ± SEM) in E11.5 or E12.5 control (Ct) and *NesCre*:*Dyrk1a*-KO (KO) embryos. n=3 embryos each genotype at E11.5; n=3-5 embryos each genotype at E12.5. MZ, mantle zone; VZ, ventricular zone. ns, not significant; *P<0.05; **P<0.01 in a two-tailed Student t-test. Scale bar: 50 µm.

5. Neural proliferation and differentiation in the *NesCre*:*Dyrk1a* mutant brain

The results presented so far suggest that, in addition to defects in cell cycle progression, dorsal *NesCre*:*Dyrk1a*-KO RG cells may present alterations in the mode of division. SOX2+ progenitors are located in the proliferative region of the dorsal and ventral telencephalon next to the ventricle (VZ). In the ganglionic eminences, most SVZ cells and some cells of the MZ also express high levels of SOX2 (see for example SOX2 immunostaining in the LGE of E13.5 embryos in **Figure R.17B**). The quantification of SOX2+ cells in the LGE of E11.5 control and mutant embryos did not shown differences between genotypes, neither in the VZ-SVZ nor in the MZ (**Figure R.17A, C**). By contrast, at E13.5 the number of cells expressing high SOX2 levels in the MZ of the LGE was significantly higher in *NesCre*:*Dyrk1a*-KO embryos than in the controls (**Figure R.17B, C**). In the LGE, SOX2 is expressed in different progenitor types, including RG cells, IP, and other progenitors such as the bRG. These distinct progenitors cycle at different rates, divide at different positions with respect to the ventricle, and undergo different modes of division (see **Figure I.4**). Therefore, the increased number of SOX2+ progenitors observed in the LGE of E13.5 KO embryos may be due to alterations in cell cycle progression and/or in RG lineage progression. The lack of specific markers for each of the distinct progenitors of the ganglionic eminences makes difficult their analysis using immunofluorescence.

A striking phenotype observed in the ventral and dorsal proliferative regions of *NesCre*:*Dyrk1a*-KO brains was the morphology of SOX2+ nuclei, that were smaller and more rounded than in the controls (see **Figures R.17B**, **R.18C and R.19D**). The nuclei of dorsal E11.5 *NesCre*:*Dyrk1a*-HET SOX2+ progenitors were also smaller than normal (control: 65.0±1.3 μm^2; *NesCre*:*Dyrk1a*-HET: 58.9±3.2 μm^2; P=0.048 in a two-tailed Student t-test. n=39-169 nuclei per genotype) although they had a normal shape (circularity index, control: 0.95±0.00; *NesCre*:*Dyrk1a*-HET: 0.96±0.01; P=0.416 in a two-tailed Student t-test). The critical role of DYRK1A in cytoskeleton dynamics (Arbones et al., 2019) may explain these nuclear morphological abnormalities, which could alter chromatin organization and gene expression and could affect the nuclear localization of mechanosensitive transcriptional activators such as YAP (Dupont et al., 2011).

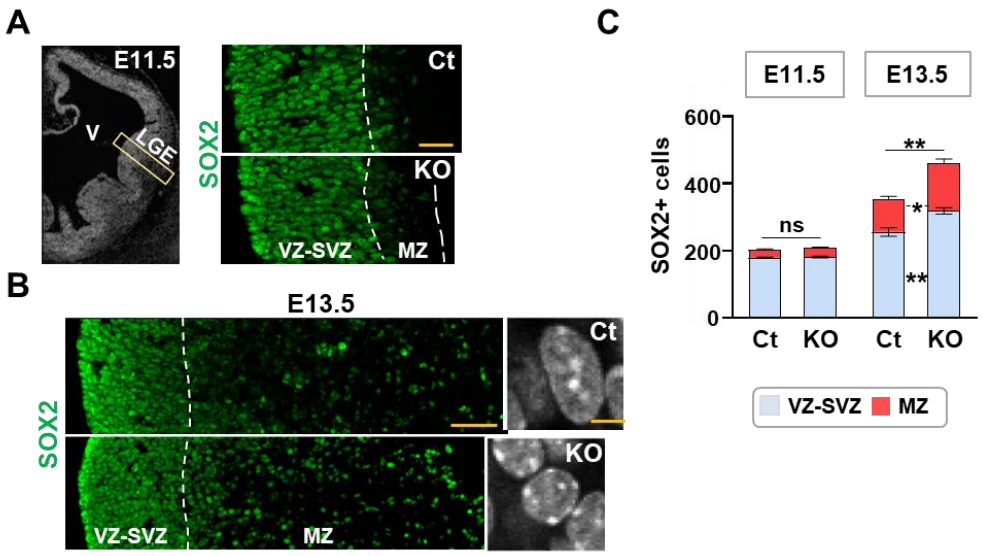

Figure R.17. Number of SOX2 progenitors in the lateral ganglionic eminence of *NesCre*:*Dyrk1a*-KO embryos. (A) Coronal brain section of an E11.5 wild-type embryo and images of the lateral ganglionic eminences (LGE) of control (Ct) and *NesCre*:*Dyrk1a*-KO (KO) brains immunostained for SOX2. Dashed lines delimit the proliferative region (ventricular and subventricular (VZ-SVZ) zones) and the tissue limit. (B) Images of a column of the LGE from E13.5 Ct and KO brains immunostained for SOX2. Dashed lines separate the VZ-SVZ from the mantel zone (MZ). Magnifications of VZ-SVZ nuclei labelled with DAPI showing the difference in shape and size between of Ct and KO nuclei. Notice that the KO LGE has more SOX2+ cells in the MZ than the Ct. (C) Histograms showing the numbers (mean ± SEM) of SOX2+ cells measured in a 150 µm column within the middle of the LGE (yellow rectangle in A). Values correspond to individual embryos. n=3 embryos each genotype at E11.5 and 4-5 embryos at E13.5. ns, not significant; *P<0.05; *P<0.01 in a two-tailed Student t-test. Scale bar: 50 µm (A, B); 4 µm magnification in B.

Next, we tested whether the increase in cell cycle length in *NesCre*:*Dyrk1a*-KO dorsal VZ cells correlates with an increased number of cells undergoing mitosis. To this end, we counted cells in the proliferative regions of E11.5 and E13.5 brains immunostained for phospho-Histone-3 (pH3; phosphorylation at Ser28), phospho-Vimentin (pVim; phosphorylation at Ser55) and SOX2 (**Figures R.18 and R.19**). Of note, H3 phosphorylation begins during G2 and it is maintained through M phase, whereas the phosphorylation of Vimentin occurs when cells enter in mitosis (Crosio et al., 2002; Yamaguchi et al., 2005) (see scheme in **Figure R.18A**). According to their position with respect to the ventricular surface, we classified the mitoses in three subtypes: ventricular mitosis, when the nuclei was next to the ventricle or separated to the ventricle from one nuclei; subapical mitosis, when the mitosis was within the VZ but separated from the ventricle for more than a nuclei; and basal mitosis, when the mitosis was located in the basal border of the VZ at E11.5 or in the SVZ at E13.5 (**Figures R.18A and R.19A**). In the dorsal VZ of E11.5 *NesCre*:*Dyrk1a*-KO embryos, the number of mitoses (pH3+ and pVim+ cells) were augmented due to the increase in subapical and basal mitoses (**Figure R.18A, B**). In addition, the percentage of

pH3+ cells immunopositive for both markers in the *NesCre*:*Dyrk1a*-KOs was very similar to that in the controls (pH3+pVim+ cells/pH3+ cells x 100, controls: 62±5; *NesCre*:*Dyrk1a*-KOs: 58±1; *P*=0.485 in a two-tailed Student *t*-test. n=3 embryos per genotype), suggesting that G2 to M phase transition in the dorsal RG of *NesCre*:*Dyrk1a*-KO embryos is not severely impaired. This data agrees with the cell cycle profiles of control and *NesCre*:*Dyrk1a*-KO dorsal telencephalic cells showing similar percentages of progenitors in G2-M in both genotypes (**Figure R.15**). The same quantifications of pH3+ and pVim+ dividing progenitors were performed in the dorsal telencephalon of E11.5 *NesCre*:*Dyrk1a*-HET littermates, but in this case, we did not detect differences with respect to the controls in the numbers of cells expressing the mitotic markers pH3 and pVim (pH3+ cells in one hemisphere, control: 51±3; *NesCre*:*Dyrk1a*-HET: 49±2; *P*=0.739 in a two-tailed Student *t*-test. pH3+pVim+ cells in one hemisphere, control: 31±2; *NesCre*:*Dyrk1a*-HET: 35±2; *P*=0.277 in a two-tailed Student *t*-test. n=3 embryos per genotype), nor in the position of the mitoses with respect to the ventricle.

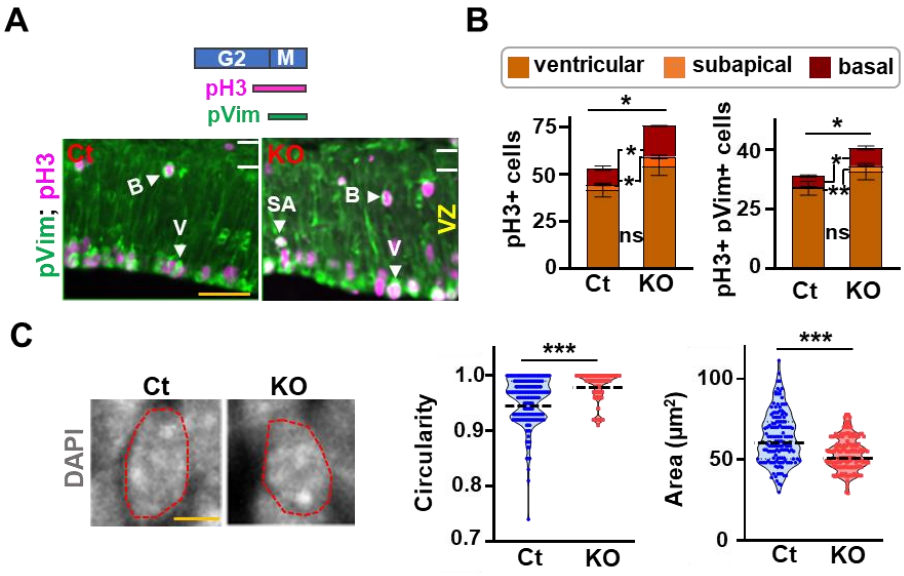

Figure R.18. Number of mitosis and nuclei shape in the dorsal telencephalon of *NesCre*:*Dyrk1a*-KO embryos at the onset of neurogenesis. (A) Scheme showing the expression in G2 and M phases of the mitotic markers pH3 and pVim and representative coronal sections of the dorsal telencephalon of E11.5 control (Ct) and *NesCre*:*Dyrk1a*-KO (KO) embryos immunostained for pH3 and pVimentin (pVim). pH3 and pVim double immunopositive nuclei in the ventricle surface (V) or in more basal positions, subapical (SA) and basal (B), are indicated. (B) Data in the histograms corresponds to the numbers (mean ± SEM) of pH3+ cells (left) and pH3+ pVim+ cells (right) counted in the dorsal telencephalon (one hemisphere). n=3 embryos per genotype. (C) Magnification of the dorsal ventricular zone (VZ) of Ct and KO brains with the nuclei labelled with DAPI and violin plots of the circularity coefficient (left) and area (right) of Ct and KO nuclei. Each point corresponds to a nucleus. Mean values are indicated by black dashed lines. n=80-140 nuclei from 3 embryos each genotype. ns, not significant; *P<0.05; **P<0.01 and ***P<0.001 in a two-tailed Student t-test. Scale bar: 50 µm (A) and 2 µm (C).

In E13.5 brains, we delimitated the SVZ of the dorsal telencephalon by immunostaining with TBR2. This transcription factor is expressed transiently in new-born neurons migrating from the ventricle to the CP and in IPs migrating to the SVZ, where they divide (Englund et al., 2005) (see pictures in **Figure R.19A**). At this developmental stage, the dorsal VZ of *NesCre*:*Dyrk1a*-KO embryos contained more SOX2+ progenitors and less TBR2+ cells than control embryos (**Figure R.19A and B**), indicating that RG differentiation is impaired. TBR2+ cells were also decreased in the SVZ of *NesCre*:*Dyrk1a*-KO embryos, but the differences with respect to the controls did not reach statistical significance (**Figure R.19B**). However, the SVZ of *NesCre*:*Dyrk1a*-KO embryos had more pH3+ cells (**Figure R.19C**), suggesting an increase in the mitotic index of mutants IPs. Ventricular and subapical mitoses were also more abundant in the dorsal VZ of *NesCre*:*Dyrk1a*-KO brains, which correlates with the increased number of progenitors (**Figure R.19B and C**). Of note, subapical mitoses were disproportionally high in the dorsal VZ of *NesCre*:*Dyrk1a*-KO brains at both E11.5 and E13.5 (**Figures R.18A, B and R.19C**), indicating that bRG cells are more abundant than normal.

At E13.5, *NesCre*:*Dyrk1a*-HETs embryos did not show statistical differences with respect to the controls in the numbers of SOX2+ cells (control: 258±4; *NesCre*:*Dyrk1a*-HET: 285±10; *P*=0.059 in a two-tailed Student *t*-test. n=3-4 embryos per genotype) nor in TBR2+ cells (numbers in the VZ, control: 32±1; *NesCre*:*Dyrk1a*-HET: 27±6; *P*=0.489 in a two-tailed Student *t*-test. Numbers in the SVZ, control: 103±9; *NesCre*:*Dyrk1a*-HET: 111±5; *P*=0.487 in a two-tailed Student *t*-test. n=3 embryos per genotype), indicating that 50% reduction in DYRK1A activity does not have an impact on the differentiation program of dorsal RG progenitors.

In the LGE of *NesCre*:*Dyrk1a*-KO embryos, mitoses were more abundant than in the controls at both E11.5 and E13.5 (**Figure R.20A and B**). Similar to the dorsal telencephalon, the number of total mitoses was increased at E11.5, due to a rise in subapical mitoses, and at E13.5, due to a rise in ventricular, subapical, and basal mitoses (**Figures R20A and B**). Double pH3+pVim+ cells in the LGE at the developmental stage analysed (E11.5) were similarly abundant in control and *NesCre*:*Dyrk1a*-KO brains. As with the cells expressing only pH3, subapical pH3+pVim+ cells were also more abundant in the LGE of the KO brains (**Figure R.20A**). Moreover, the percentages of pH3+pVim+ mitoses in the LGE of *NesCre*:*Dyrk1a*-KO embryos were similar to that of controls (control: 58±1; *NesCre*:*Dyrk1a*-KO: 62±5; *P*=0.485 in a two-tailed Student *t*-test. n=3 embryos per genotype), supporting the notion that progression through G2 and M phases in *Dyrk1a* null progenitors is not affected. Together, these results indicate that the lack of DYRK1A affects the apical-basal position in which progenitors divide or the mode of division of RG-derived progenitors favouring the formation of subapical progenitors.

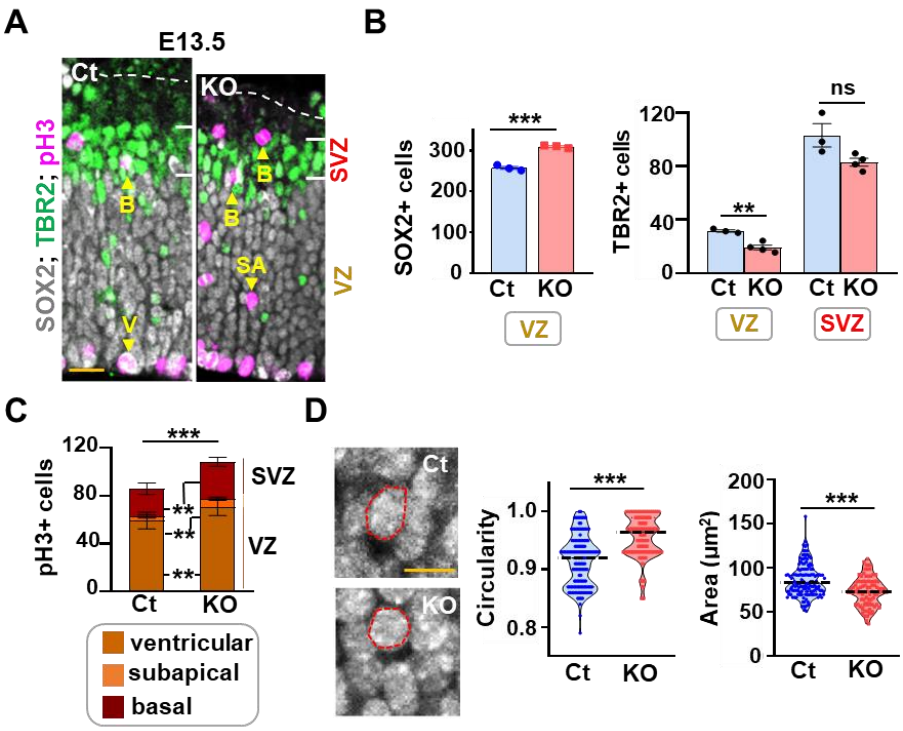

Figure R.19. Number of mitosis and nuclei shape in the dorsal telencephalon of *NesCre*:*Dyrk1a*-KO embryos at mid-neurogenesis. (A) Representative coronal sections of the dorsal telencephalon of E13.5 control (Ct) and *NesCre*:*Dyrk1a*-KO (KO) embryos immunolabelled for SOX2, TBR2 and pH3. Arrowheads point to ventricular (V), subapical (SA), and basal (B) mitosis. (B) histograms with the number of SOX2+ cells (mean ± SEM) counted in 200 µm width columns and of TBR2+ cells counted in the ventricular zone (VZ) and the subventricular zone (SVZ) of a 300 µm width column. (C) Numbers of ventricular, subapical, and basal mitosis immunolabeled for pH3 (mean ± SEM) in the whole dorsal telencephalon (one hemisphere). n=3-4 embryos each genotype. (D) Magnifications of Ct and KO VZs with the nuclei labelled with DAPI. Notice the different shape of the encircle nuclei. Violin plots showing the circularity coefficient (left) and area (right) of Ct and KO nuclei. n=80-140 nuclei from 3 embryos each genotype. Mean values are indicated by black dashed lines. ns, not significant; **P<0.01 and ***P<0.001 in a two-tailed Student t-test. Scale bar: 50 µm (A) and 7 µm (D).

Given that the integrity of ventral structures is severely altered in the *NesCre*:*Dyrk1a*-KO embryos from mid neurogenesis onwards, the analysis of mutant embryos at late embryonic stages (E15.5 and E17.5) were performed only in the dorsal telencephalon. The numbers of SOX2+ progenitors in the dorsal telencephalon of *NesCre*:*Dyrk1a*-KO embryos were normal at E15.5 but significantly decreased at E17.5 (**Figure R.21**), indicating an earlier exhaustion of the NSC pool. This could be due, at least in part, to the increased apoptosis observed in the dorsal germinal region at earlier developmental stages (**Figures R-7A, B and R.8**). In accordance with this possibility, the dorsal VZ-SVZ of E17.5 *NesCre*:*Dyrk1a*-KO brains also presented fewer cells expressing the IP marker TBR2 (**Figure R.22**). Of note, the numbers of TBR2 progenitors in the dorsal VZ-SVZ of *NesCre*:*Dyrk1a*-HET littermate embryos were normal (number in 350 µm radial columns,

control: 129±3; *NesCre*:*Dyrk1a*-HET: 122±6; *P*=0.880 in a two-tailed Student *t*-test. n=3-4 embryos each genotype), again indicating that dorsal RG differentiation in these embryos is not significantly altered.

The results presented so far show that DYRK1A depletion in dorsal RG cells during early neurogenesis alters cell cycle progression and changes their mode of division leading to an increase in pluripotent RG (SOX2+) cells at the expense of neurons or progenitors (IPs) committed to produce neurons (**Figures R.16 and R.19B**). In the ventral telencephalon, the depletion of DYRK1A causes a rapid and severe reduction of neurons (see the reduction of ventral brain parenchyma in *NesCre*:*Dyrk1a*-KO embryos at E13.5, **Figure R.5A**).

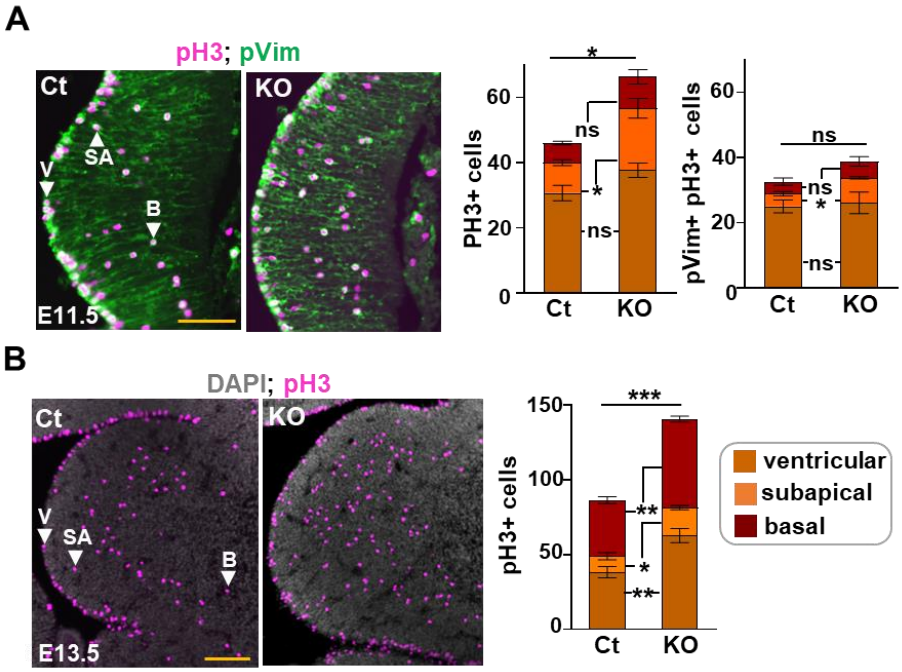

Figure R.20. Number of mitosis in the lateral ganglionic eminence of *NesCre*:*Dyrk1a*-KO embryos at early and mid-neurogenesis. (A) Representative coronal sections of the lateral ganglionic eminence (LGE) of E11.5 control (Ct) and *NesCre*:*Dyrk1a*-KO (KO) embryos immunolabeled for pH3 and pVimentin (pVim). Arrowheads point to ventricular (V), subapical (SA) and basal (B) pH3+ pVim+ progenitors. Data in the histograms corresponds to the number (mean ± SEM) of V, SA and B pH3+ cells (left) and pH3+ pVim+ cells (right) in the whole LGE. n=3 embryos per genotype. (B) Representative coronal sections of the LGE of E13.5 Ct and KO embryos. Cells in mitosis are stained for pH3. Arrowheads point to V, SA and B mitosis. Notice that the KO has more mitosis than the Ct. Data in the histogram correspond to the number (mean ± SEM) of pH3+ cells in the whole LGE. n=5-7 embryos each genotype. ns, not significant; *P<0.5; **P<0.01 and ***P<0.001 in a two-tailed Student t-test. Scale bar: 200 μm (A) and 100 μm (B).

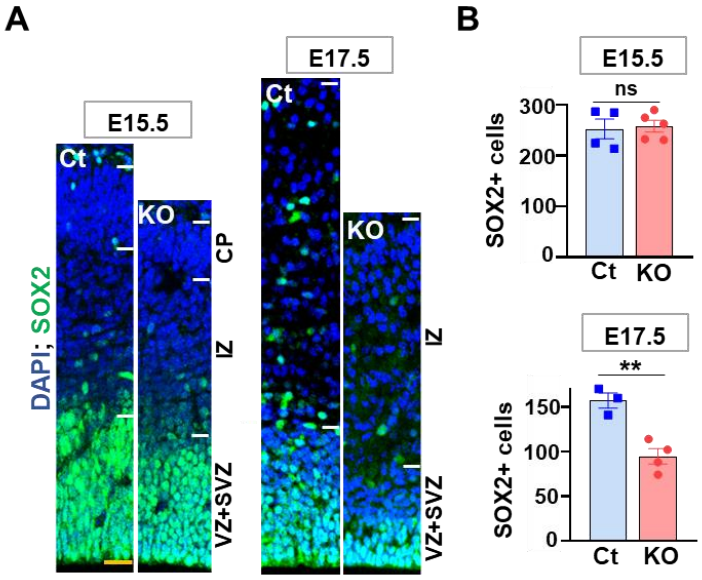

Figure R.21. Number of apical progenitors in the dorsal telencephalon of *NesCre*:*Dyrk1a*-KO embryos at late neurogenesis. (A) Representative coronal sections of E15.5 and E17.5 control (Ct) and *NesCre*:*Dyrk1a*-KO (KO) embryos immunostained for SOX2 and the nuclei labelled with DAPI. (B) Data in the histograms corresponds to the number of SOX2+ cells (mean ± SEM) counted in the VZ of a 200 µm width column of the dorsal telencephalon at the indicated developmental stages. Values correspond to individual embryos. n= 3-5 embryos each genotype. CP, cortical plate; IZ, intermediate zone; SVZ, subventricular zone; VZ, ventricular zone. ns, not significant; **P<0.01 in a two-tailed Student t-test. Scale bar: 30 µm.

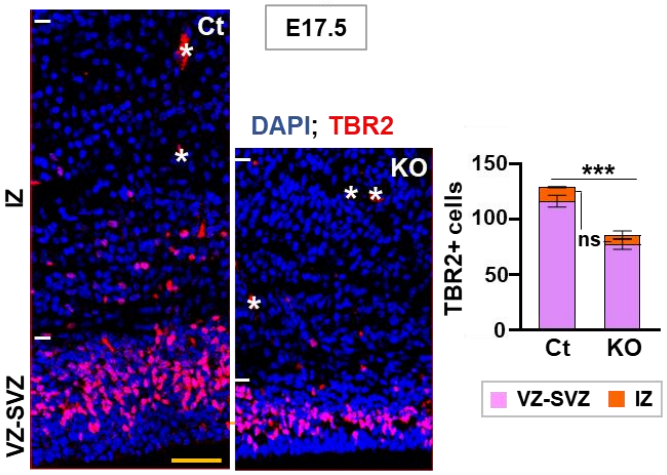

Figure R.22. Number of TBR2 progenitors in the dorsal telencephalon of *NesCre*:*Dyrk1a*-KO embryos at late neurogenesis. Representative coronal sections of E17.5 control (Ct) and *NesCre*:*Dyrk1a*-KO (KO) embryos immunostained for TBR2 and the nuclei labelled with DAPI. Asterisks point to autofluorescent signal from blood vessel cells. The histogram shows the number of TBR2+ cells (mean ± SEM) in the ventricular and subventricular zones (VZ-SVZ) and intermediate zone (IZ) counted in a 300 µm column of the dorsal telencephalon. Values correspond to individual embryos. n=3-4 embryos each genotype. ns, not significant; ***P<0.001 in a two-tailed Student t-test. Scale bar: 50 µm.

Compelling evidences obtained by the analysis of cortical neurogenesis in the mouse indicate that alterations in the duration of the cell cycle of the RG, particularly the duration

of G1 and S phases, impact on the fate of their progeny (Arai et al., 2011; Salomoni and Calegari, 2010). The reduced numbers of TBR2+ cells in the dorsal VZ of E13.5 *NesCre*:*Dyrk1a*-KO brains indicate that neuron production is compromised in these brains. Thus, we next analysed the telencephalon of control and *NesCre*:*Dyrk1a*-KO littermates before the peak of ventral (E11.5) and dorsal (E13.5) apoptosis using neuronal markers. At E11.5, there were already many cells expressing Tubulin Beta-III (TUJ1), a microtubule component expressed primarily on neurons (Sullivan and Cleveland, 1986), in the MZ of the LGE and MGE in control embryos. TUJ1 immunostaining in the ventral eminences of the KO embryos followed a similar immunostaining pattern than the controls but the staining occupied less territory (see images in **Figure R.23A**). TUJ1 immunostaining pattern was also similar in the dorsal telencephalon of control and *NesCre*:*Dyrk1a*-KO brains but the thickness of the immunostained layer (MZ) was disproportionally reduced in the KOs (**Figure R.23A**). These results suggest that neurogenesis in *NesCre*:*Dyrk1a*-KO brains is impaired or delayed. Consistent with the lack of phenotype of the *NesCre*:*Dyrk1a*-HET brain, TUJ1 immunostaining in E11.5 *NesCre*:*Dyrk1a*-HET brains was very similar than in the controls (data not shown).

Next, we immunostained control and *NesCre*:*Dyrk1a*-KO coronal brain sections with antibodies against TBR2 and TBR1 and counted TBR2+ and TBR1+ cells in the prospective somatosensory cortex. As mentioned, TBR2 is expressed in newborn neurons and intermediate progenitors produced by RG in the ventricular surface. Neurons migrating from the VZ to the MZ/CP downregulate TBR2 and upregulate TBR1 (Englund et al., 2005) (**Figure R.23B**). At E11.5, most cells in the dorsal MZ still express TBR2 in both control and *NesCre*:*Dyrk1a*-KO embryos (**Figure R.23C**). Accordingly with the immunostainings with TUJ1 (**Figure R.23A**), the MZ of the KO dorsal telencephalon had less TBR1 expressing cells than the control (**Figure R.23D**). These observations indicate a delay in the production and/or differentiation of early-born cortical neurons in *Dyrk1a* null mutant embryos. Of note, *NesCre*:*Dyrk1a*-HET embryos showed a small increase in TBR1+ cells in the dorsal MZ (TBR1+ cells in a 350 μm wide column, control: 24±0.6; *NesCre*:*Dyrk1a*-HET: 27±0.81; P=0.021 in a two-tailed Student t-test. n=3-4 embryos per genotype), which is consistent with the advanced neurogenesis observed in the *Dyrk1a*$^{+/-}$ haploinsufficiency mouse model (Najas et al., 2015).

To provide further evidence of the impact of the conditional *Dyrk1a* null mutation in dorsal neurogenesis, we immunostained E13.5 *NesCre*:*Dyrk1a*-KO, *NesCre*:*Dyrk1a*-HET and control brains for TUJ1 and TBR1. In *NesCre*:*Dyrk1a*-KO brains, the thickness of the layers immunostained for TUJ1 (IZ and CP) was reduced whereas the thickness of the proliferative layers (VZ-SVZ) was increased (**Figure R.24A**). Accordingly, the dorsal telencephalon of E13.5 *NesCre*:*Dyrk1a*-KO had less TBR1+ neurons than the controls

(**Figure R.24B and C**). These results agree with the increased number of SOX2+ progenitors observed at this developmental stage in *NesCre*:*Dyrk1a*-KO brains (**Figure R.19B**) and indicate that direct neurogenesis (neurons produced directly by RG cells; see **Figure I.6**) is impaired in the KO brains. TBR1 expression in differentiating cortical neurons is transient with the exception of layer VI neurons where the expression of this transcription factor is maintained high to adulthood (Hevner et al., 2001). At E15.5, TBR1+ neurons in the CP were less abundant in *NesCre*:*Dyrk1a*-KO embryos than in the controls (**Figure R.24B and C**), which is consistent with a role of DYRK1A in RG differentiation.

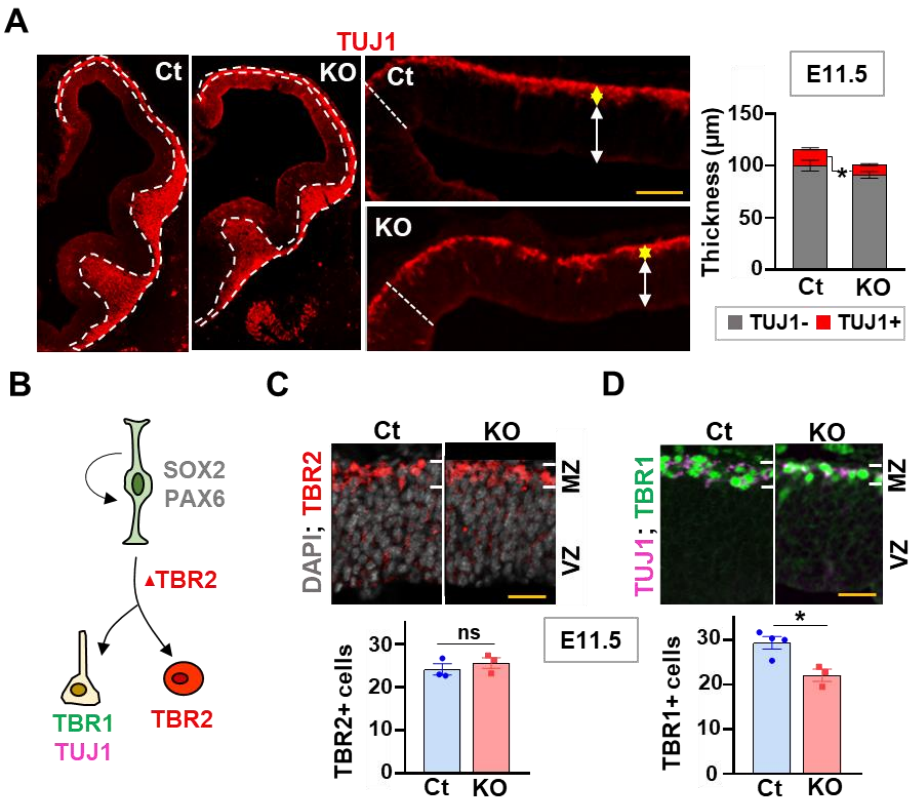

Figure R.23. Differentiation in the *NesCre*:*Dyrk1a*-KO brain at early neurogenesis. (A) Representative images of a brain hemisphere (left) and the dorsal telencephalon (right) of E11.5 control (Ct) and *NesCre*:*Dyrk1a*-KO (KO) embryos showing the immunostaining for the pan-neuronal marker TUJ1. Yellow and white double arrowheads indicate the thickness of the mantle zone (MZ; TUJ1+) and the ventricular zone (VZ; TUJ1-) of the dorsal telencephalon, respectively. Discontinuous white lines in the pictures on the right delimitate the medial part of the telencephalon. The histogram shows the average thickness of the VZ (TUJ1-) and MZ (TUJ1+) (mean ± SEM) measured in 3 regions of the dorsal telencephalon. (B) Scheme showing the expression of the transcription factors SOX2, PAX6, TBR2 and TBR1 in progenitors and postmitotic cells. (C, D) Representative images of the dorsal telencephalon of Ct and KO embryos immunostained for TBR2 and the nuclei labelled with DAPI (C) or for TUJ1 and TBR1 (D). The histograms in C and D correspond to the number (mean ± SEM) of TBR2+ cells (C) and TBR1+ cells (D) counted in a 300 µm wide column. n=3-4 embryos each genotype. ns, not significant; *P<0.05 in a two-tailed Student t-test. Scale bar: 100 µm (A) and 30 µm (C, D).

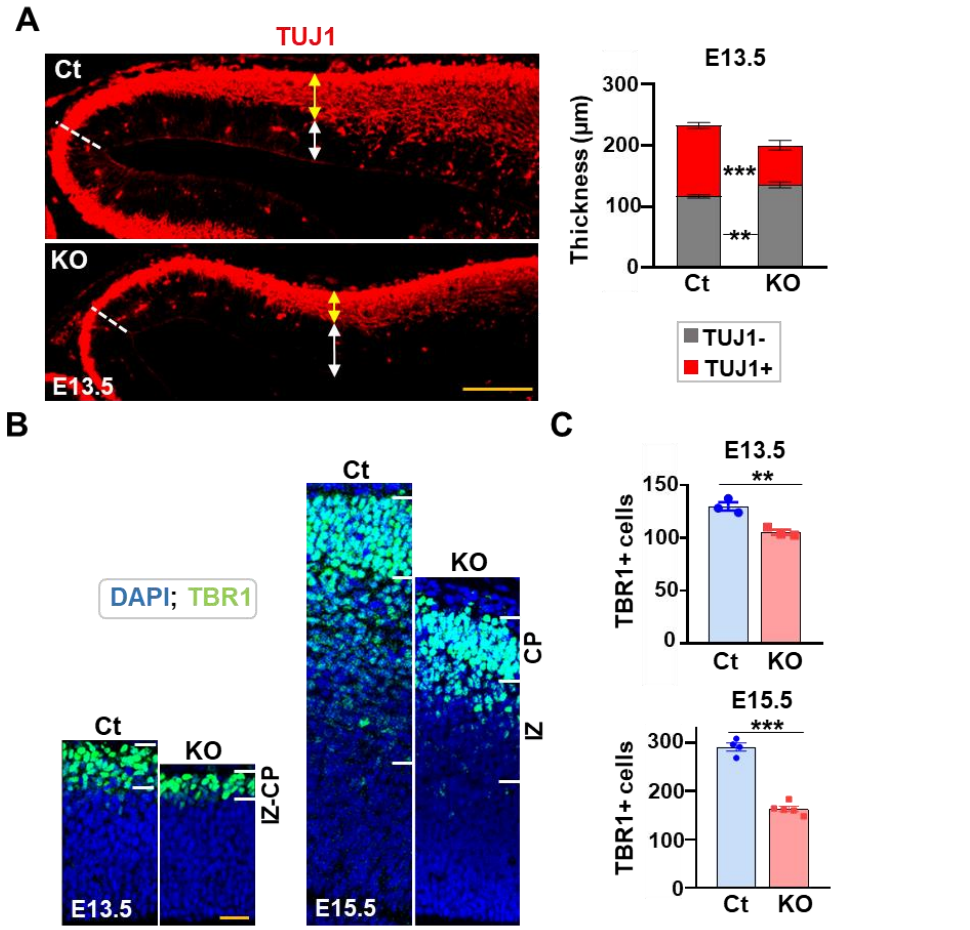

Figure R.24. Differentiation in the dorsal telencephalon of *NesCre*:*Dyrk1a*-KO embryos at mid neurogenesis. (A) Representative coronal brain sections of E13.5 control (Ct) and mutant (KO) embryos immunostained for TUJ1. Yellow and white arrowheads indicate the thickness of the intermediate zone (IZ) and cortical plate (CP) (TUJ1+) and the progenitor region (TUJ1-), respectively. Data in the histogram corresponds to the thickness of the TUJ1+ and TUJ1- regions (mean ± SEM) measured in the position indicated by double arrowheads. (B) Representative images of the dorsal telencephalon of E13.5 and E15.5 Ct and KO embryos immunostained for TBR1 and the nuclei labelled with DAPI. (C) Histograms showing the average number of TBR1 neurons (mean ± SEM) counted in the CP of a 300 µm wide column of the dorsal telencephalon in E13.5 and E15.5 embryos. Values correspond to individual embryos. n=3-4 embryos each genotype at E13.5 and 4-5 embryos at E15.5. **P<0.01 and ***P<0.001 in a two-tailed Student t-test. Scale bar: 200 µm (A) and 50 µm (B).

Next, we evaluated the impact of the *Dyrk1a* null mutation in indirect cortical neurogenesis (neurons produced by IPs; see **Figure I.6**). To this end, we immunostained E17.5 control and *NesCre:Dyrk1a*-KO brain coronal sections for the neuronal markers CTIP2, to label layer V neurons (Arlotta et al., 2005), and SATB2 to label callosal neurons, most of which layer II-III (late-born) neurons (Britanova et al., 2008). As shown in **Figure R.25A** the thickness of the dorsal telencephalon in *NesCre:Dyrk1a*-KO brains was abnormally reduced (control: 1130.32±43.20 µm; *NesCre*:*Dyrk1a*-KO: 874.11±25.08 µm; *P*=0.005 in a two-tailed Student *t*-test. n=3-4 embryos per genotype), indicating that in

addition to the defects in lateral expansion (growth of the telencephalic vesicles; see **Figure R.1**), radial expansion of the dorsal telencephalon is also affected in *NesCre*:*Dyrk1a*-KOs embryos. Layer distribution of CTIP2+ and SATB2+ neurons in these embryos was similar to the controls (**Figure R.25A**).

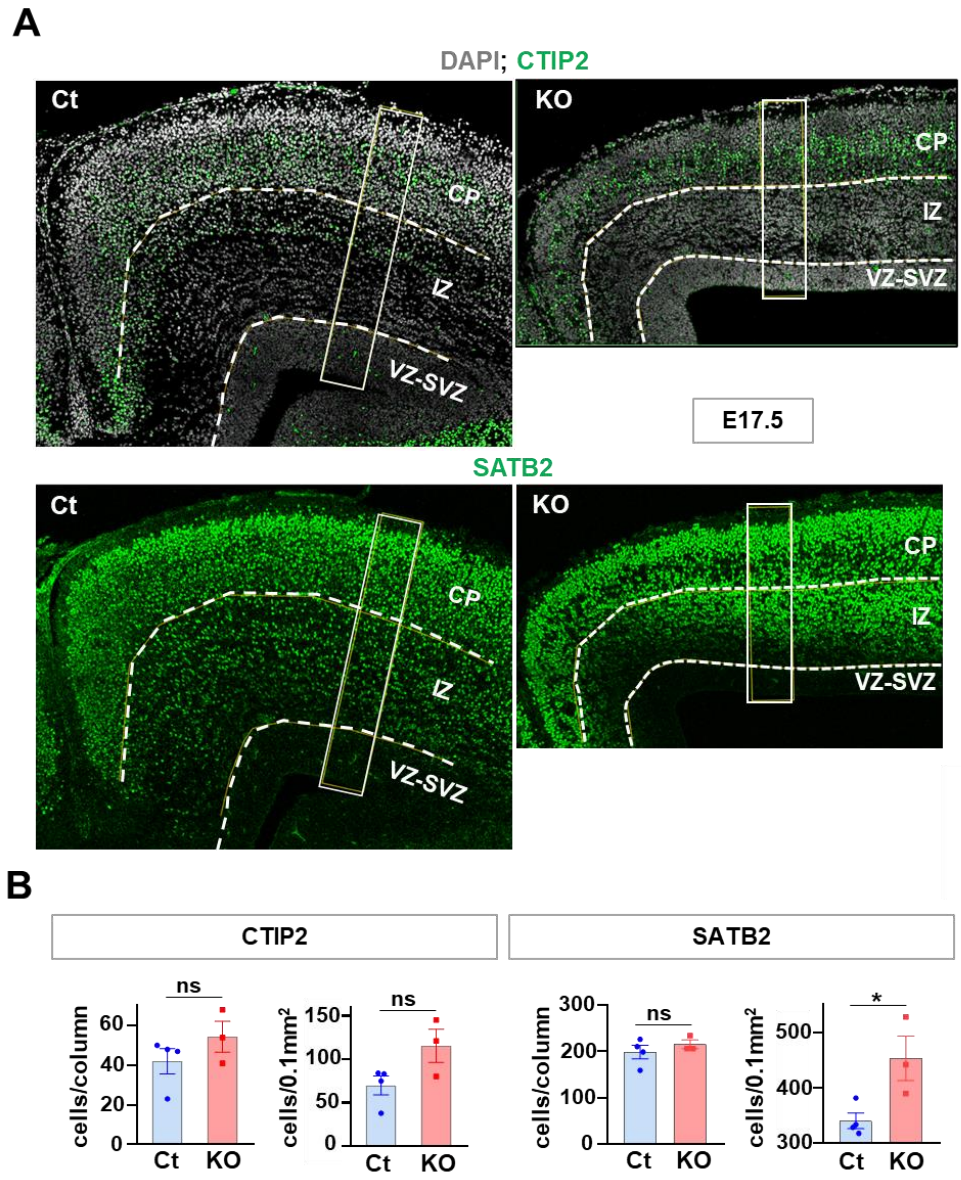

Figure R.25. Neuron numbers in the dorsal telencephalon of *NesCre*:*Dyrk1a*-KO embryos at late neurogenesis. (A) Representative images of the dorsal telencephalon in E17.5 control (Ct) and *NesCre*:*Dyrk1a*-KO (KO) brains immunostained for CTIP2 and nuclei stained with DAPI (upper panels) and for SATB2 (lower panels). (B) The histograms show the numbers of CITP2+ and SATB2+ neurons counted in a 120 µm wide column and the neuronal densities within the column. The position of the columns is indicated by a rectangle in the pictures in A. Values (mean ± SEM) correspond to individual embryos. n=3-4 embryos each genotype. CP, cortical plate; IZ, intermediate zone; VZ-SVZ, ventricular-subventricular zone. ns, not significant and *P<0.05 in a two-tailed Student t-test. Scale bar: 200 µm.

CITP2+ neurons in both genotypes were mostly located in the CP with few neurons located in the IZ. In contrast, SATB2+ neurons were abundant in both the CP and the IZ,

although in the controls these neurons were more spread than in the *NesCre*:*Dyrk1a*-KO embryos, where they tended to accumulate to the external region of these two layers (**Figure R.25A**). The quantification of CITP2 and SATB2 neurons in the prospective somatosensorial cortex of control and *NesCre*:*Dyrk1a*-KO brains did not shown differences between genotypes in the numbers of these two neuron types (**Figure R.25B**). This was an unexpected result considering the levels of apoptosis observed at E15.5 in the IZ and CP of the *NesCre*:*Dyrk1a*-KO embryos (**Figure R.8**). Due to the reduced thickness of the dorsal IZ and CP in *NesCre:Dyrk1a*-KO embryos (**Figure R. 25A**), the densities of CITP2 and SATB2 in these embryos were significantly higher than in the controls (**Figure R.25B**). At E17.5, there were fewer SOX2+ cells and TBR2 cells in the dorsal VZ-SVZ of the *NesCre*:*Dyrk1a*-KO brains (**Figure R.22**), a result that is consistent with an enhanced terminal differentiation and thus, to an earlier depletion of the progenitors.

Taken together, the analysis of the dorsal telencephalon of *NesCre*:*Dyrk1a*-KO brains throughout development indicates alterations in the neurogenic program of the RG, affecting both early and late neurogenesis.

6. Characterization of the *Sox2CreERT2*:*Dyrk1a* conditional mutant

Compelling evidences indicate that afferents from thalamic neurons are key for cortical neurogenesis (Monko et al., 2022). Thus, the severe and early brain phenotype shown by the *NesCre*:*Dyrk1a*-KO mutant precluded the study of DYRK1A functions during mid- and late-neurogenesis. To circumvent this problem, we generated the *Sox2*Cre*ERT2*:*Dyrk1a* conditional mutant mouse using the *Sox2CreERT2* transgenic mouse. In this transgenic line, Cre-recombinase expression is induced upon tamoxifen treatment in the RG of the embryonic dorsal telencephalon and in the subgranular zone of the hippocampus in postnatal and adult animals (Favaro et al., 2009). The expression of Cre-recombinase in *Sox2CreERT2* embryos was previously analysed only at mid-gestation (E14.5) and not at the cellular level (see Supplementary data in (Favaro et al., 2009). To have a better knowledge of the induction of Cre-recombinase by the *Sox2CreERT2* transgene during neurogenesis, we examined the expression of the loxP reporter tdTomato in brain sections of E11.5, E13.5, and E15.5 *Sox2CreERT2*+:*Dyrk1a*$^{Fl/Fl}$:tdTomato$^{+/-}$ embryos (*Sox2*Cre*ERT2*:*Dyrk1a*-KO:tdTomato+ embryos from now on) treated with tamoxifen 48 h before sacrifice (see crosses to obtain these embryos in **Figure M.1**). As shown in **Figure R.26**, at E11.5 *Sox2*Cre*ERT2*:*Dyrk1a*-KO:tdTomato+ embryos showed cells with high tdTomato expression in both dorsal and ventral brain structures. At E13.5, the expression was high only in cells of the dorsal telencephalon and in the LGE. The

dorsalization of the reporter in *Sox2*Cre*ERT2*:*Dyrk1a*-KO:tdTomato+ embryos was more evident at E15.5 than in earlier developmental stages (compare images in **Figure R.26A, B and C**). To have an estimation of the progenitors that carried the *Dyrk1a* null mutation, we counted cells with high tdTomato levels in the proliferative regions (VZ and SVZ) of the dorsal telencephalon and the LGE of tamoxifen treated E11.5, E13.5 and E15.5 *Sox2*Cre*ERT2*:*Dyrk1a*-KO:tdTomato+ embryos. The percentages of tdTomato+ cells were similar in the different development stages analysed and ranged from 34% to 43% in the dorsal telencephalon and from 37% to 45% in the LGE (E11.5: dorsal telencephalon 34±1% and LGE 45±2%; E13.5: dorsal telencephalon 34±2% and LGE 37±3%; E15.5: dorsal telencephalon 43±1% and LGE 40±1%. n=2 hemispheres from 1-2 embryos each developmental stage). These results indicate that tamoxifen-induced expression of Cre-recombinase is effective only in a subset of SOX2 progenitors, thus generating a mosaic of wild-type and *Dyrk1a* mutant RG cells and their derivatives (IPs and neurons).

To gain insights into the role of DYRK1A during mid-corticogenesis, when most neurons are produced by indirect neurogenesis, we injected *Dyrk1a*$^{Fl/Fl}$ pregnant females that have been crossed with *Sox2CreERT2*+:*Dyrk1a*$^{Fl/+}$:tdTomato$^{+/-}$ males (**Figure M.1**) with tamoxifen at E11.5 and analysed the embryos at the end of neurogenesis (E18.5). Preliminary observations of the resulting *Sox2*Cre*ERT2*:*Dyrk1a*-KO:tdTomato+ embryos did not reveal any notorious alterations in the thickness of the dorsal telencephalon, number of cortical neurons and progenitors nor in pyknotic nuclei (data not shown) when compared to controls (*CreERT2*- embryos; see **Figure M.1**). These observations suggest that the abrogation of DYRK1A activity in the dorsal RG after E11.5 does not have a major effect on cortical cell differentiation and survival. Next, we checked whether the deletion of *Dyrk1a* sequences in the conditional *Sox2*Cre*ERT2*:*Dyrk1a*-KO:tdTomato+ earlier in development has any effect in neurogenesis. To this end, tamoxifen injections were done at E9.5 and the embryos were collected at E14.5. The expression pattern of the loxP tdTomato reporter gene and percentages of cells expressing this gene (30±2% of the cells in the dorsal telencephalon and 38±6% of the cells in the LGE) in E14.5 *Sox2*Cre*ERT2*:*Dyrk1a*-KO:tdTomato+ brains were similar than in E13.5 embryos treated with tamoxifen 48 h before sacrifice (compare **Figures R.26B and R.27A**). This support the notion that the mosaicism of the *Dyrk1a* mutation is independent of the time of tamoxifen treatment. TUJ1 and SOX2 immunostainings of brain sections from control and *Sox2*Cre*ERT2*:*Dyrk1a*-KO:tdTomato+ littermates did not show any difference between genotypes in total cortical thickness nor in the relative thickness of layers occupied by progenitors (VZ-SVZ; SOX2+TUJ1-) and neurons (IZ and CP; SOX2-TUJ1+) (see **Figure R.27B**). This result is in contrast with the reduced number of neurons and increased number of progenitors observed in the dorsal telencephalon of the conditional *NesCre*:*Dyrk1a*-KO model at E13.5 (**Figures R.19A, B and**

R.24). According to the accepted model of mouse cortical neurogenesis (see **Figure I.6**), tamoxifen treatments at E9.5 should be sufficient to induce Cre-recombinase expression, and therefore to delete floxed sequences, when the first cortical neurons are produced. The analysis of the conditional *Sox2*Cre*ERT2*:*Dyrk1a*-KO:tdTomato+, although preliminary, suggests that cortical neurogenesis is not affected in this mutant, probably due to the fact that the mutation is in mosaicism.

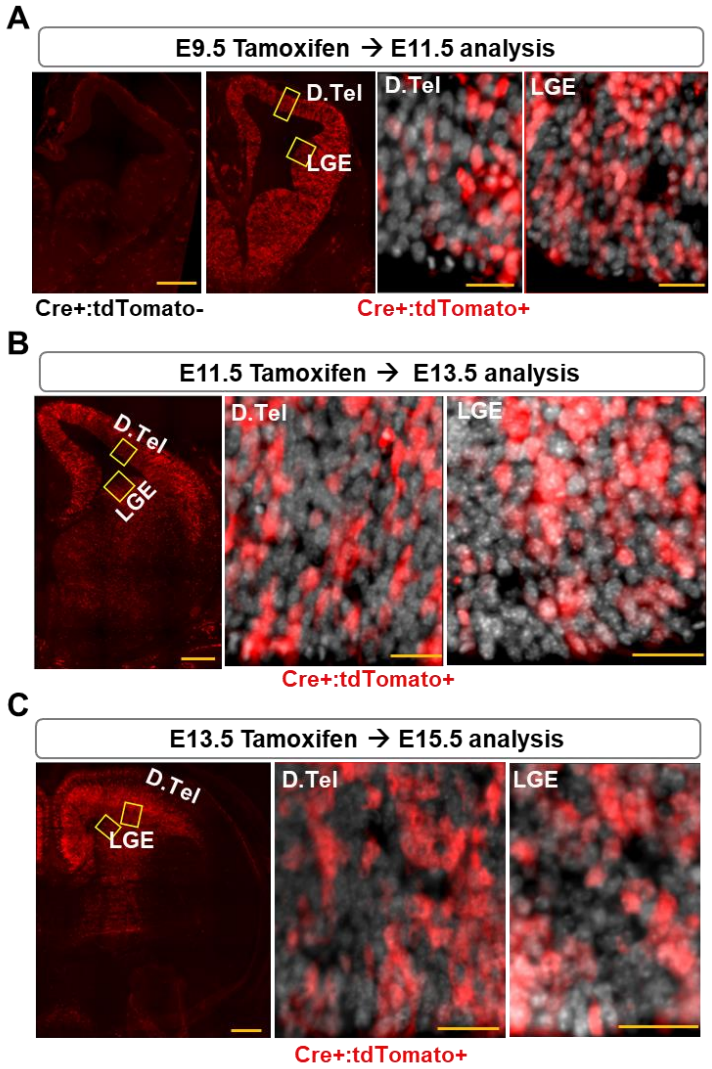

Figure R.26. Tamoxifen induced Cre-recombinase in the telencephalon of *Sox2CreERT2*:tdTomato embryos. Brain sections of the telencephalon of E11.5 (A), E13.5 (B) and E15.5 (C) embryos treated with tamoxifen 48h before sacrifice. The loxP reporter tdTomato labels cells expressing Cre-recombinase (in red). Pictures are from *Sox2CreERT2*:tdTomato (Cre+:tdTomato+) embryos except for the picture on the left in panel A that is from a Sox2Cre (Cre+:tdTomato-) embryo. The two pictures on the right in panels A to C correspond to amplifications of the regions delimited by yellow rectangles in the picture on the left. Note that in A, tdTomato in Cre+:tdTomato+ brains is equally expressed in the dorsal and the ventral telencephalon, and that this expression is more restricted to the dorsal telencephalon as neurogenesis advances (B and C). D. Tel, dorsal telencephalon; LGE, lateral ganglionic eminence. Scale bar: 300 µm (whole telencephalon), 25 µm (amplifications in D. Tel) and 30 µm (amplifications in LGE).

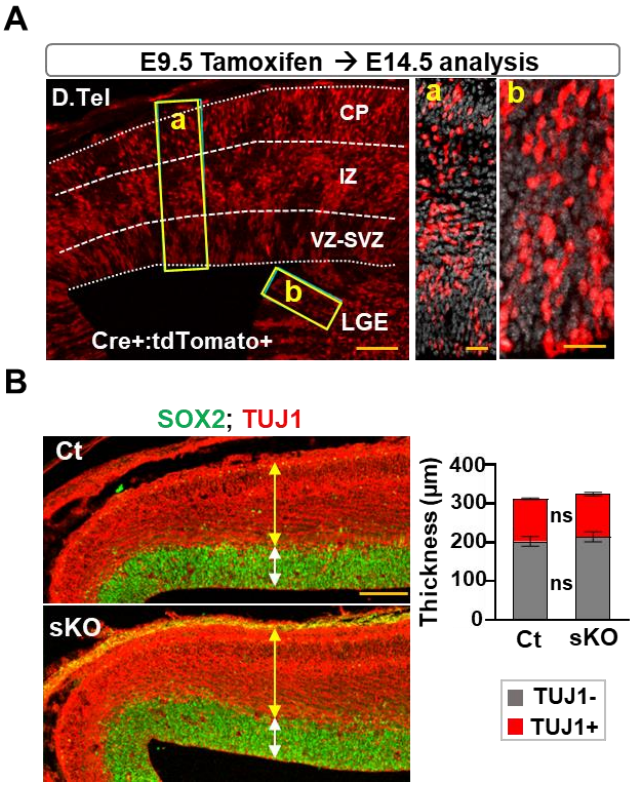

Figure R.27. Brain phenotype of *Sox2CreERT2*:*Dyrk1a*-KO:tdTomato embryos treated with tamoxifen at E9.5 and analysed at E14.5. (A) Pictures showing the expression of tdTomato (red cells) in the dorsal telencephalon (D. Tel) of a *Sox2CreERT2*:*Dyrk1a*-KO:tdTomato (Cre+:tdTomato+) embryo. Pictures on the right correspond to amplifications of the area delimited by yellow rectangles in the picture on the left. (B) Representative sections of the D. Tel of control (Ct) and *Sox2CreERT2*:*Dyrk1a*-KO:tdTomato (sKO) immunolabeled for SOX2 and TUJ1. The histogram on the right indicate the thickness (mean ± SEM) of the ventricular and subventricular zones (SOX2+; TUJ1-, white arrows) and the intermediate zone and cortical plate (SOX2-; TUJ1+, yellow arrows). ns, not significant in a two-tailed Student t-test. Scale bar: 100 µm (A and B) and 30 µm (a and b).

One of the earliest phenotypes detected in *NesCre*:*Dyrk1a*-KO brains was the anomalous nuclear morphology of dorsal and ventral SOX2 progenitors (**Figures R.17B, R.18C and R.19D**). Therefore, we next measured the circularity and area of tdTomato+ (*Dyrk1a* mutant) and tdTomato- (control) nuclei in the VZ of the dorsal telencephalon and the LGE of E14.5 *Sox2*Cre*ERT2*:*Dyrk1a*-KO:tdTomato+ embryos that were treated with tamoxifen at E9.5. As shown in **Figure R.28**, tdTomato+ nuclei had similar size (area) and shape (circularity) than control nuclei in both brain regions. Next, we assessed whether cell survival is compromised in the dorsal telencephalon of *Sox2*Cre*ERT2*:*Dyrk1a*-KO:tdTomato+ embryos. To this end, first we counted the number of pyknotic nuclei in the whole dorsal telencephalon of E14.5 *Sox2*Cre*ERT2*:*Dyrk1a*-KO:tdTomato+ embryos and control littermates treated with tamoxifen at E9.5 (**Figure 29**).

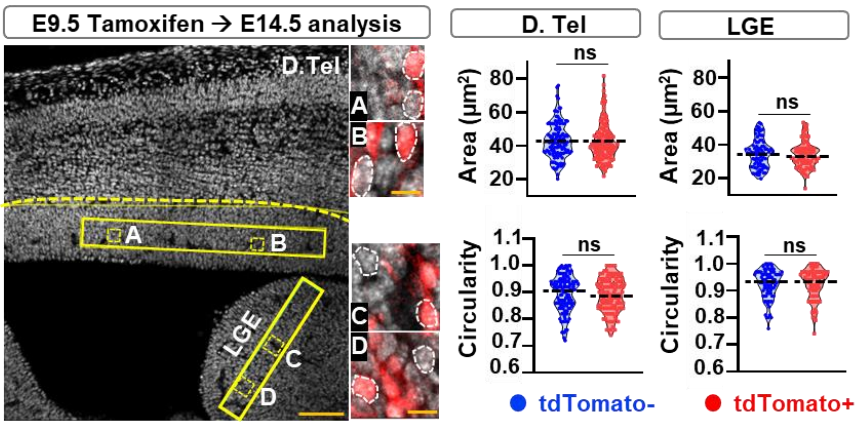

Figure R.28. Nuclear size and shape of progenitors of the telencephalon of *Sox2CreERT2*:*Dyrk1a*-KO:tdTomato embryos treated with tamoxifen at E9.5 and analysed at E14.5. Representative image of the brain of a *Sox2Cre*ERT2:*Dyrk1a*-KO:tdTomato embryo with the nuclei labelled with DAPI indicating the areas in the dorsal telencephalon (D. Tel) and the lateral ganglionic eminence (LGE) (yellow rectangles) where the nuclei where analysed. The yellow dotted line marks the separation between the proliferative region and the intermediate zone. Pictures on the right correspond to amplifications of the squares indicated by dashed lines and show representative tdTomato+ and tdTomato- nuclei. Points in the violin plots correspond to the circularity index and area of control (tdTomato-) and *Dyrk1a* mutant (tdTomato+) nuclei of the D. Tel (n=125 nuclei each genotype) and LGE (n=83 nuclei each genotype). Mean values are indicated by black dashed lines. ns, not significant in a two-tailed Student t-test. Scale bar: 100 µm and 10 µm (magnifications).

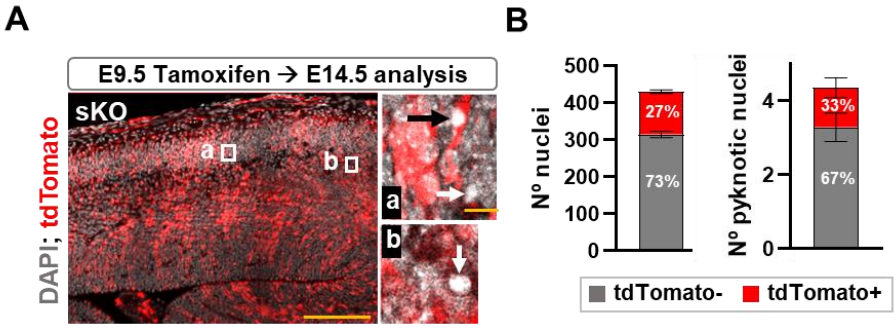

Figure R.29. Presence of pyknotic nuclei in the telencephalon of *Sox2CreERT2*:*Dyrk1a*-KO:tdTomato embryos treated with tamoxifen at E9.5 and analysed at E14.5. (A) Representative picture of the dorsal telencephalon (D. Tel) of a Sox2CreERT2:*Dyrk1a*-KO:tdTomato embryo showing the expression of the loxP reporter tdTomato. Images on the right are amplifications of the area delimited by white squares in the cortical plate (a) and intermediate zone (b). The black arrow shows a pyknotic nuclei in a *Dyrk1a* mutant (tdTomato+) cell and the white arrow in a control (tdTomato-) cell. (B) Data in the histograms correspond to the total number of tdTomato- and tdTomato+ nuclei counted in a 100 µm wide column of the D. Tel (left) and the number of pyknotic tdTomato- and tdTomato+ nuclei counted in the whole D.Tel (one hemisphere). The percentages of total tdTomato- and tdTomato+ nuclei and pyknotic tdTomato- and tdTomato+ nuclei are indicated in the histogram bars. Scale bar: 200 µm (dorsal telencephalon) and 10 µm (magnifications).

This quantification did not show difference between genotypes (pyknotic cells/hemisphere: 5±0.68 in controls; 4±0.59 in *Sox2*Cre*ERT2*:*Dyrk1a*-KO:tdTomato+; *P*=0.880 in a two-tailed Student *t*-test. n=8-14 hemispheres from 2 control and 3 *Sox2*Cre*ERT2*:*Dyrk1a*-KO:tdTomato+ embryos). Then, we counted active caspase-3 and ɣ-H2AX immunopositive cells in the whole dorsal telencephalon of control and *Sox2*Cre*ERT2*:*Dyrk1a*-KO:tdTomato+ embryos. These quantifications did not show differences between genotypes (number of active caspase-3+ cells/hemisphere: 0.75±0.25 in controls; 0.64±0.20 in *Sox2*Cre*ERT2*:*Dyrk1a*-KO:tdTomato+ ; *P*=0.737 in a two-tailed Student *t*-test. Number of ɣ-H2AX+ cells/hemisphere: 3±0.70 in controls; 3±0.57 in *Sox2CreERT2*:*Dyrk1a*-KO; *P*=0.647 in a two-tailed Student *t*-test. n=12-14 hemispheres from 4 embryos per genotype).

Together, these results indicate that the abrogation of DYRK1A activity in around 30% of RG progenitors is not sufficient to alter cortical neurogenesis.

DISCUSSION

The brain phenotype of *NesCre*:*Dyrk1a*-KO embryos reported here shows that DYRK1A is necessary to sustain neurogenesis in the developing ventral telencephalon and provides the first in vivo evidence of the implication of this kinase in DNA repair mechanisms during this process.

1. DNA damage response and cell death

We have shown that knockdown of DYRK1A in neural progenitors at the onset of neurogenesis increases the expression of the DDR marker γH2AX in the dorsal and ventral telencephalon of *NesCre*:*Dyrk1a*-KO embryos and that this increase correlates with an increased p53 activity and apoptosis.

At the onset of cortical neurogenesis (E11-E12 in the mouse), most cells of the dorsal telencephalon are RG cells that divide symmetrically to expand the progenitor pool allowing the growth (lateral expansion) of the brain (Florio and Huttner, 2014). Many studies support the idea that replication stress is the main source of DNA damage during brain neurogenesis and that defects in cell cycle functions and/or mechanism involved in DDR cause an excess of unrepaired DNA damage in NSCs inducing p53-mediated apoptosis (McKinnon, 2013).

As discuss below (section 3), alterations in cell cycle progression are critically contributing to the excess of unrepaired DNA damage in *NesCre*:*Dyrk1a*-KO brains, in particular during the early stages of neurogenesis, when proliferating rates are high. Among the DYRK1A substrates identified so far, there are several that have functions related to DDR (Rammohan et al., 2022). One of these DYRK1A substrates is the transcription factor FOXO1, a DNA damage sensor that slow-down the cell cycle giving time for DNA repair. The phosphorylation of FOXO1 by DYRK1A inhibits FOXO1 nuclear export and degradation in B cells and has been shown to be critical for B lymphopoiesis (Bhansali et al., 2021). Another DDR related substrate is the deacetylase sirtuin-1 (SIRT1). In cultured cells, the phosphorylation of SIRT1 by DYRK1A promotes the deacetylation of p53, thereby inhibiting DNA damage-induced cell death (Guo et al., 2010). The physiological significance of SIRT1 phosphorylation by DYRK1A remains unknown. Another example is the E3 ubiquitin ligase RNF169. This ubiquitin ligase is involved in DSB repair and has been identified as an interactor of DYRK1A in three independent proteomic screens (Guard et al., 2019; Menon et al., 2019; Roewenstrunk et al., 2019). It has also been shown that the phosphorylation of RNF169 by DYRK1A promotes the displacement of 53BP1 from DNA damage sites induced by ionizing irradiation (Roewenstrunk et al., 2019), which is expected to favour DSBs repair by HR over NHEJ (An et al., 2018). Therefore, it is possible to speculate that defects in different steps of the DDR, including DNA repair, are contributing to the excess of

unrepaired DNA damage and augmented cell death in the brain germinal regions of *NesCre*:*Dyrk1a*-KO embryos.

During early neurogenesis, unrepaired DNA damage and apoptosis in the brain of *NesCre*:*Dyrk1a*-KO embryos are more evident in ventral structures such as the lateral and medial ganglionic eminences, than in the dorsal telencephalon. This difference can be explained by the higher proliferative rates of ventral progenitors when compared to dorsal progenitors. Moreover, neurogenesis in the ganglionic eminences starts earlier (around E10.5) than in the dorsal telencephalon (E11.5). There are evidences claiming that during early neurogenesis the pool of progenitors in the LGE and MGE expands rapidly due to the generation of RG-derived amplifying progenitors (sub-apical and basal progenitors) and a progressive reduction of their cell cycle length as neurogenesis advances. In contrast, during early neurogenesis the dorsal VZ is mostly composed by RG cells that start dividing asymmetrically to produce the first IPs and neurons. Moreover, dorsal RG cells have longer cell cycles than the ventral (Pilz et al., 2013). The different behaviour of ventral and dorsal RG cells is likely the cause of the differences in the onset and magnitude of apoptosis between ventral and dorsal regions of *NesCre*:*Dyrk1a*-KO brains.

During embryonic brain development, apoptosis induced in response to unrepaired DNA damage takes place in progenitors as well as in differentiating neurons, although in these postmitotic cells the DNA damage is mainly triggered by oxidative stress (O'Driscoll and Jeggo, 2008; McKinnon, 2013). Cells expressing the DDR marker γH2AX and the active forms of caspase-9 and caspase-3 have been observed in proliferative as well as in non-proliferative regions (*i.e.* CP and ventral parenchyma) of *NesCre*:*Dyrk1a*-KO brains, suggesting that both replicative and oxidative stress are likely contributing to the cell death of the mutant brains. This is supported by the fact that the magnitude of apoptosis in the non-proliferative regions of the KO brains increases as neurogenesis advances. Another possibility to explain the excess of unrepaired DNA damage and apoptosis in non-proliferative regions is that apoptosis induced by unrepaired DNA in progenitors compromises the survival of postmitotic daughters. This second possibility is supported by an *in vivo* study showing that p53-dependent apoptosis induced by prolonged mitosis in dorsal RG cells compromises the survival of the direct progeny (IPs and neurons) (Pilaz et al., 2016).

Contrary to the increased apoptosis observed in the brain of *NesCre*:*Dyrk1a*-KO embryos, we did not see any increase in pyknotic nuclei nor in active-caspase3+ cells in the dorsal telencephalon of *Sox2CreERT2*:*Dyrk1a*:tdTomato+ embryos treated with tamoxifen at E9.5 and analysed at E14.5 despite the fact that more than 30% of dorsal brain cells in these mutant embryos expressed the loxP reporter tdTomato. Our tamoxifen treatments performed at different developmental times indicate that Cre-recombinase in the

Sox2CreERT2:*Dyrk1a*-KO embryos is active 48 h after tamoxifen induction. There are several possibilities to explain the lack of aberrant apoptosis in the *Sox2CreERT2*:*Dyrk1a*-KO embryos. The first possibility is that Cre-recombinase activity is sufficient to recombine the loxP sequences in the tdTomato reporter cassette in a subset of neural progenitors but not to recombine the flanking loxP sites in the two *Dyrk1a* alleles, which is necessary to generate a null mutation in these progenitors. This possibility is supported by studies showing that the efficiency of Cre-mediated loxP recombinase is locus specific (McLellan et al., 2017). DDR and apoptosis in the brain of *NesCre*:*Dyrk1a*-HET embryos (50% reduction of DYRK1A protein levels) is much more subtle than in the *NesCre*:*Dyrk1a*-KO littermates indicating that complete abrogation of DYRK1A activity is needed to critically compromise the survival of brain NSCs and their progeny. Therefore, only bona-fide *Dyrk1a* null mutant cells are expected to display a phenotype. The second possibility is that DYRK1A activity in RG cells is critical only in a specific developmental time window. Indeed, different evidences indicate that the threshold for apoptosis induced in response to DNA damage is very low during early neurogenesis and that this threshold increases as neurogenesis progresses (McKinnon, 2013). In the neural tube of transgenic *NestinCre* embryos Cre-recombinase expression starts at E8.5 (Petersen et al., 2002), but complete depletion of the DYRK1A protein in the telencephalon of *NesCre*:*Dyrk1a*-KO embryos does not take place until E11.5. Therefore, it is possible that abrogation of DYRK1A activity in the RG of *Sox2CreERT2*:*Dyrk1a*-KO brains treated with tamoxifen at E9.5 occurs after the critical time window for DYRK1A in these NSCs. To discriminate between these two possibilities, it would be informative to follow DYRK1A protein levels or DYRK1A enzymatic activity in the *Dyrk1a* mutant (tdTomato+) and wild-type (tdTomato-) cells of the dorsal telencephalon of tamoxifen treated *Sox2*Cre*ERT2*:*Dyrk1a:*tdTomato+ embryos. However, since DYRK1A immunostaining in brain tissue with the DYRK1A antibodies available is too faint to obtain reliable quantitative data, quantifications of DYRK1A levels/activity would require performing immunoblots or kinase assays in FACS sorted tdTomato+ and tdTomato- cells. A third possibility is that depletion of DYRK1A in only 30-40% of dorsal VZ progenitors in not sufficient to alter the general behaviour of the RG in all the territory because of non-cell autonomous DYRK1A functions. This possibility is supported by the similar percentages of pyknotic nuclei and similar nuclear morphology (see section 2 below) between wild-type and *Dyrk1a* mutant cells in the dorsal telencephalon of *Sox2*Cre*ERT2*:*Dyrk1a:*tdTomato+ embryos.

The apoptosis induced by unrepaired DNA lesions is mediated by the intrinsic cell death pathway and relies on caspase-9 activation (McKinnon, 2013). The expression of active caspase-9 in the telencephalon of *NesCre*:*Dyrk1a*-KO embryos is similar to the active form of the executioner caspase-3. This observation strongly indicates that the excess of

apoptosis in the conditional *NesCre*:*Dyrk1a*-KO brains is due to an over-activation of the intrinsic apoptotic pathway. *In vivo* studies performed in the retina and ventral mesencephalon of postnatal *Dyrk1a*$^{+/-}$ mice indicate that in these CNS structures, DYRK1A modulates developmental apoptosis by phosphorylating a threonine residue in caspase-9 that inhibits its cleavage and the subsequent activation of the apoptotic pathway (Laguna et al., 2008; Barallobre et al., 2014). Immunoblotting experiments performed with total protein extracts from the ventral telencephalon of E11.5 *NesCre*:*Dyrk1a*-KO and control embryos show that the phosphorylation status of caspase-9 is the same in both genotypes suggesting that kinases other than DYRK1A, such as the CDK1 and ERK1 and 2 (Allan and Clarke, 2009), are phosphorylating this inhibitory caspase-9 residue. Increased cell death has also been detected in the postnatal brain of the *Emx1Cre*:*Dyrk1a*-HET mouse, which carries a conditional *Dyrk1a* mutation in heterozygosity in all the neurons generated in the dorsal telencephalon (Levy et al., 2021). In this heterozygous *Dyrk1a* mutant there is a decreased number of cortical neurons from P7 onwards resulting from an exacerbated postnatal apoptosis. Given that in the *NesCre*:*Dyrk1a* mutant mouse reported here, *Dyrk1a* is mutated in all the cells of the dorsal and ventral telencephalon, it would be interesting to analyse cell death in the *NesCre*:*Dyrk1a*-HET model not only during embryonic development but also in postnatal stages.

2. Cell cycle regulation in cortical radial glia

Compelling evidences indicate that DYRK1A can act as an inhibitor of proliferation due to its ability to inhibit cell cycle promoters or activate cell cycle inhibitors (Fernandez-Martinez et al., 2015; see also **Figure I.13**). In neural cells in culture, DYRK1A can inhibit G1 to S phase transition by different means: i) phosphorylating Cyclin D1 at Thr125 (Soppa et al., 2014), which induces Cyclin D1 nuclear export and its degradation through the ubiquitin proteasome pathway (Chen et al., 2013); ii) phosphorylating p27^{KIP1} at Ser10, which promotes the stabilization of the protein (Soppa et al., 2014); and iii) phosphorylating p53 at Ser15, which leads to the induction of the p53 target gene *p21^{CIP1}*.

The analysis of cell cycle parameters in the dorsal RG of E11.5 mBACTg*Dyrk1a* embryos revealed that a 50% increase in DYRK1A protein causes a significant lengthening of the cell cycle due to a specific lengthening of the G1 and S phases. The cell cycle alterations detected in dorsal mBACTg*Dyrk1a* RG agree with an antiproliferative role of DYRK1A and correlate with a decrease in the levels of Cyclin D1 detected by immunofluorescence and immunoblotting. Conversely, Cyclin D1 levels are augmented in the dorsal RG of E11.5 *Dyrk1a*$^{+/-}$ brains. However, p27^{KIP1} and p21^{CIP1} levels in the dorsal

telencephalon of *Dyrk1a*$^{+/-}$ and mBACTg*Dyrk1a* embryos are normal (Najas et al., 2015), suggesting that phosphorylation of p27^{KIP1} and p53 by DYRK1A is dispensable for cell cycle regulation in neurogenic cortical RG cells. This notion is supported by the normal levels of p27^{KIP1} and p21^{CIP1} (preliminary data not included in this work) detected by immunoblotting in extracts from the dorsal telencephalon of *NesCre*:*Dyrk1a*-KO embryos. Of note, Cyclin D1 were significantly augmented in all brain extracts obtained from E11.5 and E12.5 *NesCre*:*Dyrk1a*-KO embryos that we have analysed. Together, these results reinforce the idea that DYRK1A phosphorylations/functions are cell type and context specific. The cell context specificity of the kinase has been illustrated in cancer cells, where DYRK1A can act as a tumour suppressor or an oncogene depending on the type of cancer (Birger and Izraeli, 2012; Fernandez-Martinez et al., 2015; Rammohan et al., 2022).

The increase in Cyclin D1 levels in the dorsal brain of E11.5 *NesCre*:*Dyrk1a*-KO embryos correlates with a moderate but significant increase in hyperphosphorylated Rb, indicating that CD4/6 activity is augmented. However, our data shows that cell cycle in dorsal *NesCre*:*Dyrk1a*-KO RGs is longer than normal and that this increase is due to a lengthening of the S phase and, although not directly measured, also to the G1. These cell cycle alterations are similar to that previously observed in the dorsal RG of mBACTg*Dyrk1a* mutant embryos just mentioned. The analysis by FACs of cells isolated from the dorsal telencephalon of E11.5 *NesCre*:*Dyrk1a*-HET and *Dyrk1a*$^{+/-}$ mutant brains does not indicate relevant cell cycle alterations (unpublished data of the laboratory), suggesting that 50% reduction in DYRK1A activity is not sufficient to dysregulate cell cycle progression in cortical RG cells despite the increased levels of Cyclin D1. In the dorsal RG, Cyclin D1 levels are high at the beginning of neurogenesis, and they decrease as neurogenesis progresses and cell cycle duration increases. Thus, it is possible that Cyclin D1 at the onset of neurogenesis is not limiting the formation of active Cyclin D1/CDK4/6 complexes and that an increase in the levels of nuclear Cyclin D1 in not affecting cell cycle duration.

In cycling cells, DNA repair by HR takes place mainly in S phase (Karanam et al., 2012). Therefore, S phase lengthening observed in *NesCre*:*Dyrk1a*-KO cortical progenitors could be the consequence of defective DNA replication and/or DNA repair mechanisms. Interestingly, growing evidences indicate that Cyclin D1 in tumour cells interacts with proteins involved in DNA repair by HR such as BRCA1 (Wang et al., 2005), BRCA2 (Jirawatnotai et al., 2011) and RAD53 (Li et al., 2010). We have recently performed a RNAseq experiment using total RNA from the dorsal telencephalon of E11.5 control, *NesCre*:*Dyrk1a*-HET and *NesCre*:*Dyrk1a*-KO embryos. The results showed an enrichment on genes involved in DNA replication and DNA repair by HR, including *Brac1* and *Brac2*, among the differentially expressed genes in the *NesCre*:*Dyrk1a*-KO samples. In the *NesCre*:*Dyrk1a*-HET samples, there were a few dysregulated genes and none of them are

related to cell cycle regulation/function (unpublished data). These results agree with the moderate cell cycle phenotype and moderate increase in unrepaired DNA lesions in *NesCre*:*Dyrk1a*-HET brains compared to the null mutants, and strongly indicate that DYRK1A plays a fundamental role in cell cycle regulation and DNA repair in RG brain progenitors during developmental neurogenesis.

3. Characteristics of the radial glia

In the dorsal and ventral telencephalon of *NesCre*:*Dyrk1a*-KO embryos, SOX2 progenitors are smaller than in control embryos, a phenotype that is evident from approximately E12.5 and that becomes more pronounced as neurogenesis progress. Since the size of the nucleus in a specific cell type is usually proportional to the size of the cell, nuclear size reduction in SOX2 progenitors suggests the possibility that DYRK1A activity is necessary for normal cell growth. Measurements of the RG apical domain (apical foot) in open-book preparations of conditional *NesCre:Dyrk1a* mutant brains are consistent with a possible size reduction of dorsal RG (laboratory unpublished data). Several evidences suggest that reducing DYRK1A dosage also has a negative impact on the growth/size of cortical neurons during development. These are the following: I) in the conditional *Emx1:Dyrk1a* mutant, the soma of cortical neurons in both newborn *Emx1*:*Dyrk1a*-KO and *Emx1*;*Dyrk1a*-HET mice is smaller than normal, although size reduction in the KOs is greater than in the HETs (Levy et al., 2021); II) in *Emx1:Dyrk1a*-HET mutants, the reduction in soma size is maintained until adulthood; III) the soma of pyramidal neurons in the neocortex of adult *Dyrk1a*$^{+/-}$ haploinsufficient mice is also smaller than normal (Benavides-Piccione et al., 2005); and IV) in E17.5 *NesCre:Dyrk1a*-KO embryos, the nuclei of cortical SATB2+ and CITP2+ neurons are smaller than in control littermates (unpublished data from the laboratory). Together, these observations suggest that the smaller size of the neurons in the *Emx1:Dyrk1a*-KO, *Emx1:Dyrk1a*-HET, and *Dyrk1a*$^{+/-}$ mutants (Arranz et al., 2019; Levy et al., 2021) and in the new conditional *NesCre:Dyrk1a*-KO causes or contributes to the reduced thickness and increased neuronal density observed in the neocortex of these LoF *Dyrk1a* mutant mice.

In addition to an abnormal size, the nucleus of SOX2 progenitors in *NesCre:Dyrk1a*-KO brains present an altered shape. Abnormal nuclear shape is a diagnostic marker for human diseases and may alter different cell functions including cell cycle progression, DNA replication and repair and the activity of mechanotransduction pathways (Manda et al., 2023) that active key transcription regulators of organ size control, such us YAP/TAZ (Yu et al., 2015; Torato et al., 2018; Mosassad et al., 2021). The ability of the nucleus to maintain

its shape and mechanical behaviour depends on the external cytoskeleton, nuclear Lamins and other associated proteins, and chromatin (Stephens et al., 2019; Karoutas and Akhtar, 2021; Manda et al., 2023). DYRK1A is strongly implicated in the regulation of actin and microtubule assembly by phosphorylating N-WASP (Park et al., 2012), β-tubulin (Ori-McKenney et al., 2016), and the microtubule-associated protein tau (Woods et al., 2001). Therefore, it is possible that the abnormal rounded shape of *NesCre:Dyrk1a*-KO progenitors is caused by alterations in cytoskeletal networks.

Perturbations in the levels of Lamin B1 alter the physiology of the cell and is linked to several human diseases including premature aging syndrome progeria (Dreesen et al., 2013). People with Down syndrome present clinical signs of accelerating ageing (Roizen and Patterson, 2003). Recently, it has been shown that the overexpression of DYRK1A causes a progeroid status in Down syndrome that correlates with reduced Lamin B1 levels and increased DNA damage in blood cell and other cell types. Notably, normalization of DYRK1A dosage in Down syndrome cells by genetic means or pharmacological inhibition of DYRK1A activity normalizes Lamin B1 levels and reduces the number of unrepaired DNA lesions (Murray et al., 2023). Thus, it is likely that Lamin B1 levels in *NesCre:Dyrk1a*-KO mutant cells are perturbed, and that this perturbation contributes to the abnormal nuclear shape and function of highly polarized progenitors such as the RG.

As already mentioned, a characteristic feature of the RG (apical radial glia) is that the dividing cells are in contact to the ventricle (Taverna and Huttner, 2010). In primates, in addition to this RG there is another type of progenitors that divide within the VZ but in a more basal (subapical o basal) position. These progenitors, mostly bRG, are very abundant in humans but scarce in the mouse and other lissencephalic species (Pinson et al., 2019). In the dorsal VZ of E11.5 *NesCre:Dyrk1a*-KO brains, there was an increase in subapical and basal mitoses, whereas the number of mitosis touching the ventricle was normal. Of note, ventricular mitosis in the mutant brain were disproportionately decreased. There are at least two possibilities to explain this phenotype. The first one is that dorsal RG in the mutant brain produces more bRG at the expenses of RG. As bRG does not have apical foot (Pinson et al., 2019), this possibility could also explain the increased number of SOX2 progenitors per radial column observed in the dorsal telencephalon of *NesCre:Dyrk1a*-KO embryos from E11.5 to E13.5, without increasing the ventricular surface (see next section). The second possibility is that the excess of subapical and basal mitoses results from RG dividing in an aberrant (basal) position. The characteristic interkinetic nuclear migration of the RG depends on microtubules and associated motor proteins (Bertipaglia et al., 2018). Thus, dysfunctions in the microtubule cytoskeleton could be the cause of both mislocalized mitoses and altered nuclear morphology. Immunostainings for pH3 and pVim are underway to discriminate between these two possibilities.

In the telencephalon of tamoxifen treated E14.5 *Sox2*Cre*ERT2*:*Dyrk1a:*tdTomato+ embryos, nuclear morphology in the RG that expresses the tdTomato reporter is very similar than in the RG that do not express the reporter, indicating that DYRK1A activity in the surrounding wild-type cells is sufficient to maintain the elongated nuclear morphology in the mutant cells. The elongated nuclear morphology of the RG is a characteristic of all pseudostratified neuroepithelium, facilitating the interkinetic nuclear migration (Bertipaglia et al., 2018). Around 70% of the RG in the dorsal VZ of *Sox2CreERT2*:*Dyrk1a*-KO embryos are wild-type. Thus, it is possible that lateral forces exerted by wild-type nuclei help to maintain the normal elongated shape of migrating *Dyrk1a* mutant nuclei.

4. Cortical radial glia differentiation

The generation of cortical neurons follows a prolonged histogenic program in which pluripotent RG cells divide symmetrically, producing two RG cells (proliferative divisions), or asymmetrically (differentiative divisions), producing one RG and either a neuron or a progenitor (usually an IP) that is committed to produce only neurons. During neurogenesis, proliferative divisions allow to the expansion of the ventricular surface (lateral expansion) whereas differentiative divisions lead to the production of neurons (direct neurogenesis) and IPs, which divide symmetrically producing two IPs or two neurones (indirect neurogenesis). Both direct and indirect neurogenesis contribute to the radial growth (thickness and cellularity) of the CP (Florio and Huttner, 2014). At the end of neurogenesis, both *NesCre:Dyrk1a*-KO and *NesCre:Dyrk1a*-HET embryos showed smaller telencephalic vesicles, although size reduction was greater in the *NesCre:Dyrk1a*-KO embryos. A significant size reduction of the telencephalic vesicles was also observed in the haploinsufficient *Dyrk1a*$^{+/-}$ mouse model at perinatal stages (Fotaki et al., 2002) (unpublished data of the laboratory). The similar phenotype of *NesCre:Dyrk1a*-HET and *Dyrk1a*$^{+/-}$ mutants indicates that a 50% reduction of DYRK1A during neurogenesis compromises brain growth (lateral expansion) and suggest that alterations in the proliferation features (such as proliferation rates and mode of division) of the dorsal RG likely contribute to the microcephaly commonly observed in infants with DYRK1A syndrome (van Bon et al., 2016). In the *Dyrk1a*$^{+/-}$ model, cortical neurogenesis is advanced, which correlates with an excess of neocortical neurons at postnatal stages (Najas et al., 2015; Arranz et al., 2019). However, neuron densities in the neocortex of the *NesCre:Dyrk1a*-HET mouse are normal (unpublished data of the laboratory), suggesting that neurogenesis in this mutant is preserved. The fact that cortical neurogenesis is affected in the mouse constitutive *Dyrk1a*$^{+/-}$ mutant but not in the conditional *NesCre:Dyrk1a*-HET mutant implies

that 50% reduction of DYRK1A at the onset of neurogenesis does not alter the histogenic program of the dorsal RG, suggesting that the neurogenic problems in the haploinsufficient *Dyrk1a*$^{+/-}$ mouse arise from earlier defects, likely during the transition between neuroepithelial to RG cells.

The quantification of cell expressing differentiating markers (TBR2 and TBR1) in the dorsal telencephalon of *NesCre:Dyrk1a*-KO embryos suggests defects in direct neurogenesis. This is supported by the significant decrease in early-born (TBR1+) neurons in the CP of the KO brains observed at mid-neurogenesis. However, at later developmental stages (E17.5), and despite the prominent apoptosis that takes places in the CP after mid-neurogenesis, the number of CTIP2 and SATB2 neurons in the IZ and CP of *NesCre:Dyrk1a*-KO brains was normal. CITP2 and the majority of SATB2 neurons are late-born neurons generated by indirect neurogenesis (*via* IPs) and/or by terminal mitosis of the RG. In the dorsal germinal region of E17.5 *NesCre:Dyrk1a*-KO brains there are less SOX2 and TBR2 progenitors than normal, which is in line with an increased production of late-born neuros, thereby compensating the loss of neurons caused by apoptosis. Of note, the dorsal SVZ of *NesCre:Dyrk1a*-KO brains has a deficit in IPs but an excess of mitoses, suggesting that these progenitors have shorter cell cycles, thus increasing the neuronal output, or longer mitoses. To discriminate between these two possibilities, it would be necessary to analyse cell cycle parameters in the dorsal SVZ of *NesCre*:*Dyrk1a*-KO embryos using similar methods as the ones used in this work.

5. Development of the striatum and implications in autism

As already mentioned, despite the size reduction of the telencephalic vesicles, morphological abnormalities in *NesCre*:*Dyrk1a*-HET brains are restricted to ventral structures, being the *striatum* one of the subcortical structures that show a notorious size reduction. This observation suggests that haploinsufficiency of *Dyrk1a* in LGE progenitors might affect the production of striatal MSN. The postnatal *striatum* of both *Dyrk1a*$^{+/-}$ and *Emx1Cre*:*Dyrk1a*-HET mutant mice also displays a significant size reduction (Fotaki et al., 2002; Levy et al., 2021). In the conditional *Emx1Cre*:*Dyrk1a*-HET mutant, the mutation is restricted to the projection neurons of the neocortex (Levy et al., 2021), which implies that the striatal phenotype in this mutant mouse is caused by defects in cortical inputs. Notably, both *Dyrk1a*$^{+/-}$ and *Emx1Cre*:*Dyrk1a*-HET mutant mice present deficits in social communication and stereotypic movements, which are common behaviours in mouse models of autism (Arranz et al., 2019; Levy et al., 2021).

The *striatum*, which is the gateway of the basal ganglia, receives massive inputs from the neocortex and there are evidences showing that the development of these two structures is interconnected (Shepherd, 2013). Dysfunctions in corticostriatal pathways have been related to the development of repetitive behaviours in patients with autism (Fuccillo, 2016). Moreover, several genes associated with ASD, including *DYRK1A*, have been implicated in axonal growth abnormalities, imbalanced of the synaptic excitation/inhibition ratio and altered long-term synaptic plasticity in the corticostriatal pathway (Li and Pozzo-Miller, 2020). Based on all this knowledge and on the striatal phenotypes of *NesCre*:*Dyrk1a*-HET embryos shown in this work and postnatal *Emx1Cre*:*Dyrk1a*-HET mutant mice (Levy et al., 2021), it is possible to speculate that both defects in striatal neuron production and synaptic cortical inputs affect the connections of striatal circuits in patients with DYRK1A syndrome, thus contributing to the autistic behaviours that are characteristic in this syndrome.

CONCLUSIONS

1.- The phenotype of the mouse conditional *NesCre*:*Dyrk1a* null mutant indicates an essential role of DYRK1A in the development of the embryonic telencephalon.

2.- At the end of neurogenesis, *NesCre*:*Dyrk1a* embryos with a single functional copy of *Dyrk1a* (*NesCre*:*Dyrk1a*-HET) display a significant reduction in the size of the *striatum* and other *subpallium* structures, indicating that alterations in subcortical brain circuits could contribute to the neurological features in DYRK1A syndrome.

3.- The *NesCre*:*Dyrk1a*-KO conditional mutant exhibits a severe loss of brain parenchyma caused by overactivation of the intrinsic apoptotic pathway resulting from persistent DNA replication stress and/or dysfunctions in DNA repair mechanisms.

4.- At the beginning of neurogenesis, the dorsal radial glia of *NesCre*:*Dyrk1a*-KO brains presents an elongation of the G1 and S phases of the cell cycle, which correlates with a transient increase in radial glia and a concomitant decrease in intermediate progenitors and neurons.

5.- In the *NesCre*:*Dyrk1a*-KO mutant, the shape and size of apical telencephalic progenitors are altered, a phenotype that could contribute to the nuclear dysfunctions shown by these progenitors.

6.- At the end of neurogenesis, *NesCre*:*Dyrk1a*-KO embryos show a prominent size reduction of the telencephalic vesicles, an earlier exhaustion of cortical progenitors and a deficit of new-born cortical neurons, indicating that DYRK1A critically contributes to the lateral expansion and differentiation program of the neocortex.

7.- The dorsal telencephalon of the mouse conditional *Sox2CreERT2*:*Dyrk1a*-KO embryo does not show any obvious morphological alteration, probably because the *Dyrk1a* mutation in this embryo is in mosaicism.

BIBLIOGRAPHY

Abner, C.W., and McKinnon, P.J. (2004). The DNA double-strand break response in the nervous system. DNA Repair (Amst) 3, 1141-1147.

Allan, L.A., and Clarke, P.R. (2009). Apoptosis and autophagy: Regulation of caspase-9 by phosphorylation. FEBS J *276*, 6063-6073.

Altafaj, X., Dierssen, M., Baamonde, C., Marti, E., Visa, J., Guimera, J., Oset, M., Gonzalez, J.R., Florez, J., Fillat, C., and Estivill, X. (2001). Neurodevelopmental delay, motor abnormalities and cognitive deficits in transgenic mice overexpressing Dyrk1A (minibrain), a murine model of Down's syndrome. Hum Mol Genet *10*, 1915-1923.

Alvarez, M., Altafaj, X., Aranda, S., and de la Luna, S. (2007). DYRK1A autophosphorylation on serine residue 520 modulates its kinase activity via 14-3-3 binding. Mol Biol Cell *18*, 1167-1178.

Alvarez, M., Estivill, X., and de la Luna, S. (2003). DYRK1A accumulates in splicing speckles through a novel targeting signal and induces speckle disassembly. J Cell Sci *116*, 3099-3107.

Amemori, K., Gibb, L.G., and Graybiel, A.M. (2011). Shifting responsibly: the importance of striatal modularity to reinforcement learning in uncertain environments. Front Hum Neurosci *5*, 47.

An, L., Dong, C., Li, J., Chen, J., Yuan, J., Huang, J., Chan, K.M., Yu, C.H., and Huen, M.S.Y. (2018). RNF169 limits 53BP1 deposition at DSBs to stimulate single-strand annealing repair. Proc Natl Acad Sci U S A *115*, E8286-E8295.

Anthony, T.E., Klein, C., Fishell, G., and Heintz, N. (2004). Radial glia serve as neuronal progenitors in all regions of the central nervous system. Neuron *41*, 881-890.

Antonarakis, S.E., Skotko, B.G., Rafii, M.S., Strydom, A., Pape, S.E., Bianchi, D.W., Sherman, S.L., and Reeves, R.H. (2020). Down syndrome. Nat Rev Dis Primers *6*, 9.

Arai, Y., Pulvers, J.N., Haffner, C., Schilling, B., Nusslein, I., Calegari, F., and Huttner, W.B. (2011). Neural stem and progenitor cells shorten S-phase on commitment to neuron production.

Aranda, S., Alvarez, M., Turro, S., Laguna, A., and de la Luna, S. (2008). Sprouty2-mediated inhibition of fibroblast growth factor signaling is modulated by the protein kinase DYRK1A. Mol Cell Biol *28*, 5899-5911.

Aranda, S., Laguna, A., and de la Luna, S. (2011). DYRK family of protein kinases: evolutionary relationships, biochemical properties, and functional roles. FASEB J *25*, 449-462.

Arbones, M.L., Thomazeau, A., Nakano-Kobayashi, A., Hagiwara, M., and Delabar, J.M. (2019). DYRK1A and cognition: A lifelong relationship. Pharmacol Ther *194*, 199-221.

Arlotta, P., Molyneaux, B.J., Chen, J., Inoue, J., Kominami, R., and Macklis, J.D. (2005). Neuronal subtype-specific genes that control corticospinal motor neuron development in vivo. Neuron *45*, 207-221.

Arque, G., Fotaki, V., Fernandez, D., Martinez de Lagran, M., Arbones, M.L., and Dierssen, M. (2008). Impaired spatial learning strategies and novel object recognition in mice haploinsufficient for the dual specificity tyrosine-regulated kinase-1A (Dyrk1A). PLoS One *3*, e2575, e2575.

Arranz, J., Balducci, E., Arato, K., Sanchez-Elexpuru, G., Najas, S., Parras, A., Rebollo, E., Pijuan, I., Erb, I., Verde, G., et al. (2019). Impaired development of neocortical circuits

contributes to the neurological alterations in DYRK1A haploinsufficiency syndrome. Neurobiol Dis *127*, 210-222.

Ashe, P.C., and Berry, M.D. (2003). Apoptotic signaling cascades. Prog Neuropsychopharmacol Biol Psychiatry *27*, 199-214.

Azevedo, F.A., Carvalho, L.R., Grinberg, L.T., Farfel, J.M., Ferretti, R.E., Leite, R.E., Jacob Filho, W., Lent, R., and Herculano-Houzel, S. (2009). Equal numbers of neuronal and nonneuronal cells make the human brain an isometrically scaled-up primate brain. J Comp Neurol *513*, 532-541.

Azzarelli, R., Hardwick, L.J., and Philpott, A. (2015). Emergence of neuronal diversity from patterning of telencephalic progenitors. Wiley Interdiscip Rev Dev Biol *4*, 197-214.

Bao, Q., and Shi, Y. (2007). Apoptosome: a platform for the activation of initiator caspases. Cell Death Differ *14*, 56-65.

Barallobre, M.J., Perier, C., Bove, J., Laguna, A., Delabar, J.M., Vila, M., and Arbones, M.L. (2014). DYRK1A promotes dopaminergic neuron survival in the developing brain and in a mouse model of Parkinson's disease. Cell Death Dis *5*, e1289.

Becker, W., Soppa, U., and Tejedor, F.J. (2014). DYRK1A: a potential drug target for multiple Down syndrome neuropathologies. CNS Neurol Disord Drug Targets *13*, 26-33.

Becker, W., Weber, Y., Wetzel, K., Eirmbter, K., Tejedor, F.J., and Joost, H.G. (1998). Sequence characteristics, subcellular localization, and substrate specificity of DYRK-related kinases, a novel family of dual specificity protein kinases. J Biol Chem *273*, 25893-25902.

Benavides-Piccione, R., Dierssen, M., Ballesteros-Yanez, I., Martinez de Lagran, M., Arbones, M.L., Fotaki, V., DeFelipe, J., and Elston, G.N. (2005). Alterations in the phenotype of neocortical pyramidal cells in the Dyrk1A+/- mouse. Neurobiol Dis *20*, 115-122.

Bertipaglia, C., Goncalves, J.C., and Vallee, R.B. (2018). Nuclear migration in mammalian brain development. Semin Cell Dev Biol *82*, 57-66.

Bhansali, R.S., Rammohan, M., Lee, P., Laurent, A.P., Wen, Q., Suraneni, P., Yip, B.H., Tsai, Y.C., Jenni, S., Bornhauser, B., et al. (2021). DYRK1A regulates B cell acute lymphoblastic leukemia through phosphorylation of FOXO1 and STAT3. J Clin Invest *131*.

Birger, Y., and Izraeli, S. (2012). DYRK1A in Down syndrome: an oncogene or tumor suppressor? J Clin Invest *122*, 807-810.

Blackburn, A.T.M., Bekheirnia, N., Uma, V.C., Corkins, M.E., Xu, Y., Rosenfeld, J.A., Bainbridge, M.N., Yang, Y., Liu, P., Madan-Khetarpal, S., et al. (2019). DYRK1A-related intellectual disability: a syndrome associated with congenital anomalies of the kidney and urinary tract. Genet Med *21*, 2755-2764.

Blackford, A.N., and Jackson, S.P. (2017). ATM, ATR, and DNA-PK: The Trinity at the Heart of the DNA Damage Response. Mol Cell *66*, 801-817.

Blanquie, O., Yang, J.W., Kilb, W., Sharopov, S., Sinning, A., and Luhmann, H.J. (2017). Electrical activity controls area-specific expression of neuronal apoptosis in the mouse developing cerebral cortex. Elife *6*.

Blaschke, A.J., Staley, K., and Chun, J. (1996). Widespread programmed cell death in proliferative and postmitotic regions of the fetal cerebral cortex. Development *122*, 1165-1174.

Boni, J., Rubio-Perez, C., Lopez-Bigas, N., Fillat, C., and de la Luna, S. (2020). The DYRK Family of Kinases in Cancer: Molecular Functions and Therapeutic Opportunities. Cancers (Basel) *12*.

Borello, U., and Pierani, A. (2010). Patterning the cerebral cortex: traveling with morphogens. Curr Opin Genet Dev *20*, 408-415.

Brault, V., Nguyen, T.L., Flores-Gutierrez, J., Iacono, G., Birling, M.C., Lalanne, V., Meziane, H., Manousopoulou, A., Pavlovic, G., Lindner, L., et al. (2021). Dyrk1a gene dosage in glutamatergic neurons has key effects in cognitive deficits observed in mouse models of MRD7 and Down syndrome. PLoS Genet *17*, e1009777.

Brimblecombe, K.R., and Cragg, S.J. (2017). The Striosome and Matrix Compartments of the Striatum: A Path through the Labyrinth from Neurochemistry toward Function. ACS Chem Neurosci *8*, 235-242.

Britanova, O., de Juan Romero, C., Cheung, A., Kwan, K.Y., Schwark, M., Gyorgy, A., Vogel, T., Akopov, S., Mitkovski, M., Agoston, D., et al. (2008). Satb2 is a postmitotic determinant for upper-layer neuron specification in the neocortex. Neuron *57*, 378-392.

Bronicki, L.M., Redin, C., Drunat, S., Piton, A., Lyons, M., Passemard, S., Baumann, C., Faivre, L., Thevenon, J., Riviere, J.B., et al. (2015). Ten new cases further delineate the syndromic intellectual disability phenotype caused by mutations in DYRK1A. Eur J Hum Genet *23*, 1482-1487.

Bujarrabal-Dueso, A., Sendtner, G., Meyer, D.H., Chatzinikolaou, G., Stratigi, K., Garinis, G.A., and Schumacher, B. (2023). The DREAM complex functions as conserved master regulator of somatic DNA-repair capacities. Nat Struct Mol Biol *30*, 475-488.

Calabresi, P., Picconi, B., Tozzi, A., Ghiglieri, V., and Di Filippo, M. (2014). Direct and indirect pathways of basal ganglia: a critical reappraisal. Nat Neurosci *17*, 1022-1030.

Causeret, F., Coppola, E., and Pierani, A. (2018). Cortical developmental death: selected to survive or fated to die. Curr Opin Neurobiol *53*, 35-42.

Caviness, V.S., Jr., Goto, T., Tarui, T., Takahashi, T., Bhide, P.G., and Nowakowski, R.S. (2003). Cell output, cell cycle duration and neuronal specification: a model of integrated mechanisms of the neocortical proliferative process. Cereb Cortex *13*, 592-598.

Chen, J.Y., Lin, J.R., Tsai, F.C., and Meyer, T. (2013). Dosage of Dyrk1a shifts cells within a p21-cyclin D1 signaling map to control the decision to enter the cell cycle. Mol Cell *52*, 87-100.

Chrzanowska, K.H., Gregorek, H., Dembowska-Baginska, B., Kalina, M.A., and Digweed, M. (2012). Nijmegen breakage syndrome (NBS). Orphanet J Rare Dis *7*, 13.

Chun, H.H., and Gatti, R.A. (2004). Ataxia-telangiectasia, an evolving phenotype. DNA Repair (Amst) *3*, 1187-1196.

Crittenden, J.R., and Graybiel, A.M. (2011). Basal Ganglia disorders associated with imbalances in the striatal striosome and matrix compartments. Front Neuroanat *5*, 59.

Crosio, C., Fimia, G.M., Loury, R., Kimura, M., Okano, Y., Zhou, H., Sen, S., Allis, C.D., and Sassone-Corsi, P. (2002). Mitotic phosphorylation of histone H3: spatio-temporal regulation by mammalian Aurora kinases. Mol Cell Biol *22*, 874-885.

De Rubeis, S., He, X., Goldberg, A.P., Poultney, C.S., Samocha, K., Cicek, A.E., Kou, Y., Liu, L., Fromer, M., Walker, S., et al. (2014). Synaptic, transcriptional and chromatin genes disrupted in autism. Nature *515*, 209-215.

Demuro, S., Di Martino, R.M.C., Ortega, J.A., and Cavalli, A. (2021). GSK-3beta, FYN, and DYRK1A: Master Regulators in Neurodegenerative Pathways. Int J Mol Sci *22*.

Dhumale, P., Menon, S., Chiang, J., and Puschel, A.W. (2018). The loss of the kinases SadA and SadB results in early neuronal apoptosis and a reduced number of progenitors. PLoS One *13*, e0196698.

Dreesen, O., Chojnowski, A., Ong, P.F., Zhao, T.Y., Common, J.E., Lunny, D., Lane, E.B., Lee, S.J., Vardy, L.A., Stewart, C.L., and Colman, A. (2013). Lamin B1 fluctuations have differential effects on cellular proliferation and senescence. J Cell Biol *200*, 605-617.

Dupont, S., Morsut, L., Aragona, M., Enzo, E., Giulitti, S., Cordenonsi, M., Zanconato, F., Le Digabel, J., Forcato, M., Bicciato, S., et al. (2011). Role of YAP/TAZ in mechanotransduction. Nature *474*, 179-183.

Englund, C., Fink, A., Lau, C., Pham, D., Daza, R.A., Bulfone, A., Kowalczyk, T., and Hevner, R.F. (2005). Pax6, Tbr2, and Tbr1 are expressed sequentially by radial glia, intermediate progenitor cells, and postmitotic neurons in developing neocortex. J Neurosci *25*, 247-251.

Faivre, L., Le Merrer, M., Lyonnet, S., Plauchu, H., Dagoneau, N., Campos-Xavier, A.B., Attia-Sobol, J., Verloes, A., Munnich, A., and Cormier-Daire, V. (2002). Clinical and genetic heterogeneity of Seckel syndrome. Am J Med Genet *112*, 379-383.

Favaro, R., Valotta, M., Ferri, A.L., Latorre, E., Mariani, J., Giachino, C., Lancini, C., Tosetti, V., Ottolenghi, S., Taylor, V., and Nicolis, S.K. (2009). Hippocampal development and neural stem cell maintenance require Sox2-dependent regulation of Shh. Nat Neurosci *12*, 1248-1256.

Fernandez-Martinez, P., Zahonero, C., and Sanchez-Gomez, P. (2015). DYRK1A: the double-edged kinase as a protagonist in cell growth and tumorigenesis. Mol Cell Oncol *2*, e970048.

Ferrini, A., Steel, D., Barwick, K., and Kurian, M.A. (2021). An Update on the Phenotype, Genotype and Neurobiology of ADCY5-Related Disease. Mov Disord *36*, 1104-1114.

Fishell, G., and van der Kooy, D. (1991). Pattern formation in the striatum: neurons with early projections to the substantia nigra survive the cell death period. J Comp Neurol *312*, 33-42.

Fjodorova, M., Noakes, Z., and Li, M. (2015). How to make striatal projection neurons. Neurogenesis (Austin) *2*, e1100227.

Flandin, P., Kimura, S., and Rubenstein, J.L. (2010). The progenitor zone of the ventral medial ganglionic eminence requires Nkx2-1 to generate most of the globus pallidus but few neocortical interneurons. J Neurosci *30*, 2812-2823.

Floresco, S.B. (2015). The nucleus accumbens: an interface between cognition, emotion, and action. Annu Rev Psychol *66*, 25-52.

Florio, M., and Huttner, W.B. (2014). Neural progenitors, neurogenesis and the evolution of the neocortex. Development *141*, 2182-2194.

Fotaki, V., Dierssen, M., Alcantara, S., Martinez, S., Marti, E., Casas, C., Visa, J., Soriano, E., Estivill, X., and Arbones, M.L. (2002). Dyrk1A haploinsufficiency affects viability and causes developmental delay and abnormal brain morphology in mice. Mol Cell Biol *22*, 6636-6647.

Fotaki, V., Martinez De Lagran, M., Estivill, X., Arbones, M., and Dierssen, M. (2004). Haploinsufficiency of Dyrk1A in mice leads to specific alterations in the development and regulation of motor activity. Behav Neurosci *118*, 815-821.

Friedman, A., Homma, D., Gibb, L.G., Amemori, K., Rubin, S.J., Hood, A.S., Riad, M.H., and Graybiel, A.M. (2015). A Corticostriatal Path Targeting Striosomes Controls Decision-Making under Conflict. Cell *161*, 1320-1333.

Fuccillo, M.V. (2016). Striatal Circuits as a Common Node for Autism Pathophysiology. Front Neurosci *10*, 27.

Gorski, J.A., Talley, T., Qiu, M., Puelles, L., Rubenstein, J.L., and Jones, K.R. (2002). Cortical excitatory neurons and glia, but not GABAergic neurons, are produced in the Emx1-expressing lineage. J Neurosci *22*, 6309-6314.

Gotz, M., and Huttner, W.B. (2005). The cell biology of neurogenesis. Nat Rev Mol Cell Biol *6*, 777-788.

Gotz, M., Stoykova, A., and Gruss, P. (1998). Pax6 controls radial glia differentiation in the cerebral cortex. Neuron *21*, 1031-1044.

Graybiel, A.M., and Ragsdale, C.W. (1978). Histochemically distinct compartments in the striatum of human, monkey, and cat demonstrated by acetylthiocholinesterase staining. Proceedings of the National Academy of Sciences of the United States of America 75, 5723–26.

Guard, S.E., Poss, Z.C., Ebmeier, C.C., Pagratis, M., Simpson, H., Taatjes, D.J., and Old, W.M. (2019). The nuclear interactome of DYRK1A reveals a functional role in DNA damage repair. Sci Rep *9*, 6539.

Guedj, F., Pereira, P.L., Najas, S., Barallobre, M.J., Chabert, C., Souchet, B., Sebrie, C., Verney, C., Herault, Y., Arbones, M., and Delabar, J.M. (2012). DYRK1A: a master regulatory protein controlling brain growth. Neurobiol Dis *46*, 190-203.

Guimera, J., Casas, C., Estivill, X., and Pritchard, M. (1999). Human minibrain homologue (MNBH/DYRK1): characterization, alternative splicing, differential tissue expression, and overexpression in Down syndrome. Genomics *57*, 407-418.

Guimera, J., Pritchard, M., Nadal, M., and Estivill, X. (1997). Minibrain (MNBH) is a single copy gene mapping to human chromosome 21q22.2. Cytogenet Cell Genet *77*, 182-184.

Guo, X., Williams, J.G., Schug, T.T., and Li, X. (2010). DYRK1A and DYRK3 promote cell survival through phosphorylation and activation of SIRT1. J Biol Chem *285*, 13223-13232.

Hakem, R., Hakem, A., Duncan, G.S., Henderson, J.T., Woo, M., Soengas, M.S., Elia, A., de la Pompa, J.L., Kagi, D., Khoo, W., et al. (1998). Differential requirement for caspase 9 in apoptotic pathways in vivo. Cell *94*, 339-352.

Hammerle, B., Carnicero, A., Elizalde, C., Ceron, J., Martinez, S., and Tejedor, F.J. (2003). Expression patterns and subcellular localization of the Down syndrome candidate protein MNB/DYRK1A suggest a role in late neuronal differentiation. Eur J Neurosci *17*, 2277-2286.

Hammerle, B., Elizalde, C., and Tejedor, F.J. (2008). The spatio-temporal and subcellular expression of the candidate Down syndrome gene Mnb/Dyrk1A in the developing mouse brain suggests distinct sequential roles in neuronal development. Eur J Neurosci *27*, 1061-1074.

Hammerle, B., Vera-Samper, E., Speicher, S., Arencibia, R., Martinez, S., and Tejedor, F.J. (2002). Mnb/Dyrk1A is transiently expressed and asymmetrically segregated in neural progenitor cells at the transition to neurogenic divisions. Dev Biol *246*, 259-273.

Hawkes K., and Finlay B.L. (2018). Mammalian brain development and our grandmothering life history. Physiol Behav. 193(Pt A), 55-68.

Haydar, T.F., and Reeves, R.H. (2012). Trisomy 21 and early brain development. Trends Neurosci 35, 81-91.

Hebert, J.M., and Fishell, G. (2008). The genetics of early telencephalon patterning: some assembly required. Nat Rev Neurosci *9*, 678-685.

Herault, Y., Delabar, J.M., Fisher, E.M.C., Tybulewicz, V.L.J., Yu, E., and Brault, V. (2017). Rodent models in Down syndrome research: impact and future opportunities. Dis Model Mech *10*, 1165-1186.

Hevner, R.F., Shi, L., Justice, N., Hsueh, Y., Sheng, M., Smiga, S., Bulfone, A., Goffinet, A.M., Campagnoni, A.T., and Rubenstein, J.L. (2001). Tbr1 regulates differentiation of the preplate and layer 6. Neuron *29*, 353-366.

Hibaoui, Y., Grad, I., Letourneau, A., Sailani, M.R., Dahoun, S., Santoni, F.A., Gimelli, S., Guipponi, M., Pelte, M.F., Bena, F., et al. (2014). Modelling and rescuing neurodevelopmental defect of Down syndrome using induced pluripotent stem cells from monozygotic twins discordant for trisomy 21. EMBO Mol Med *6*, 259-277.

Hikosaka, O., Kim, H.F., Yasuda, M., and Yamamoto, S. (2014). Basal ganglia circuits for reward value-guided behavior. Annu Rev Neurosci *37*, 289-306.

Himpel, S., Panzer, P., Eirmbter, K., Czajkowska, H., Sayed, M., Packman, L.C., Blundell, T., Kentrup, H., Grotzinger, J., Joost, H.G., and Becker, W. (2001). Identification of the autophosphorylation sites and characterization of their effects in the protein kinase DYRK1A. Biochem J *359*, 497-505.

Hoess, R., Abremski, K., and Sternberg, N. (1984). The nature of the interaction of the P1 recombinase Cre with the recombining site loxP. Cold Spring Harb Symp Quant Biol *49*, 761-768.

Jabaudon, D. (2017). Fate and freedom in developing neocortical circuits. Nat Commun *8*, 16042.

Jackson, S.P., and Bartek, J. (2009). The DNA-damage response in human biology and disease. Nature *461*, 1071-1078.

Ji, J., Lee, H., Argiropoulos, B., Dorrani, N., Mann, J., Martinez-Agosto, J.A., Gomez-Ospina, N., Gallant, N., Bernstein, J.A., Hudgins, L., et al. (2015). DYRK1A haploinsufficiency causes a new recognizable syndrome with microcephaly, intellectual disability, speech impairment, and distinct facies. Eur J Hum Genet *23*, 1473-1481.

Jiang, Y., and Chu, W.K. (2018). Potential Roles of the Retinoblastoma Protein in Regulating Genome Editing. Front Cell Dev Biol *6*, 81.

Jirawatnotai, S., Hu, Y., Michowski, W., Elias, J.E., Becks, L., Bienvenu, F., Zagozdzon, A., Goswami, T., Wang, Y.E., Clark, A.B., et al. (2011). A function for cyclin D1 in DNA repair uncovered by protein interactome analyses in human cancers. Nature *474*, 230-234.

Kale, J., Liu, Q., Leber, B., and Andrews, D.W. (2012). Shedding light on apoptosis at subcellular membranes. Cell *151*, 1179-1184.

Karanam, K., Kafri, R., Loewer, A., and Lahav, G. (2012). Quantitative live cell imaging reveals a gradual shift between DNA repair mechanisms and a maximal use of HR in mid S phase. Mol Cell *47*, 320-329.

Karoutas, A., and Akhtar, A. (2021). Functional mechanisms and abnormalities of the nuclear lamina. Nat Cell Biol *23*, 116-126.

Kawaguchi, Y., Wilson, C.J., Augood, S.J., and Emson, P.C. (1995). Striatal interneurones: chemical, physiological and morphological characterization. Trends Neurosci *18*, 527-535.

Kelly, S.M., Raudales, R., He, M., Lee, J.H., Kim, Y., Gibb, L.G., Wu, P., Matho, K., Osten, P., Graybiel, A.M., and Huang, Z.J. (2018). Radial Glial Lineage Progression and Differential Intermediate Progenitor Amplification Underlie Striatal Compartments and Circuit Organization. Neuron *99*, 345-361 e344.

Kerr, J.F., Wyllie, A.H., and Currie, A.R. (1972). Apoptosis: a basic biological phenomenon with wide-ranging implications in tissue kinetics. Br J Cancer *26*, 239-257.

Kravitz, A.V., and Matikainen-Ankney, B.A. (2020). Motor Control: Memory and Motor Control in the Dorsal Striatum. Curr Biol *30*, R1366-R1368.

Kuan, C.Y., Roth, K.A., Flavell, R.A., and Rakic, P. (2000). Mechanisms of programmed cell death in the developing brain. Trends Neurosci *23*, 291-297.

Kuhn, C., Frank, D., Will, R., Jaschinski, C., Frauen, R., Katus, H.A., and Frey, N. (2009). DYRK1A is a novel negative regulator of cardiomyocyte hypertrophy. J Biol Chem *284*, 17320-17327.

Kuida, K., Haydar, T.F., Kuan, C.Y., Gu, Y., Taya, C., Karasuyama, H., Su, M.S., Rakic, P., and Flavell, R.A. (1998). Reduced apoptosis and cytochrome c-mediated caspase activation in mice lacking caspase 9. Cell *94*, 325-337.

Kurabayashi, N., Nguyen, M.D., and Sanada, K. (2015). DYRK1A overexpression enhances STAT activity and astrogliogenesis in a Down syndrome mouse model. EMBO Rep *16*, 1548-1562.

Laguna, A., Aranda, S., Barallobre, M.J., Barhoum, R., Fernandez, E., Fotaki, V., Delabar, J.M., de la Luna, S., de la Villa, P., and Arbones, M.L. (2008). The protein kinase DYRK1A regulates caspase-9-mediated apoptosis during retina development. Dev Cell *15*, 841-853.

Laguna, A., Barallobre, M.J., Marchena, M.A., Mateus, C., Ramirez, E., Martinez-Cue, C., Delabar, J.M., Castelo-Branco, M., de la Villa, P., and Arbones, M.L. (2013). Triplication of DYRK1A causes retinal structural and functional alterations in Down syndrome. Hum Mol Genet *22*, 2775-2784.

Laham, A.J., El-Awady, R., Lebrun, J.J., and Ayad, M.S. (2022). A Bioinformatics Evaluation of the Role of Dual-Specificity Tyrosine-Regulated Kinases in Colorectal Cancer. Cancers (Basel) *14*.

Lange, C., Huttner, W.B., and Calegari, F. (2009). Cdk4/cyclinD1 overexpression in neural stem cells shortens G1, delays neurogenesis, and promotes the generation and expansion of basal progenitors. Cell Stem Cell *5*, 320-331.

LeBlanc, A.C. (2003). Natural cellular inhibitors of caspases. Prog Neuropsychopharmacol Biol Psychiatry *27*, 215-229.

Levy, J.A., LaFlamme, C.W., Tsaprailis, G., Crynen, G., and Page, D.T. (2021). Dyrk1a Mutations Cause Undergrowth of Cortical Pyramidal Neurons via Dysregulated Growth Factor Signaling. Biol Psychiatry *90*, 295-306.

Li, W., and Pozzo-Miller, L. (2020). Dysfunction of the corticostriatal pathway in autism spectrum disorders. J Neurosci Res *98*, 2130-2147.

Li, Y.L., Zhang, M.M., Wu, L.W., Liu, Y.H., Zhang, Z.Y., Zeng, L.H., Lin, N.M., and Zhang, C. (2022). DYRK1A reinforces epithelial-mesenchymal transition and metastasis of hepatocellular carcinoma via cooperatively activating STAT3 and SMAD. J Biomed Sci *29*, 34.

Li, Z., Jiao, X., Wang, C., Shirley, L.A., Elsaleh, H., Dahl, O., Wang, M., Soutoglou, E., Knudsen, E.S., and Pestell, R.G. (2010). Alternative cyclin D1 splice forms differentially regulate the DNA damage response. Cancer Res *70*, 8802-8811.

Liebl, M.C., and Hofmann, T.G. (2019). Cell Fate Regulation upon DNA Damage: p53 Serine 46 Kinases Pave the Cell Death Road. Bioessays *41*, e1900127.

Lim, L., Mi, D., Llorca, A., and Marin, O. (2018). Development and Functional Diversification of Cortical Interneurons. Neuron *100*, 294-313.

Liu, T., Wang, Y., Wang, J., Ren, C., Chen, H., and Zhang, J. (2022). DYRK1A inhibitors for disease therapy: Current status and perspectives. Eur J Med Chem *229*, 114062.

Lochhead, P.A., Sibbet, G., Morrice, N., and Cleghon, V. (2005). Activation-loop autophosphorylation is mediated by a novel transitional intermediate form of DYRKs. Cell *121*, 925-936.

Lodato, S., and Arlotta, P. (2015). Generating neuronal diversity in the mammalian cerebral cortex. Annu Rev Cell Dev Biol *31*, 699-720.

Lu, M., Zheng, L., Han, B., Wang, L., Wang, P., Liu, H., and Sun, X. (2011). REST regulates DYRK1A transcription in a negative feedback loop. J Biol Chem *286*, 10755-10763.

Luco, S.M., Pohl, D., Sell, E., Wagner, J.D., Dyment, D.A., and Daoud, H. (2016). Case report of novel DYRK1A mutations in 2 individuals with syndromic intellectual disability and a review of the literature. BMC Med Genet *17*, 15.

Luna, J., Boni, J., Cuatrecasas, M., Bofill-De Ros, X., Nunez-Manchon, E., Gironella, M., Vaquero, E.C., Arbones, M.L., de la Luna, S., and Fillat, C. (2019). DYRK1A modulates c-MET in pancreatic ductal adenocarcinoma to drive tumour growth. Gut *68*, 1465-1476.

Luo, L., Ambrozkiewicz, M.C., Benseler, F., Chen, C., Dumontier, E., Falkner, S., Furlanis, E., Gomez, A.M., Hoshina, N., Huang, W.H., et al. (2020). Optimizing Nervous System-Specific Gene Targeting with Cre Driver Lines: Prevalence of Germline Recombination and Influencing Factors. Neuron *106*, 37-65 e35.

Ma, S., Meng, Z., Chen, R., and Guan, K.L. (2019). The Hippo Pathway: Biology and Pathophysiology. Annu Rev Biochem *88*, 577-604.

Manda, N.K., Golla, U., Sesham, K., Desai, P., Joshi, S., Patel, S., Nalla, S., Kondam, S., Singh, L., Dewansh, D., et al. (2023). Tuning between Nuclear Organization and Functionality in Health and Disease. Cells *12*.

Mandal, R., Barron, J.C., Kostova, I., Becker, S., and Strebhardt, K. (2020). Caspase-8: The double-edged sword. Biochim Biophys Acta Rev Cancer *1873*, 188357.

Manning, G., Whyte, D.B., Martinez, R., Hunter, T., and Sudarsanam, S. (2002). The protein kinase complement of the human genome. Science *298*, 1912-1934.

Marin, O., Anderson, S.A., and Rubenstein, J.L. (2000). Origin and molecular specification of striatal interneurons. J Neurosci *20*, 6063-6076.

Marti, E., Altafaj, X., Dierssen, M., de la Luna, S., Fotaki, V., Alvarez, M., Perez-Riba, M., Ferrer, I., and Estivill, X. (2003). Dyrk1A expression pattern supports specific roles of this kinase in the adult central nervous system. Brain Res *964*, 250-263.

Martin, L.J. (2008). DNA damage and repair: relevance to mechanisms of neurodegeneration. J Neuropathol Exp Neurol *67*, 377-387.

Martynoga, B., Morrison, H., Price, D.J., and Mason, J.O. (2005). Foxg1 is required for specification of ventral telencephalon and region-specific regulation of dorsal telencephalic precursor proliferation and apoptosis. Dev Biol *283*, 113-127.

Mayhew, T.M., and Olsen, D.R. (1991). Magnetic resonance imaging (MRI) and model-free estimates of brain volume determined using the Cavalieri principle. J Anat *178*, 133-144.

McKinnon, P.J. (2013). Maintaining genome stability in the nervous system. Nat Neurosci *16*, 1523-1529.

McKinnon, P.J. (2017). Genome integrity and disease prevention in the nervous system. Genes Dev *31*, 1180-1194.

McLellan, M.A., Rosenthal, N.A., and Pinto, A.R. (2017). Cre-loxP-Mediated Recombination: General Principles and Experimental Considerations. Curr Protoc Mouse Biol *7*, 1-12.

Menon, V.R., Ananthapadmanabhan, V., Swanson, S., Saini, S., Sesay, F., Yakovlev, V., Florens, L., DeCaprio, J.A., Washburn, M.P., Dozmorov, M., and Litovchick, L. (2019). DYRK1A regulates the recruitment of 53BP1 to the sites of DNA damage in part through interaction with RNF169. Cell Cycle *18*, 531-551.

Mihalas, A.B., and Hevner, R.F. (2018). Clonal analysis reveals laminar fate multipotency and daughter cell apoptosis of mouse cortical intermediate progenitors. Development *145*.

Molyneaux, B.J., Arlotta, P., Menezes, J.R., and Macklis, J.D. (2007). Neuronal subtype specification in the cerebral cortex. Nat Rev Neurosci *8*, 427-437.

Mosaddad, S.A., Salari, Y., Amookhteh, S., Soufdoost, R.S., Seifalian, A., Bonakdar, S., Safaeinejad, F., Moghaddam, M.M., and Tebyanian, H. (2021). Response to Mechanical Cues by Interplay of YAP/TAZ Transcription Factors and Key Mechanical Checkpoints of the Cell: A Comprehensive Review. Cell Physiol Biochem *55*, 33-60.

Murray, A., Gough, G., Cindric, A., Vuckovic, F., Koschut, D., Borelli, V., Petrovic, D.J., Bekavac, A., Plecas, A., Hribljan, V., et al. (2023). Dose imbalance of DYRK1A kinase causes systemic progeroid status in Down syndrome by increasing the un-repaired DNA damage and reducing LaminB1 levels. EBioMedicine *94*, 104692.

Najas, S. (2014). Role of DYRK1A in the development of the cerebral cortex. Implication in Down Syndrome. In Departament de Ciències Experimentals i de la Salut (Universitat Pompeu Fabra).

Najas, S., Arranz, J., Lochhead, P.A., Ashford, A.L., Oxley, D., Delabar, J.M., Cook, S.J., Barallobre, M.J., and Arbones, M.L. (2015). DYRK1A-mediated Cyclin D1 Degradation in Neural Stem Cells Contributes to the Neurogenic Cortical Defects in Down Syndrome. EBioMedicine *2*, 120-134.

Newman, H., Liu, F.C., and Graybiel, A.M. (2015). Dynamic ordering of early generated striatal cells destined to form the striosomal compartment of the striatum. J Comp Neurol *523*, 943-962.

Nieuwenhuys R., Voogd N., and Van Huijzen C. (2007). The Human Central Nervous System (4th Edition) A Synopsis and Atlas. Steinkopff, Heidelberg.

O'Driscoll, M., and Jeggo, P.A. (2008). The role of the DNA damage response pathways in brain development and microcephaly: insight from human disorders. DNA Repair (Amst) *7*, 1039-1050.

Okui, M., Ide, T., Morita, K., Funakoshi, E., Ito, F., Ogita, K., Yoneda, Y., Kudoh, J., and Shimizu, N. (1999). High-level expression of the Mnb/Dyrk1A gene in brain and heart during rat early development. Genomics *62*, 165-171.

Ori-McKenney, K.M., McKenney, R.J., Huang, H.H., Li, T., Meltzer, S., Jan, L.Y., Vale, R.D., Wiita, A.P., and Jan, Y.N. (2016). Phosphorylation of beta-Tubulin by the Down Syndrome Kinase, Minibrain/DYRK1a, Regulates Microtubule Dynamics and Dendrite Morphogenesis. Neuron *90*, 551-563.

Park, J., Oh, Y., Yoo, L., Jung, M.S., Song, W.J., Lee, S.H., Seo, H., and Chung, K.C. (2010). Dyrk1A phosphorylates p53 and inhibits proliferation of embryonic neuronal cells. J Biol Chem *285*, 31895-31906.

Park, J., Sung, J.Y., Park, J., Song, W.J., Chang, S., and Chung, K.C. (2012). Dyrk1A negatively regulates the actin cytoskeleton through threonine phosphorylation of N-WASP. J Cell Sci *125*, 67-80.

Parras, A., Anta, H., Santos-Galindo, M., Swarup, V., Elorza, A., Nieto-Gonzalez, J.L., Pico, S., Hernandez, I.H., Diaz-Hernandez, J.I., Belloc, E., et al. (2018). Autism-like phenotype and risk gene mRNA deadenylation by CPEB4 mis-splicing. Nature *560*, 441-446.

Penaloza, C., Orlanski, S., Ye, Y., Entezari-Zaher, T., Javdan, M., and Zakeri, Z. (2008). Cell death in mammalian development. Curr Pharm Des *14*, 184-196.

Petersen, P.H., Zou, K., Hwang, J.K., Jan, Y.N., and Zhong, W. (2002). Progenitor cell maintenance requires numb and numblike during mouse neurogenesis. Nature *419*, 929-934.

Phillips, E.R., and McKinnon, P.J. (2007). DNA double-strand break repair and development. Oncogene *26*, 7799-7808.

Pijuan, I., Balducci, E., Soto-Sanchez, C., Fernandez, E., Barallobre, M.J., and Arbones, M.L. (2022). Impaired macroglial development and axonal conductivity contributes to the neuropathology of DYRK1A-related intellectual disability syndrome. Sci Rep *12*, 19912.

Pilaz, L.J., McMahon, J.J., Miller, E.E., Lennox, A.L., Suzuki, A., Salmon, E., and Silver, D.L. (2016). Prolonged Mitosis of Neural Progenitors Alters Cell Fate in the Developing Brain. Neuron *89*, 83-99.

Pilaz, L.J., Patti, D., Marcy, G., Ollier, E., Pfister, S., Douglas, R.J., Betizeau, M., Gautier, E., Cortay, V., Doerflinger, N., et al. (2009). Forced G1-phase reduction alters mode of division, neuron number, and laminar phenotype in the cerebral cortex. Proc Natl Acad Sci U S A *106*, 21924-21929.

Pilz, G.A., Shitamukai, A., Reillo, I., Pacary, E., Schwausch, J., Stahl, R., Ninkovic, J., Snippert, H.J., Clevers, H., Godinho, L., et al. (2013). Amplification of progenitors in the mammalian telencephalon includes a new radial glial cell type. Nat Commun *4*, 2125.

Pinson, A., Namba, T., and Huttner, W.B. (2019). Malformations of Human Neocortex in Development - Their Progenitor Cell Basis and Experimental Model Systems. Front Cell Neurosci *13*, 305.

Poulsen, M., Lukas, C., Lukas, J., Bekker-Jensen, S., and Mailand, N. (2012). Human RNF169 is a negative regulator of the ubiquitin-dependent response to DNA double-strand breaks. J Cell Biol *197*, 189-199.

Priya, R., Paredes, M.F., Karayannis, T., Yusuf, N., Liu, X., Jaglin, X., Graef, I., Alvarez-Buylla, A., and Fishell, G. (2018). Activity Regulates Cell Death within Cortical Interneurons through a Calcineurin-Dependent Mechanism. Cell Rep *22*, 1695-1709.

Rachdi, L., Kariyawasam, D., Guez, F., Aiello, V., Arbones, M.L., Janel, N., Delabar, J.M., Polak, M., and Scharfmann, R. (2014). Dyrk1a haploinsufficiency induces diabetes in mice through decreased pancreatic beta cell mass. Diabetologia *57*, 960-969.

Rammohan, M., Harris, E., Bhansali, R.S., Zhao, E., Li, L.S., and Crispino, J.D. (2022). The chromosome 21 kinase DYRK1A: emerging roles in cancer biology and potential as a therapeutic target. Oncogene *41*, 2003-2011.

Recasens, A., Humphrey, S.J., Ellis, M., Hoque, M., Abbassi, R.H., Chen, B., Longworth, M., Needham, E.J., James, D.E., Johns, T.G., et al. (2021). Global phosphoproteomics reveals DYRK1A regulates CDK1 activity in glioblastoma cells. Cell Death Discov *7*, 81.

Reinhardt, H.C., and Schumacher, B. (2012). The p53 network: cellular and systemic DNA damage responses in aging and cancer. Trends Genet *28*, 128-136.

Roewenstrunk, J., Di Vona, C., Chen, J., Borras, E., Dong, C., Arato, K., Sabido, E., Huen, M.S.Y., and de la Luna, S. (2019). A comprehensive proteomics-based interaction screen that links DYRK1A to RNF169 and to the DNA damage response. Sci Rep *9*, 6014.

Rogakou, E.P., Pilch, D.R., Orr, A.H., Ivanova, V.S., and Bonner, W.M. (1998). DNA double-stranded breaks induce histone H2AX phosphorylation on serine 139. J Biol Chem *273*, 5858-5868.

Roizen, N.J., and Patterson, D. (2003). Down's syndrome. Lancet *361*, 1281-1289.

Roth, K.A., Kuan, C., Haydar, T.F., D'Sa-Eipper, C., Shindler, K.S., Zheng, T.S., Kuida, K., Flavell, R.A., and Rakic, P. (2000). Epistatic and independent functions of caspase-3 and Bcl-X(L) in developmental programmed cell death. Proc Natl Acad Sci U S A *97*, 466-471.

Sadasivam, S., and DeCaprio, J.A. (2013). The DREAM complex: master coordinator of cell cycle-dependent gene expression. Nat Rev Cancer *13*, 585-595.

Salomoni, P., and Calegari, F. (2010). Cell cycle control of mammalian neural stem cells: putting a speed limit on G1. Trends Cell Biol *20*, 233-243.

Schindelin, J., Arganda-Carreras, I., Frise, E., Kaynig, V., Longair, M., Pietzsch, T., Preibisch, S., Rueden, C., Saalfeld, S., Schmid, B., et al. (2012). Fiji: an open-source platform for biological-image analysis. Nat Methods *9*, 676-682.

Sessa, A., Mao, C.A., Hadjantonakis, A.K., Klein, W.H., and Broccoli, V. (2008). Tbr2 directs conversion of radial glia into basal precursors and guides neuronal amplification by indirect neurogenesis in the developing neocortex. Neuron *60*, 56-69.

Shen, W., Taylor, B., Jin, Q., Nguyen-Tran, V., Meeusen, S., Zhang, Y.Q., Kamireddy, A., Swafford, A., Powers, A.F., Walker, J., et al. (2015). Inhibition of DYRK1A and GSK3B induces human beta-cell proliferation. Nat Commun *6*, 8372.

Shepherd, G.M. (2013). Corticostriatal connectivity and its role in disease. Nat Rev Neurosci *14*, 278-291.

Shiloh, Y., and Ziv, Y. (2013). The ATM protein kinase: regulating the cellular response to genotoxic stress, and more. Nat Rev Mol Cell Biol *14*, 197-210.

Soppa, U., Schumacher, J., Florencio Ortiz, V., Pasqualon, T., Tejedor, F.J., and Becker, W. (2014). The Down syndrome-related protein kinase DYRK1A phosphorylates p27(Kip1) and Cyclin D1 and induces cell cycle exit and neuronal differentiation. Cell Cycle *13*, 2084-2100.

Southwell, D.G., Paredes, M.F., Galvao, R.P., Jones, D.L., Froemke, R.C., Sebe, J.Y., Alfaro-Cervello, C., Tang, Y., Garcia-Verdugo, J.M., Rubenstein, J.L., et al. (2012). Intrinsically determined cell death of developing cortical interneurons. Nature *491*, 109-113.

Sprick, M.R., Rieser, E., Stahl, H., Grosse-Wilde, A., Weigand, M.A., and Walczak, H. (2002). Caspase-10 is recruited to and activated at the native TRAIL and CD95 death-inducing signalling complexes in a FADD-dependent manner but can not functionally substitute caspase-8. EMBO J *21*, 4520-4530.

Stephens, A.D., Banigan, E.J., and Marko, J.F. (2019). Chromatin's physical properties shape the nucleus and its functions. Curr Opin Cell Biol *58*, 76-84.

Stessman, H.A., Xiong, B., Coe, B.P., Wang, T., Hoekzema, K., Fenckova, M., Kvarnung, M., Gerdts, J., Trinh, S., Cosemans, N., et al. (2017). Targeted sequencing identifies 91 neurodevelopmental-disorder risk genes with autism and developmental-disability biases. Nat Genet *49*, 515-526.

Stracker, T.H., Usui, T., and Petrini, J.H. (2009). Taking the time to make important decisions: the checkpoint effector kinases Chk1 and Chk2 and the DNA damage response. DNA Repair (Amst) *8*, 1047-1054.

Sullivan, K.F., and Cleveland, D.W. (1986). Identification of conserved isotype-defining variable region sequences for four vertebrate beta tubulin polypeptide classes. Proc Natl Acad Sci U S A *83*, 4327-4331.

Takahashi, T., Nowakowski, R.S., and Caviness, V.S., Jr. (1995). The cell cycle of the pseudostratified ventricular epithelium of the embryonic murine cerebral wall. J Neurosci *15*, 6046-6057.

Taverna, E., and Huttner, W.B. (2010). Neural progenitor nuclei IN motion. Neuron *67*, 906-914.

Tejedor, F., Zhu, X.R., Kaltenbach, E., Ackermann, A., Baumann, A., Canal, I., Heisenberg, M., Fischbach, K.F., and Pongs, O. (1995). minibrain: a new protein kinase family involved in postembryonic neurogenesis in Drosophila. Neuron *14*, 287-301.

Tepper, J.M., Koos, T., and Wilson, C.J. (2004). GABAergic microcircuits in the neostriatum. Trends Neurosci *27*, 662-669.

Thompson, B.J., Bhansali, R., Diebold, L., Cook, D.E., Stolzenburg, L., Casagrande, A.S., Besson, T., Leblond, B., Desire, L., Malinge, S., and Crispino, J.D. (2015). DYRK1A controls the transition from proliferation to quiescence during lymphoid development by destabilizing Cyclin D3. J Exp Med *212*, 953-970.

Totaro, A., Panciera, T., and Piccolo, S. (2018). YAP/TAZ upstream signals and downstream responses. Nat Cell Biol *20*, 888-899.

Tschop, K., Conery, A.R., Litovchick, L., Decaprio, J.A., Settleman, J., Harlow, E., and Dyson, N. (2011). A kinase shRNA screen links LATS2 and the pRB tumor suppressor. Genes Dev *25*, 814-830.

Turrero Garcia, M., and Harwell, C.C. (2017). Radial glia in the ventral telencephalon. FEBS Lett *591*, 3942-3959.

van Bon, B.W., Coe, B.P., Bernier, R., Green, C., Gerdts, J., Witherspoon, K., Kleefstra, T., Willemsen, M.H., Kumar, R., Bosco, P., et al. (2016). Disruptive de novo mutations of DYRK1A lead to a syndromic form of autism and ID. Mol Psychiatry *21*, 126-132.

Varjosalo, M., Keskitalo, S., Van Drogen, A., Nurkkala, H., Vichalkovski, A., Aebersold, R., and Gstaiger, M. (2013). The protein interaction landscape of the human CMGC kinase group. Cell Rep *3*, 1306-1320.

Vidaki, M., Drees, F., Saxena, T., Lanslots, E., Taliaferro, M.J., Tatarakis, A., Burge, C.B., Wang, E.T., and Gertler, F.B. (2017). A Requirement for Mena, an Actin Regulator, in Local mRNA Translation in Developing Neurons. Neuron *95*, 608-622 e605.

Villalba, A., Gotz, M., and Borrell, V. (2021). The regulation of cortical neurogenesis. Curr Top Dev Biol *142*, 1-66.

Wamsley, B., and Fishell, G. (2017). Genetic and activity-dependent mechanisms underlying interneuron diversity. Nat Rev Neurosci *18*, 299-309.

Wang, C., Fan, S., Li, Z., Fu, M., Rao, M., Ma, Y., Lisanti, M.P., Albanese, C., Katzenellenbogen, B.S., Kushner, P.J., et al. (2005). Cyclin D1 antagonizes BRCA1 repression of estrogen receptor alpha activity. Cancer Res *65*, 6557-6567.

Wang, P., Wang, L., Chen, L., and Sun, X. (2017). Dual-specificity tyrosine-phosphorylation regulated kinase 1A Gene Transcription is regulated by Myocyte Enhancer Factor 2D. Sci Rep *7*, 7240.

Waterman, D.P., Haber, J.E., and Smolka, M.B. (2020). Checkpoint Responses to DNA Double-Strand Breaks. Annu Rev Biochem *89*, 103-133.

Weerasinghe, P., and Buja, L.M. (2012). Oncosis: an important non-apoptotic mode of cell death. Exp Mol Pathol *93*, 302-308.

Wegiel, J., Kuchna, I., Nowicki, K., Frackowiak, J., Dowjat, K., Silverman, W.P., Reisberg, B., DeLeon, M., Wisniewski, T., Adayev, T., et al. (2004). Cell type- and brain structure-specific patterns of distribution of minibrain kinase in human brain. Brain Res *1010*, 69-80.

Wei, H., Alberts, I., and Li, X. (2014). The apoptotic perspective of autism. Int J Dev Neurosci *36*, 13-18.

Weinberg, R.A. (1995). The retinoblastoma protein and cell cycle control. Cell *81*, 323-330.

Widowati, E.W., Bamberg-Lemper, S., and Becker, W. (2018). Mutational analysis of two residues in the DYRK homology box of the protein kinase DYRK1A. BMC Res Notes *11*, 297.

Williams, A.B., and Schumacher, B. (2016). p53 in the DNA-Damage-Repair Process. Cold Spring Harb Perspect Med *6*.

Wilson, C.J., and Groves, P.M. (1980). Fine structure and synaptic connections of the common spiny neuron of the rat neostriatum: a study employing intracellular inject of horseradish peroxidase. J Comp Neurol *194*, 599-615.

Wonders, C.P., and Anderson, S.A. (2006). The origin and specification of cortical interneurons. Nat Rev Neurosci *7*, 687-696.

Wong, F.K., Bercsenyi, K., Sreenivasan, V., Portales, A., Fernandez-Otero, M., and Marin, O. (2018). Pyramidal cell regulation of interneuron survival sculpts cortical networks. Nature *557*, 668-673.

Wong, F.K., and Marin, O. (2019). Developmental Cell Death in the Cerebral Cortex. Annu Rev Cell Dev Biol *35*, 523-542.

Woods, Y.L., Cohen, P., Becker, W., Jakes, R., Goedert, M., Wang, X., and Proud, C.G. (2001). The kinase DYRK phosphorylates protein-synthesis initiation factor eIF2Bepsilon at Ser539 and the microtubule-associated protein tau at Thr212: potential role for DYRK as a glycogen synthase kinase 3-priming kinase. Biochem J *355*, 609-615.

Xing, L., Wilsch-Brauninger, M., and Huttner, W.B. (2021). How neural stem cells contribute to neocortex development. Biochem Soc Trans *49*, 1997-2006.

Yamaguchi, T., Goto, H., Yokoyama, T., Sillje, H., Hanisch, A., Uldschmid, A., Takai, Y., Oguri, T., Nigg, E.A., and Inagaki, M. (2005). Phosphorylation by Cdk1 induces Plk1-mediated vimentin phosphorylation during mitosis. J Cell Biol *171*, 431-436.

Yan, G. (2020). Multiple cell death modalities and their key features. World Academy of Sciences Journal 2, 39–48.

Yehia, L., Keel, E., and Eng, C. (2020). The Clinical Spectrum of PTEN Mutations. Annu Rev Med *71*, 103-116.

Yoshida, H., Kong, Y.Y., Yoshida, R., Elia, A.J., Hakem, A., Hakem, R., Penninger, J.M., and Mak, T.W. (1998). Apaf1 is required for mitochondrial pathways of apoptosis and brain development. Cell *94*, 739-750.

Young, R.W. (1984). Cell death during differentiation of the retina in the mouse. J Comp Neurol *229*, 362-373.

Yu, F.X., Zhao, B., and Guan, K.L. (2015). Hippo Pathway in Organ Size Control, Tissue Homeostasis, and Cancer. Cell *163*, 811-828.

Zappone, M.V., Galli, R., Catena, R., Meani, N., De Biasi, S., Mattei, E., Tiveron, C., Vescovi, A.L., Lovell-Badge, R., Ottolenghi, S., and Nicolis, S.K. (2000). Sox2 regulatory sequences direct expression of a (beta)-geo transgene to telencephalic neural stem cells and precursors of the mouse embryo, revealing regionalization of gene expression in CNS stem cells. Development *127*, 2367-2382.

Zilles, K., Palomero-Gallagher, N., and Amunts, K. (2013). Development of cortical folding during evolution and ontogeny. Trends Neurosci *36*, 275-284.

ANNEXE

Table M1. Primers used for genotyping

***Dyrk1a* allele/ transgene**	**Primers**	**Sequence 5'-3'**	**Ta (ºC) (cycles)**	**Amplicon (bp)**
Dyrk1a-flox	Dyrk1a-I3 (F) Dyrk1a-E4 (R)	ATTACCTGGAGAAGAGGGCAAG TTCTTATGACTGGAATCGTCCC	58 (30)	500/**600**
Dyrk1a-flox *Dyrk1a*-Δ	Dyrk1a-I3 (F) Dyrk1a-E4 (R) Dyrk1aR-R4 (R)	ATTACCTGGAGAAGAGGGCAAG TTCTTATGACTGGAATCGTCCC CACCGGCTTTGATGAATGTA	58 (35)	500/ **600, 700**
Cre-recombinase	CRE (F) CRE-228 (R) WT (F) WT (R)	GCGGTCTGGCAGTAAAAACTATC AGCATACCTGGAAAATGCTTCTG CTAGGCCACGAATTGAAAGATCT GTAGGTGGAAATTCTAGCATCATCC	51 (35)	**228** 325
*td*Tomato	Td-MF (F) Td-MR (R) Td-WT (F) Td-WT (R)	GGCATTAAAGCAGCGTATCC CTGTTCCTGTACGGCATGG AAGGGAGCTGCAGTGGAGTA CCGAAAATCTGTGGGAAGTC	63 (35)	**196** 297

*All primers were used at 10 µM. *In bold the size of the amplicon in the mutant allele. bp: base pairs; F: forward; R: reverse; Ta: annealing temperature.*

Table M2. Primary antibodies used for Immunoblotting

Primary antibody	**Host**	**Dilution**	**#Identifier, RRID, provider**
Active Caspase-9	Mouse	1:200	#9508, AB_2068620, Cell Signalling
Caspase-9 (Thr125)	Rabbit	1:500	#bs-3082R, AB_10857093, Bioss antibodies
Cre-recombinase	Mouse	1:1000	#mab3120, AB_2085748, Merck Millipore
Cyclin D1	Rabbit	1:200	#MA5-16356, AB_2537875, Invitrogen
DYRK1A	Mouse	1:1000	#H00001859-M01, AB_2230676, Abnova
P27 (KIP1)	Mouse	1:500	#610242, AB_397637, BD Bioscience
Retinoblastoma	Mouse	1:500	#554136, AB_395259, BD Biosciences

Table M3. Primary antibodies used for immunofluorescence

Primary antibody	Host	Dilution	#Identifier, RRID, provider
BrdU+	Rat	1:100	#NB500-169, AB_10002608, Novus Biologicals
Active Caspase-3	Rabbit	1:400	#559565, AB_397274, BD Pharmigen
Active Caspase-9	Rabbit	1:400	#9509, AB_2073476, Cell Signalling
CTIP2*	Rat	1:200	#ab18465, AB_2064130, Abcam
Ki67	Rat	1:75	#M7249, AB_2250503, DAKO
p53	Rabbit	1:100	NCL-L-p53-CM5p, AB_2895247, Novocastra
Phospho-histone H2AX*	Rabbit	1:100	#9718, AB_2118009, Cell Signalling
Phospho-histone 3 (Ser28)	Rat	1:400	#H9908, AB_260096, Sigma
Phospho-vimentin (Ser55)	Mouse	1:200	D076-3. AB_502063, MBL Life Science
SATB2	Mouse	1:200	#ab51502, AB_882455, Abcam
SOX2*	Goat	1:100	#sc17320, AB_2286684, Santa Cruz
SOX2*	Goat	1:100	AF2018, AB_355110, R&D Biosystem
TBR1	Rabbit	1:100	#ab183032, AB_2313773, Abcam
TBR2	Rabbit	1:200	#ab23345, AB_778267, Abcam
TUJ1	Mouse	1:400	#801202, AB_10063408, Biolegend

(*) Citrate pre-treatment needed. (+) Hydroxide Chloride pre-treatment needed.

Table M4. Secondary antibodies used for immunofluorescence

Secondary antibody	Host	Dilution	Source
Alexa Fluor 488-conjugated anti-mouse	Donkey	1:1000	Life Technologies
Alexa Fluor 8488-conjugated anti-rabbit	Goat	1:1000	Life Technologies
Alexa Fluor 488-conjugated anti-rat	Donkey	1:1000	Life Technologies
Alexa Fluor 488-conjugated anti-goat	Donkey	1:1000	Life Technologies
Alexa Fluor 568-conjugated anti-mouse	Donkey	1:1000	Life Technologies
Alexa Fluor 568-conjugated anti-rabbit	Donkey	1:1000	Life Technologies
Alexa Fluor 647-conjugated anti-rat	Donkey	1:1000	Life Technologies
Biotinylated anti-goat	Horse	1:200	Vector Laboratories
Biotinylated anti-mouse	Goat	1:200	Vector Laboratories
Streptavidin Alexa Fluor 633-conjugated	-	1:1000	Thermo scientific
Streptavidin Alexa Fluor 488-conjugated	-	1:1000	Thermo scientific